Influence of compositions and size on the giant magnetocaloric effect in (Mn,Fe)2(P,Si)-based compounds

Nguyên, Thang

DOI
10.4233/uuid:b40864fa-cc4b-43b2-816d-98f810296a24

Publication date
2017

Document Version
Publisher's PDF, also known as Version of record

INFLUENCE OF COMPOSITIONS AND SIZE ON THE GIANT MAGNETOCALORIC EFFECT IN $(Mn,Fe)_2(P,Si)$-BASED COMPOUNDS

INFLUENCE OF COMPOSITIONS AND SIZE ON THE GIANT MAGNETOCALORIC EFFECT IN $(Mn,Fe)_2(P,Si)$-BASED COMPOUNDS

Proefschrift

ter verkrijging van de graad van doctor
aan de Technische Universiteit Delft,
op gezag van de Rector Magnificus prof. ir. K.C.A.M. Luyben,
voorzitter van het College voor Promoties,
in het openbaar te verdedigen op maandag 15 mei 2017 om 10:00 uur

door

Thang VAN NGUYEN

Master in Inorganic Chemistry,
VNU University of Science, Vietnam
geboren te Binh Dinh, Vietnam.

This dissertation has been approved by

promotor: Prof. dr. E.H. Brück
copromotor: Dr. ir. N.H. van Dijk

Composition of the doctoral committee:

Rector Magnificus	voorzitter
Prof. dr. E.H. Brück	Technische Universiteit Delft
Dr. ir. N.H. van Dijk	Technische Universiteit Delft
Independent members:	
Prof. dr. C. Pappas	Technische Universiteit Delft
Prof. dr. A. Schmidt-Ott	Technische Universiteit Delft
Prof. dr. G.C.A.M Janssen	Technische Universiteit Delft
Prof. dr. N. Dempsey	Institut NEEL CNRS, France
Assoc. Prof. dr. N.P. Duong	Hanoi University of Science and Technology, Vietnam

The work presented in this PhD thesis is financially supported by the Foundation for Fundamental Research on Matter (FOM), the Netherlands, via the Industrial Partnership Program IPP I28 and co-financed by BASF New Business, carried out at the section Fundamental Aspects of Materials and Energy, Faculty of Applied Sciences, Delft University of Technology (TUD).

Printed by: Gildeprint, Enschede

Casimir PhD Series, Delft-Leiden 2017-12

ISBN 978-94-92516-48-0

An electronic version of this dissertation is available at
http://repository.tudelft.nl/.

Dedicated to my beloved parents for their blessings and support.

CONTENTS

1

INTRODUCTION

Cooling technologies for both industrial and residential applications account for 15 % of the total worldwide energy consumption [1]. Limited natural resources and the growing global energy demand call for an efficient and environmentally friendly energy consumption. Thus the UN Advisory on Energy and Climate Change requests a 40 % improved energy efficiency by the year 2030 [2]. Vapor-compression refrigeration is the most commonly used method of cooling. However, it seems that cooling efficiency of latest generation vapor-compression refrigerators has reached its upper limit. Moreover, the use of the dangerous and environmentally unfriendly refrigerants such as ozone-depleting chemicals (e.g., chlorofluorocarbons (CFCs)), hazardous chemicals (e.g., ammonia (NH_3)) or greenhouse gases (e.g., hydrofluorocarbons (HFCs) and hydrochlorofluorocarbons (HCFCs)) in this technology has raised serious environmental concerns [1]. The CFCs and HCFCs have been prohibited, and the HFCs will also be completely banned in the coming years according to the Montreal Protocol [3]. Therefore, it is highly desirable to develop a novel refrigeration technology with a minimum negative impact on the environment and a higher cooling efficiency in order to replace the conventional vapor-compression refrigeration. A promising alternative to the conventional vapor-compression technology is magnetic refrigeration using advanced magnetocaloric materials. Refrigerators based on the magnetic cooling technology use environmentally friendly materials and it has been calculated that the efficiency can exceed the efficiency of conventional refrigeration. Furthermore, magnetic cooling allows the design of a more compact and silent refrigerator compared to conventional refrigerators [4] , [5], [6], [7]. In this chapter, an overview of the magnetocaloric effect, magnetic refrigeration and giant magnetocaloric materials is given.

1

1.1. MAGNETOCALORIC EFFECT

The magnetocaloric effect (MCE) is a magneto-thermodynamic phenomenon that is intrinsic to all magnetic materials and originates from the interplay between the magnetic and the crystal lattices. For long it was accepted within the magnetic refrigeration research community that the MCE was discovered by the German physicist E. Warburg in 1881 [8]. However, Anders Smith re-examined the original literature and showed that the discovery of the MCE should be attributed to Weiss and Piccard in 1917 [9]. Weiss and Piccard experimentally discovered the MCE by observing a reversible temperature change of 0.7 K in pure nickel under a magnetic change of 1.5 T near its Curie temperature (T_C = 627 K) [10].

The magnetocaloric effect is observed in magnetic materials under the application of an external magnetic field. Depending on whether the magnetic field is changed under adiabatic or isothermal conditions, an adiabatic temperature change $\Delta T_{ad}(T, \Delta B)$ or an isothermal magnetic entropy change $\Delta S_m(T, \Delta B)$ is obtained, respectively. The mechanism for the changes in temperature and entropy arises from the manipulation of the magnetic moments in the material. Temperature and entropy changes will be maximal around phase transitions, where a reconfiguration of the magnetic order in a material spontaneously takes place at a given critical temperature and field.

The MCE is mainly investigated for magnetic heat pumping applications [11], [12]. MCE materials could also be used as hyperthermia (MCE nanoparticles) [13] and show potential for heat-to-power conversion in thermomagnetic generators [14]. The main focus of this thesis is the potential application of MCE materials for near room-temperature magnetic refrigeration.

1.2. MAGNETIC REFRIGERATION

Magnetic refrigeration (MR) based on the MCE is a well-established cooling technology to achieve ultra-low temperatures (below 1 K) [15]. Over the past decade, since the discovery of magnetic materials that show a giant MCE near room temperature, the interest in this cooling technology has been revived as a highly efficient alternative to the traditional vapor-compression refrigeration.

In general, a magnetic refrigerator consists of: a solid-state magnetic refrigerant, a permanent magnet to generate the field changes, hot/cold heat exchangers and a heat-transfer medium [16]. Depending on the operating temperature, the heat-transfer medium can be a gas (e.g., air or helium) or a liquid (e.g., water with antifreeze). A magnetic refrigeration cycle is analogous to the conventional vapor compression cycle. However, a change in external magnetic field is used as driving force rather than a change in pressure.

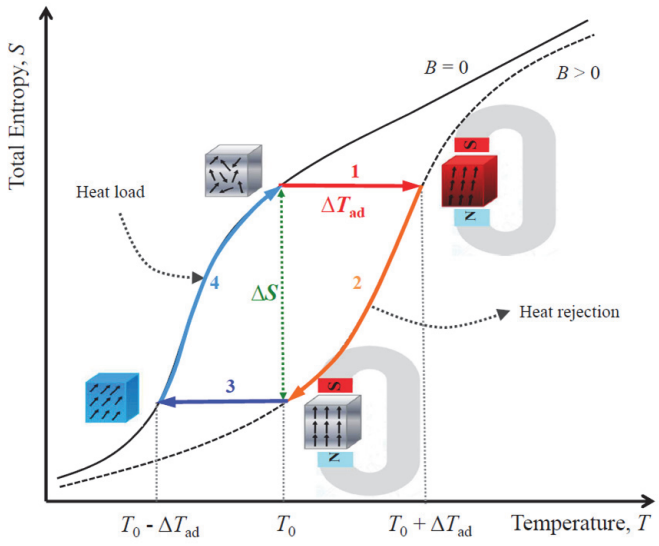

Figure 1.1: $T-S$ diagram representing a Brayton cycle for first-order magnetocaloric materials [17].

The Brayton cycle illustrated in Fig. 1.1 is commonly used as the basis for current MR prototypes. This cycle consists of two adiabatic processes (1 and 3) and two isofield processes (2 and 4). The cycle starts at a temperature (T_0) just above the Curie temperature in zero magnetic field. The solid-state magnetic refrigerant is magnetized under adiabatic conditions, resulting in an increase in the temperature of the refrigerant ($T_0 + \Delta T_{ad}$). This additional heat is expelled from the refrigerant to the surroundings under isofield conditions by a heat transfer medium. The adiabatic removal of the magnetic field leads to cooling the refrigerant below its initial temperature ($T_0 - \Delta T_{ad}$). Finally the heat exchanger transfers heat to the refrigerant to provide cooling power, thereby completing the cycle. The temperature span of such a cycle is directly proportional to the adiabatic temperature change of the refrigerant, which is relatively low for the presently known MCE materials (3 K for ΔB = 1 T). A larger temperature span can be achieved by combining MCE materials with various Curie temperatures in a so-called Active Magnetic Regenerative Refrigeration cycle, which comprises of a cascade of Brayton cycles [17].

1

1.3. GIANT MAGNETOCALORIC EFFECT IN $(MN,FE)_2(P,SI)$

The realization of magnetic refrigeration for domestic purposes requires an active magnetic refrigerant, a low-cost magnetic field source and a proper design of the thermodynamic refrigeration cycle. The use of permanent magnets generating fields below 1 T are desirable for domestic applications [18] to reduce the costs. However, the MCE is relatively low for these low-field changes. This calls for novel materials that show large MCE in a small applied magnetic field.

Since the MCE is maximal close to the phase transition, most of attention is paid to materials that undergo a first-order magnetic phase transition near room temperature. A large MCE in the vicinity of room temperature has been observed in several materials: $Gd_5(Si,Ge)_4$ [19]; MnAs and Mn(As,Sb) [20],[21]; $Fe_{49}Rh_{51}$ [22],[23]; $(Mn,Fe)_2(P,X)$ with X = As, Ge, Si [24],[25],[26]; $(Mn,Fe)_2(P,Si,B)$ [27]; $La(Fe,Si)_{13}$ and their hydrides [28],[29],[30]; $La(Mn,Fe,Si)_{13}H_z$ [31], $MnCoGeB_x$ [32]; $MnCoGe_{1-x}Ga_x$ [33]; $MnCo_{1-x}Fe_xSi$ [34]; and Heusler alloys [35],[36],[37],[38]. Based on the nature of the first-order magnetic phase transition, MCE materials can be divided into materials with a first-order magneto-structural (change in crystal symmetry) and a first-order magneto-elastic transition (contraction/elongation of lattice parameters, while keeping the same crystal structure). Compared to systems with first-order magneto-structural transitions such as $Gd_5(Si,Ge)_4$, MnAs and $MnCoGeB_x$, systems with first-order magneto-elastic transitions, $La(Fe,Si)_{13}$ and $(Mn,Fe)_2(P,X)$, are preferred as it is generally easier to tailor MCE properties by modifying the chemical composition.

Along with $La(Fe,Si)_{13}$-based compounds, $(Mn,Fe)_2(P,Si)$-based compounds are currently the best candidates for the commercial realization of near room-temperature magnetic refrigeration due to their large magnetocaloric effect in a small applied magnetic field, limited thermal hysteresis, tunability of the Curie temperature over a broad range of temperatures and non-toxic abundantly available ingredients [39], [40]. A milestone for the magnetic refrigeration community was the realization of a first commercial prototype of a MCE wine cooler, which utilized a magnetic refrigerant based on the $(Mn,Fe)_2(P,Si)$ material developed at the TU Delft. This prototype was produced and presented by Haier, Astronautics and BASF at the International Consumer Electronics Show in Las Vegas (January 2015).

1.4. NANO SCALING

Large scale production of MCE bulk materials usually consumes large amounts of energy during the annealing process in order to achieve a high degree of homogeneity. The use of nanoscale particles in the annealing process reduces the required temperatures and annealing times, while maintaining the same degree

of homogeneity. This could effectively lower the total energy consumption of the production process. MCE nanoscale particles could be used as treatment for malignant tumors by means of hyperthermia [41]. In this treatment the dispersing magnetic particles in the target tissue are heated by applying an AC magnetic field of sufficient strength at a certain frequency. This heat eliminates cancer cells if the temperature can be maintained above the therapeutic threshold of 42 °C for 30 minutes. In addition, these nano structured materials may provide some new features in the MCE and magnetic properties because the surface-to-volume ratio in nanoparticles is larger compared to bulk materials.

1.5. SCOPE AND OUTLINE OF THIS THESIS

One of the shortcomings of $(Mn,Fe)_2(P,Si)$-based compounds is that they undergo a large change in lattice parameters at the phase transition. This may lead to cracks and poor mechanical stability, which is not suitable for long-term use in magnetic refrigerators. Furthermore, relatively low adiabatic temperature change of these compounds is a problem for practical applications. To cover a wide temperature range, a series of compositions with gradual changes in T_C are required, while keeping good magnetic, thermal and mechanical properties. Hence, it is highly desirable to find additional parameters to tailor the magnetocaloric properties and improve the mechanical stability of $(Mn,Fe)_2(P,Si)$-based compounds.

The aim of the present work is to optimize the properties of $(Mn,Fe)_2(P,Si)$-based compounds utilizing two different approaches: (i) exploring the possibility to produce nano-scale $(Mn,Fe)_2(P,Si)$ particles without losing the magnetocaloric properties, (ii) optimizing this system by changing compositions or/and heat treatment conditions.

Chapter 2 provides an overview on the theoretical aspects of the MCE. Direct and indirect measurements to determine the magnetocaloric quantities $\Delta S_m(T,\Delta B)$ and $\Delta T_{ad}(T,\Delta B)$ are also presented. **Chapter 3** describes the main experimental techniques employed in this thesis, including the sample preparation and characterization. In **Chapter 4** the possibility to produce nano-scale $(Mn,Fe)_2(P,Si)$ particles by surfactant-assisted high-energy ball milling is explored. The effect of milling conditions on $Mn_{1.25}Fe_{0.70}P_{0.60}Si_{0.40}$ nanoparticles is investigated by X-ray diffraction (XRD) and magnetic measurements. **Chapter 5** is devoted to find optimal annealing conditions to either lower the annealing temperature or shorten the annealing time, while keeping a uniform phase in $(Mn,Fe)_2(P,Si,B)$-based materials. Furthermore, the influence of heat treatment conditions on the structural properties and magnetic phase transition of $Mn_{1.000}Fe_{0.950}P_{0.595}Si_{0.330}B_{0.075}$ is discussed. **Chapter 6** examines the influence of nitrogen added to $(Mn,Fe)_2(P,Si)$-based materials on the magnetic phase tran-

sition and the mechanical stability. The aim of **Chapter 7** is to investigate the influence of Co-B and Ni-B co-doping on the structural, magnetic and magnetocaloric properties of $(Mn,Fe)_2(P,Si)$ compounds using X-ray diffraction, differential scanning calorimetry, magnetic and direct temperature change measurements. Finally, **Chapter 8** focuses on a systematic study of the effect of carbon addition on the structural, magnetic and magnetocaloric properties of $(Mn,Fe)_2(P,Si)$-based materials.

REFERENCES

[1] S. L. Russek and C. B. Zimm, *Potential for cost effective magnetocaloric air conditioning systems,* International Journal of Refrigeration **29**, 1366 (2006).

[2] *Remarks at Fourth World Future Energy Summit,* Secretary-General Ban Ki-moon, Abu Dhabi (United Arab Emirates) , 1 (2011).

[3] *Handbook for the montreal protocol on substances that deplete the ozone layer* (2012).

[4] K. Gschneidner and V. Pecharsky, *Thirty years of near room temperature magnetic cooling: Where we are today and future prospects,* International Journal of Refrigeration **31**, 945 (2008).

[5] B. Yu, M. Liu, P. W. Egolf, and A. Kitanovski, *A review of magnetic refrigerator and heat pump prototypes built before the year 2010,* International Journal of Refrigeration **33**, 1029 (2010).

[6] K. Gschneidner Jr, V. Pecharsky, and A. Tsokol, *Recent developments in magnetocaloric materials,* Reports on Progress in Physics **68**, 1479 (2005).

[7] E. Brück, *Developments in magnetocaloric refrigeration,* Journal of Physics D: Applied Physics **38**, R381 (2005).

[8] E. Warburg, *Emil 1881 Magnetishe Untersuchungen . Über einige Wirkungen der Coercitivkraft,* Annalen der Physik **249**, 141 (1881).

[9] A. Smith, *Who discovered the magnetocaloric effect?* The European Physical Journal H **38**, 507 (2013).

[10] P. Weiss and A. Picard, *Le phènomène magnètocalorique,* Journal de Physique Théorique et Appliquée **7**, 103 (1917).

[11] O. Gutfleisch, M. A. Willard, E. Brück, C. H. Chen, S. G. Sankar, and J. P. Liu, *Magnetic materials and devices for the 21st century: stronger, lighter, and more energy efficient.* Advanced materials **23**, 821 (2011).

[12] A. Smith, C. R. Bahl, R. Bjørk, K. Engelbrecht, K. K. Nielsen, and N. Pryds, *Materials challenges for high performance magnetocaloric refrigeration devices,* Advanced Energy Materials **2**, 1288 (2012).

[13] V. Srivastava, Y. Song, K. Bhatti, and R. D. James, *The direct conversion of heat to electricity using multiferroic alloys,* Advanced Energy Materials **1**, 97 (2011).

[14] A. Kitanovski, A. and Tušek, J. and Tomc, U. and Plaznik, U. and Ozbolt, M. and Poredoš, *Magnetocaloric energy conversion From theory to applications* (Springer, Berlin, 2015).

[15] W. F. Giauque, *A thermodynamic treatment of certain magnetic effects. A proposed method of producing temperatures considerably below 1° Absolute,* Journal of the American Chemical Society **49**, 1864 (1927).

[16] R. F. Garcia, A. D. M. Catoira, and M. R. Go, *Magnetocaloric effect : A review of the thermodynamic cycles in magnetic refrigeration,* Renewable and Sustainable Energy Reviews **17**, 74 (2013).

[17] H. Yibole, *Nature of the first-order magnetic phase transition in giant-magnetocaloric materials*, Ph.D. thesis, TU Delft (2016).

[18] O. Tegus, *Novel materials for magnetic refrigeration*, Ph.D. thesis, University of Amsterdam (2003).

[19] V. K. Pecharsky and K. A. Gschneidner, *Giant magnetocaloric effect in $Gd_5(Si_2Ge_2)$,* Physical Review Letters **78**, 4494 (1997).

[20] H. Wada and Y. Tanabe, *Giant magnetocaloric effect of $MnAs_{1-x}Sb_x$,* Applied Physics Letters **79**, 3302 (2001).

[21] H. Wada, T. Morikawa, K. Taniguchi, T. Shibata, Y. Yamada, and Y. Akishige, *Giant magnetocaloric effect of $MnAs_{1-x}$ Sb_x in the vicinity of first-order magnetic transition,* Physica B: Condensed Matter **328**, 114 (2003).

[22] S. A. Nikitin, G. Myalikgulyev, A. M. Tishin, M. P. Annaorazov, K. A. Asatryan, and A. L. Tyurin, *The magnetocaloric effect in $Fe_{49}Rh_{51}$ compound,* Physical Letters A **148**, 363 (1990).

[23] M. P. Annaorazov, K. A. Asatryan, G. Myalikgulyev, S. A. Nikitin, A. M. Tishin, and A. L. Tyurin, *Alloys of the Fe-Rh system as a new class of working material for magnetic refrigerators,* Renewable and Sustainable Energy Reviews **32**, 867 (1992).

[24] O. Tegus, E. Brück, K. H. J. Buschow, and F. R. de Boer, *Transition-metal-based magnetic refrigerants for room-temperature applications.* Nature **415**, 150 (2002).

[25] N. T. Trung, Z. Q. Ou, T. J. Gortenmulder, O. Tegus, K. H. J. Buschow, and E. Brück, *Tunable thermal hysteresis in MnFe(P,Ge) compounds,* Applied Physics Letters **94**, 102513 (2009).

[26] D. T. Cam Thanh, E. Brück, N. T. Trung, J. C. P. Klaasse, K. H. J. Buschow, Z. Q. Ou, O. Tegus, and L. Caron, *Structure, magnetism, and magnetocaloric properties of $MnFeP_{1-x}Si_x$ compounds,* Journal of Applied Physics **103**, 07B318 (2008).

[27] F. Guillou, H. Yibole, G. Porcari, L. Zhang, N. H. van Dijk, and E. Brück, *Magnetocaloric effect, cyclability and coefficient of refrigerant performance in the MnFe(P,Si,B) system,* Journal of Applied Physics **116**, 063903 (2014).

[28] F. Hu, B. Shen, J. Sun, Z. Cheng, G. Rao, and X. Zhang, *Influence of negative lattice expansion and metamagnetic transition on magnetic entropy change in the compound $LaFe_{11.4}Si_{1.6}$,* Applied Physics Letters **78**, 3675 (2001).

[29] F. X. Hu, M. Ilyn, A. M. Tishin, J. R. Sun, G. J. Wang, Y. F. Chen, F. Wang, Z. H. Cheng, and B. G. Shen, *Direct measurements of magnetocaloric effect in the first-order system $LaFe_{11.7}Si_{1.3}$,* Journal of Applied Physics **93**, 5503 (2003).

[30] A. Fujita, S. Fujieda, Y. Hasegawa, and K. Fukamichi, *Itinerant-electron metamagnetic transition and large magnetocaloric effects in $La(Fe_xSi_{1-x})_{13}$ compounds and their hydrides,* Physical Review B **67**, 104416 (2003).

[31] A. Barcza, M. Katter, V. Zellmann, S. Russek, S. Jacobs, and C. Zimm, *Stability and magnetocaloric properties of sintered $La(Fe,Mn,Si)_{13}H_z$ alloys,* IEEE Transactions on Magnetics **47**, 3391 (2011).

[32] N. Trung, L. Zhang, L. Caron, K. Buschow, and E. Bruck, *Giant magnetocaloric effects by tailoring the phase transitions,* Applied Physics Letters **96**, 172504 (2010).

[33] D. Zhang, Z. Nie, Z. Wang, L. Huang, Q. Zhang, and Y. D. Wang, *Giant magnetocaloric effect in MnCoGe with minimal Ga substitution,* Journal of Magnetism and Magnetic Materials **387**, 107 (2015).

[34] J. Chen, Z. Wei, E. Liu, X. Qi, W. Wang, and G. Wu, *Structural and magnetic properties of $MnCo_{1-x}Fe_xSi$ alloys,* Journal of Magnetism and Magnetic Materials **387**, 159 (2015).

[35] F. Hu, B. Shen, and J. Sun, *Magnetic entropy change in $Ni_{51.5}Mn_{22.7}Ga_{25.8}$ alloy,* Applied Physics Letters **76**, 3460 (2000).

[36] F. Hu, B. Shen, J. Sun, and G. Wu, *Large magnetic entropy change in a Heusler alloy $Ni_{52.6}Mn_{23.1}Ga_{24.3}$ single crystal,* Physical Review B **64**, 132412 (2001).

[37] T. Krenke, E. Duman, M. Acet, E. F. Wassermann, X. Moya, L. Mañosa, and A. Planes, *Inverse magnetocaloric effect in ferromagnetic Ni-Mn-Sn alloys.* Nature Materials **4**, 450 (2005).

[38] J. Liu, T. Gottschall, K. P. Skokov, J. D. Moore, and O. Gutfleisch, *Giant magnetocaloric effect driven by structural transitions,* Nature Materials , 620 (2012).

[39] N. Dung, *Moment formation and giant magnetocaloric effects in hexagonal Mn-Fe-P-Si compounds,* Ph.D. thesis, TU Delft (2012).

[40] Z. Ou, *Magnetic structure and phase formation of magnetocaloric Mn-Fe-P-X compounds,* Ph.D. thesis, TU Delft (2013).

[41] A. Tishin and Y. Spichkin, *Recent progress in magnetocaloric effect: Mechanisms and potential applications,* International Journal of Refrigeration **37**, 223 (2014).

2

THEORETICAL ASPECTS

This chapter provides the key theoretical aspects of the magnetocaloric effect (MCE). First, a general description of the thermodynamic concepts is given. Then the focus is directed towards the different methods to determine the magnetocaloric quantities $\Delta S_m(T, \Delta B)$ and $\Delta T_{ad}(T, \Delta B)$. These theoretical aspects will be applied in the studied $(Mn,Fe)_2(P,Si)$-based materials. Finally, nano-scale magnetism is discussed.

2.1. THERMODYNAMIC APPROACH TO THE MAGNETOCALORIC EFFECT

2.1.1. THERMODYNAMIC FUNCTIONS AND ORDER OF PHASE TRANSITIONS

In general, the thermodynamic properties of a magnetic system in a magnetic field B at a temperature T and under a pressure p are described by the Gibbs free energy $G(T,p,B)$ [1],[2]:

$$G = U - TS + pV - MB \tag{2.1}$$

where U, S, V and M are the internal energy, entropy, volume and magnetization of the system, respectively. The total differential of the Gibbs free energy can be expressed by:

$$dG = -SdT + Vdp - MdB \tag{2.2}$$

The internal parameter S, V and M (generalized thermodynamic quantities), conjugated to the state variables T, p and B, can be obtained in terms of the partial derivatives of the Gibbs free energy G [2]:

$$S(T,B,p) = -\left(\frac{\partial G}{\partial T}\right)_{B,p} \tag{2.3}$$

$$V(T,B,p) = \left(\frac{\partial G}{\partial p}\right)_{T,B} \tag{2.4}$$

$$M(T,B,p) = -\left(\frac{\partial G}{\partial B}\right)_{T,p} \tag{2.5}$$

From a thermodynamic point of view, the order of a phase transition depends on the behavior of the derivatives of the Gibbs free energy. The order of the phase transition is labeled by the lowest derivative of the Gibbs free energy that is discontinuous at the phase transition [3]. First-order phase transitions exhibit a discontinuity in the first derivatives of the Gibbs free energy as a function of the state variables, while second-order phase transitions are continuous in the first derivatives and discontinuous in the second derivatives of the Gibbs free energy. Hence, the entropy, volume and magnetization of the magnetic material are discontinuous at a first-order phase transition, and continuous for a second-order transition.

2.1.2. TOTAL ENTROPY, ISOTHERMAL MAGNETIC ENTROPY CHANGE AND ADIABATIC TEMPERATURE CHANGE

In general, the total entropy change of a magnetic material can be described as the sum of magnetic, lattice and electronic contributions:

$$S(T,B,p) = S_{mag}(T,B,p) + S_{lat}(T,B,p) + S_{el}(T,B,p) \tag{2.6}$$

where S_{mag} presents the magnetic entropy, S_{lat} the entropy of the lattice and S_{el} the entropy of the conduction electrons. These three contributions generally depend on both temperature and magnetic field, and are difficult to separate experimentally.

Since the entropy S is a state function, the full differential of the total entropy in a closed system can be written as:

$$dS = \left(\frac{\partial S}{\partial T}\right)_{B,p} dT + \left(\frac{\partial S}{\partial B}\right)_{T,p} dB + \left(\frac{\partial S}{\partial p}\right)_{T,B} dp \tag{2.7}$$

From above-mentioned three contributions to the total entropy, the magnetic entropy is strongly field dependent, while the lattice and electronic entropy show a much weaker field dependence. For the sake of simplicity, one supposes that S_{lat} and S_{el} only depend on temperature. Hence, the total entropy change induced by the magnetic field variation is attributed to the change in the magnetic entropy.

Under an isobaric-isothermal process ($dp = 0$, $dT = 0$), Eq. (2.7) becomes:

$$dS = \left(\frac{\partial S}{\partial B}\right)_{T,p} dB \tag{2.8}$$

The change in entropy from an initial magnetic field B_i to a final magnetic field $B_f = B_i + \Delta B$ can be obtained by numerical integration of Eq. (2.8):

$$\Delta S_m(T,\Delta B) = \int_{B_i}^{B_f} \left(\frac{\partial S}{\partial B}\right)_{T,p} dB \tag{2.9}$$

Moreover, from

$$\frac{\partial^2 G}{\partial T \partial B} = \frac{\partial^2 G}{\partial B \partial T} \tag{2.10}$$

and Eq. (2.3) and (2.5), one can obtain the following Maxwell relation:

$$\left(\frac{\partial S}{\partial B}\right)_{T,p} = \left(\frac{\partial M}{\partial T}\right)_{B,p} \tag{2.11}$$

Eq. (2.9) can be rewritten as:

$$\Delta S_m(T,\Delta B) = \int_{B_i}^{B_f} \left(\frac{\partial M}{\partial T}\right)_{B,p} dB \tag{2.12}$$

The heat capacity at constant magnetic field and pressure $C_p(T,B)$ is defined as:

$$C_p(T,B) = \left(\frac{\delta Q}{dT}\right)_{B,p} \tag{2.13}$$

where δQ is the heat required to change the system temperature by dT. The second law of thermodynamics indicates that for internally reversible processes one finds:

$$dS = \frac{\delta Q}{T} \tag{2.14}$$

The heat capacity can then be represented as:

$$C_p(T,B) = T\left(\frac{\partial S}{\partial T}\right)_{B,p} \tag{2.15}$$

Combining Eq. (2.7) and (2.15), the entropy in a magnetic field B under isobaric conditions ($dp = 0$) can be expressed by:

$$S(T,B) = \int_0^T \frac{C_p(T^{'},B)}{T^{'}} dT^{'} + S_0 \tag{2.16}$$

Thus, we obtain:

$$\Delta S_m(T,\Delta B) = \int_0^T \frac{C_p(T^{'},B_f) - C_p(T^{'},B_i)}{T^{'}} dT^{'} \tag{2.17}$$

where $C_p(T^{'},B_f)$ and $C_p(T^{'},B_i)$ represent the specific heat at constant pressure p at magnetic field B_f and B_i, respectively. Under an adiabatic–isobaric process ($dp = 0$, $dS = 0$), which is usually realized in magnetocaloric experiments, the infinitesimal adiabatic temperature change due to the magnetic field change can be obtained by combining Eq. (2.7), (2.11) and (2.15) as:

$$dT = -\frac{T}{C_p(T,B)}\left(\frac{\partial M}{\partial T}\right)_{B,p} dB \tag{2.18}$$

The adiabatic temperature change for a magnetic field change from B_i to B_f can be obtained by numerical integration of Eq. (2.18):

$$\Delta T_{ad}(T,\Delta B) = -\int_{B_i}^{B_f} \frac{T}{C_p(T,B)}\left(\frac{\partial M}{\partial T}\right)_{B,p} dB \tag{2.19}$$

2.2. CLASSIFICATION OF THE MAGNITUDE OF THE MCE OF A MAGNETIC MATERIAL

There are various ways to classify magnetocaloric materials. From a thermodynamic point of view, the isothermal magnetic entropy change $\Delta S_m(T,\Delta B)$ and the adiabatic temperature change $\Delta T_{ad}(T,\Delta B)$ are two quantitative parameters to evaluate the magnetocaloric effect of a magnetic material. $\Delta S_m(T,\Delta B)$ determines the cooling capacity, while, $\Delta T_{ad}(T,\Delta B)$ determines the temperature span that can be achieved by the change in magnetic field . Hence, it is essential that both magnetocaloric parameters $\Delta S_m(T,\Delta B)$ and $\Delta T_{ad}(T,\Delta B)$ have large values in order to apply a magnetocaloric material for magnetic refrigeration.

According to equation (2.12) and (2.19), it can be seen that, the MCE will be large if $\left({}^{\partial M}/_{\partial T}\right)_{B,p}$ is large and $C_p(T,B)$ is small [4]. Both $\Delta S_m(T,\Delta B)$ and $\Delta T_{ad}(T,\Delta B)$ reach a maximum value around a phase transition because $\left({}^{\partial M}/_{\partial T}\right)_{B,p}$ peaks around the magnetic ordering temperature. A large MCE is expected for systems with a first-order magnetic phase transition (FOMT), as a consequence of the large discontinuous change in magnetization, which is observed within a narrow temperature and field interval [5].

2.3. DETERMINATION OF THE MAGNETOCALORIC EFFECT

To determine the magnetocaloric effect, different experimental methods have been suggested in literature [6],[7],[8],[9],[10]. The methods to determine the MCE can be divided into direct and indirect measurements. Compared to direct measurements, indirect measurements are much simpler to perform due to the availability of commercial experimental devices, such as magnetometers and calorimeters. Direct measurements, however, have been extensively utilized more recently with the help of home-built experimental setups.

2.3.1. DETERMINATION OF THE ISOTHERMAL MAGNETIC ENTROPY CHANGE

According to Eq. (2.12) and (2.17), the isothermal magnetic entropy change $\Delta S_m(T,\Delta B)$ can be determined by either magnetization or calorimetric measurements. In case of the magnetization method, by measuring the magnetization at various temperatures and fields, the isothermal magnetic entropy change

can be extracted with Eq. (2.12). Considering controversies in the literature about the applicability of the Maxwell relation (Eq. (2.11)) for the calculation of the magnetic entropy change in first-order magnetocaloric materials, it is worth summarizing briefly the requirements for the validity of this Maxwell relation [11],[12],[13],[14],[15],[16],[17]. First of all, the system should be in thermodynamic equilibrium. This can be problematic in the case of a first-order phase transition due to the presence of significant thermal or magnetic hysteresis. Moreover, the system should be homogeneous, since it can be problematic in case of a phase coexistence at the phase transition. In addition, the first derivative of the magnetization with respect to temperature $\left(\partial M/\partial T\right)_{B,p}$ should be continuous. In other words, Eq. (2.12) can be only used for second-order phase transitions because the $\left(\partial M/\partial T\right)_{B,p}$ becomes infinite at a first-order phase transition. In the case of first-order phase transitions, the Clausius-Clapeyron equation was proposed to calculate the magnetic entropy change [1],[18]. The Clausius-Clapeyron equation is a way of describing a discontinuous transformation (phase 1 to phase 2). In a temperature - field diagram, the transition line separating the two phases is known as the co-existence curve.

Under an isobaric transformation ($dp = 0$), Eq. (2.2) can be rewritten as:

$$dG = -SdT - MdB \tag{2.20}$$

Hence, the derivative of the Gibbs free energy of phase 1 and phase 2 can be expressed by:

$$dG_1 = -S_1 dT - M_1 dB \tag{2.21}$$

$$dG_2 = -S_2 dT - M_2 dB \tag{2.22}$$

Under equilibrium conditions, the derivative of the Gibbs free energy of phase 1 and phase 2 along their coexistence curve is identical to one another : ($dG_1 = dG_2$)

$$-S_1 dT - M_1 dB = -S_2 dT - M_2 dB \tag{2.23}$$

The slope of the coexistence line is given by:

$$\left(\frac{dT_C}{dB}\right)_p = -\frac{(M_2 - M_1)}{(S_2 - S_1)} = -\frac{\Delta M}{\Delta S} \tag{2.24}$$

Thus,

$$\Delta S_m = -\frac{\Delta M}{\left(dT_C/dB\right)_p} \tag{2.25}$$

where ΔM is the difference in magnetization between the low-and high-field phases and $\left(dT_C/dB\right)_p$ re-presents the change in the Curie temperature as a function of the change in magnetic field.

The application of the Maxwell relation for the determination of the magnetic entropy change remains the most commonly used method for first-order magnetocaloric materials because an infinite $\left(\partial M/\partial T\right)_{B,p}$ can only arise in an ideal first-order phase transition. In reality, the first-order magnetocaloric materials always have a finite transition width rather than a discontinuous change in magnetization [19]. It is worth mentioning that the Clausius-Clapeyron equation is used to quantify the difference in total entropy between the low-and high-field phases at transition point. Hence, the value of the magnetic entropy change obtained from the application of the Maxwell relation and the Clausius-Clapeyron equation are not directly comparable.

For the calorimetric method, the values of $\Delta S_m(T,\Delta B)$ can be determined indirectly or directly from isofield in-field DSC or isothermal DSC measurements, respectively. By measuring the specific heat as a function of temperature at different applied magnetic fields, one can obtain the isothermal magnetic entropy change using Eq. (2.17). On the other hand, the isothermal magnetic entropy change can be determined directly by measuring the heat released (or absorbed) by the sample when the magnetic field changes under isothermal conditions using Eq. (2.14).

It has been confirmed that there is a good agreement in the values of $\Delta S_m(T,\Delta B)$ derived from both magnetization and calorimetric measurements [20],[21]. Experimentally, the magnetic entropy change of a given magnetic system is often calculated through the measurement of the magnetization as a function of temperature and magnetic field because calorimetric measurements require specialized equipment.

2.3.2. DETERMINATION OF THE ADIABATIC TEMPERATURE CHANGE

The adiabatic temperature change of an MCE material can be measured either directly by means of a thermocouple in contact with the sample, or indirectly by means of in-field DSC. According to Eq. (2.19), the determination of $\Delta T_{ad}(T,\Delta B)$ is very difficult because both the specific heat and magnetization are unknown functions of magnetic field and temperature in the vicinity of the magnetic phase transition. If C_p is weakly temperature dependent, the change in $\frac{T}{C_p(T,B)}$ is small compared to the change in the magnetization as a function of temperature. Then, Eq. (2.19) can be simplified:

$$\Delta T_{ad}(T,\Delta B) = -\frac{T}{C_p(T,B)}\Delta S_m(T,\Delta B) \tag{2.26}$$

Hence, $\Delta T_{ad}(T,\Delta B)$ can be obtained from the specific heat, or from the combination of the specific heat and magnetization data.

For measurements of the direct adiabatic temperature change, the temperature of the MCE material is recorded during continuous oscillation of the external field while slowly scanning the surrounding temperature (at a rate of 0.5–1.5 K/min) over the temperature range of interest. For measurements of the direct temperature change, a rapid change of the magnetic field is required, while the sample is kept quasi-adiabatic. The measurements can be carried out either by keeping the sample stationary and changing the applied magnetic field [22], or by moving the sample relative to a constant magnetic field [23]. In the context of this thesis, a custom-built setup with the latter approach was used to measure the temperature change. Experimentally, apart from the direct adiabatic temperature change measurements, $\Delta T_{ad}(T,\Delta B)$ is often determined from the entropy curves (isofield in-field DSC measurements).

2.4. NANO-SCALE MAGNETISM

Based on the response of a material to an applied magnetic field, materials can be classified into five major groups: (i) diamagnetic, (ii) paramagnetic, (iii) ferromagnetic, (iv) antiferromagnetic and (v) ferrimagnetic. The first two groups, which exhibit no collective interaction of atomic magnetic moments and are not magnetically ordered, are the two most common types of magnetism. In contrast, materials in the last three groups exhibit very strong interaction between the atomic moments. These materials exhibit long-range magnetic order below a certain critical temperature.

In the case of ferromagnetic and ferrimagnetic materials, domain formation is a way to minimize the magnetostatic energy in the total volume. Within each domain, the spins align parallel, but different domains have different spin orientations. These domains are separated by the domain walls. When the particle size decreases, a critical size, at which the energy cost of domain wall formation exceeds the advantages of decreasing the magnetostatic energy, will be reached. Hence, below this critical size, the grain contains a single domain (SD) rather than multi domains (MD).

For MD grains the reversal of direction of magnetization can occur via domain wall movement or coherent spin rotation that requires nucleation. When domain wall movement is an energetically easy process, the ferromagnetic material can be easily magnetized in relatively low fields. This kind of ferromagnetic material is categorized as soft magnetic materials. When domain wall movement

is difficult, the reversal of direction of magnetization only occurs as a high magnetic field is applied. This type of ferromagnetic material is called hard magnetic and is used in motors, loudspeakers, meters, and holding devices. In contrast, a reversal of magnetization in SD grains must occur via coherent spin rotation due to the absence of domain walls. Spin rotation is an energetically more difficult process due to the energy barrier arising from magnetocrystalline anisotropy. Hence, SD grains have a larger coercivity and remanence compared to MD grains.

The magnetic anisotropy K is the dependence of magnetic energy on the spin orientation and provides a preferred spin orientation. Magnetocrystalline anisotropy and shape anisotropy are two important and common types of magnetic anisotropy. Magnetocrystalline anisotropy is an intrinsic property while shape anisotropy is an extrinsic property that depends on the particle shape. The ease of reaching saturation magnetization of ferromagnetic materials is different for different crystallographic directions due to the magnetocrystalline anisotropy. The direction in which the saturation magnetization is most easily obtained is called the easy direction. In contrast, in the hard directions, it is more difficult to magnetize the materials compared to the easy direction.

The magnetocrystalline anisotropy is the energy required to switch the magnetic moment from the easy to hard directions. In the case of a hexagonal crystal symmetry of Fe_2P type the anisotropy energy density can expressed by:

$$K_a = K_0 + K_1 \sin^2\theta + K_2 \sin^4\theta + (K_3 + K_3^{'} \cos 6\phi)\sin^6\theta \tag{2.27}$$

where K_0, K_1, K_2, K_3 and $K_3^{'}$ are anisotropy constants, θ is the angle between the magnetization vector and the c-axis, and ϕ is the angle between the magnetization component in the basal plane and the a-axis (Fig. 2.1). K_0 does not depend on either θ or ϕ, while K_3 and $K_3^{'}$ are relatively small compared to K_1 and K_2 and are often neglected. In most cases, considering the magnitude and sign of K_1 and K_2, it is sufficient to determine the preferred direction of the magnetization vector, which has a minimum anisotropy energy. Different categories are shown in Table 2.1 [24].

Table 2.1: Various categories for the easy magnetization direction.

If	$K_{a(min)}$ for	the directions of easy magnetization	category
$K_1 > 0$, $K_1 + K_2 > 0$	$\theta = 0°$ and $180°$	the c-axis	easy axis
$K_1 < 0$, $K_1 + K_2 < 0$	$\theta = 90°$	the basal plane	easy plane
$K_1 < 0$, $2K_2 > -K_1$	$\theta = \sin^{-1}\sqrt{\frac{-K_1}{2K_2}}$	a cone with angle θ ($0° < \theta < 90°$)	easy cone

In the case of SD grains with an easy axis configuration without external magnetic field there are two equal minima along the easy axis. However, un-

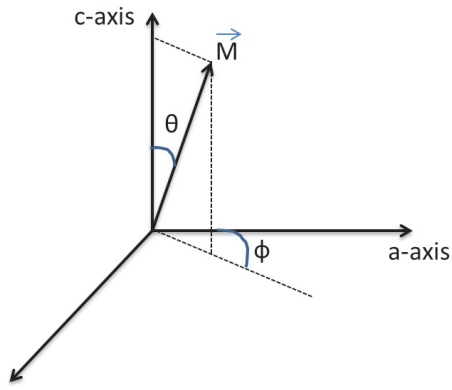

Figure 2.1: Direction of the magnetic moment vector with respect to the c-axis and a-axis

der the application of an external field, one of the minima obtains a lower energy, shown in Fig. 2.2. To switch the magnetic moment direction from 0 to 180° and vise versa, an anisotropy energy $K_a V$ (K_a: anisotropy energy per volume or anisotropy energy density, V: the particle volume) has to be overcome, which often requires a strong external magnetic field.

As the grain size continues to go down within the SD range, the anisotropy energy $K_a V$, which is proportional to the particle size, decreases. When the energy barrier becomes smaller than the prevailing thermal energy $k_B T$ (k_B: Boltzmann's constant; T: absolute temperature), a reversal of the magnetization over very short time scales occurs. This is called super-paramagnetism. In other words, super-paramagnetism occurs when the collective magnetic moments flip their direction over a very short time scales because the anisotropy energy is overcome by the thermal energy. When this happens, the particle is in a super-paramagnetic state. The average time for moment reversal to occur is presented by the relaxation time:

$$\tau = \tau_0 e^{\frac{-K_a V}{k_B T}} \tag{2.28}$$

where τ_0 is a time constant characteristic for the probed substance, which is of the order of 10^{-9} - 10^{-12} s and depends only weakly on temperature [26].

It is worth mentioning that whether the super-paramagnetic state is observed depends not only on the temperature, but also on the time window of the experimental measurement τ_m. If $\tau_m >> \tau$, the reversal of the direction of magnetization is relatively fast with respect to the experimental time window, the particles are expected to behave super-paramagnetic. In contrast, if $\tau_m << \tau$, reorienting

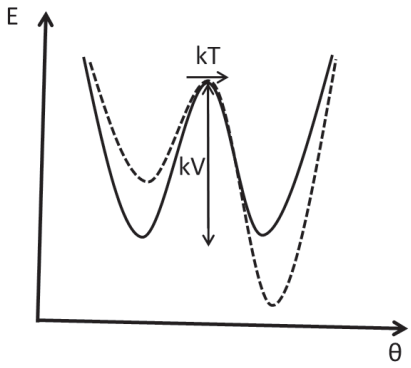

Figure 2.2: Orientation dependence of the magnetic energy as a function of θ without (solid line) and with (dashed line) the presence of an applied field along the anisotropy axis (adapted from [25]).

the direction of the collective magnetic moment is relatively slow and thus the so-called 'blocked' state of the system is observed. The blocking temperature T_B is defined as the temperature between the blocked and the super-paramagnetic state, where $\tau \sim \tau_m$. Depending on the experimental techniques used, τ_m can be 10^2 s for DC magnetization, 10^{-1} to 10^{-5} s for AC susceptibility, and 10^{-7} to 10^{-9} s for ^{57}Fe Mössbauer spectroscopy [27].

For measurements of the blocking temperature T_B, zero-field-cooled (ZFC) and field-cooled (FC) magnetization curves are recorded. At first, the sample is cooled down to a temperature well below the expected T_B in zero applied field: so-called zero-field cooling (ZFC). Then, a small applied field of 0.01 T, which is generally insufficient to induce spin reorientation away from the anisotropy axis at low temperature, is applied before starting measuring the magnetization as a function of temperature upon heating. When the temperature is below T_B, the individual particle's moments randomize in different directions, so the induced magnetization is small. As the temperature approaches T_B, the thermal energy $k_B T$ assists in reorienting the moment in the direction of the applied magnetic field, resulting in an increase in the induced magnetization. At T_B, the collective magnetic moments are coupled and free to align with the applied field to yield a large total magnetization. With further increasing temperature, the induced magnetization decreases due to fluctuation of collective magnetic moments.

Nano-scale magnetic materials may show a variety of unusual behavior compared to the bulk due to surface/interface effects. Since the coordination number of atoms on the surface of nanoparticles is smaller than that of the bulk, their d-band of transition-metal atoms is narrower. This may lead to a higher density of

states and enhanced surface magnetic moments [28], [29].

REFERENCES

[1] A. M. Tishin and Y. I. Spichkin, *The magnetocaloric effect and its applications* (Institue of Physics Publishing, Bristol, 2003).

[2] T. Gibbs, *Magnetocaloric effect. Part 1: An introduction to various aspects of theory and practice,* Cryogenics **32**, 545 (1992).

[3] E. Sci, *The Ehrenfest Classification of Phase Transitions : Introduction and Evolution,* Archive for History of Exact Sciences **53**, 51 (1998).

[4] K. A. Gschneidner Jr, V. K. Pecharsky, and A. O. Tsokol, *Recent developments in magnetocaloric materials,* Reports on Progress in Physics **68**, 1479 (2005).

[5] E. Brück, *Developments in magnetocaloric refrigeration,* Journal of Physics D: Applied Physics **38**, R381 (2005).

[6] V. K. Pecharsky and K. A. Gschneidner, *Magnetocaloric effect from indirect measurements: Magnetization and heat capacity,* Journal of Applied Physics **86**, 565 (1999).

[7] T. Plackowski, Y. Wang, and A. Junod, *Specific heat and magnetocaloric effect measurements using commercial heat-flow sensors,* Review of Scientific Instruments **73**, 2755 (2002).

[8] S. Jeppesen, S. Linderoth, N. Pryds, L. T. Kuhn, and J. B. Jensen, *Indirect measurement of the magnetocaloric effect using a novel differential scanning calorimeter with magnetic field.* Review of Scientific Instruments **79**, 083901 (2008).

[9] H. Yibole, F. Guillou, L. Zhang, N. H. van Dijk, and E. Brück, *Direct measurement of the magnetocaloric effect in MnFe(P, X) (X = As, Ge, Si) materials,* Journal of Physics D: Applied Physics **47**, 075002 (2014).

[10] F. X. Hu, M. Ilyn, A. M. Tishin, J. R. Sun, G. J. Wang, Y. F. Chen, F. Wang, Z. H. Cheng, and B. G. Shen, *Direct measurements of magnetocaloric effect in the first-order system $LaFe_{11.7}Si_{1.3}$,* Journal of Applied Physics **93**, 5503 (2003).

[11] A. Giguere, M. Foldeaki, B. R. Gopal, R. Chahine, T. K. Bose, A. Frydman, and J. A. Barclay, *Direct measurement of the "giant" adiabatic temperature change in $Gd_5Si_2Ge_2$,* Physical Review Letters **83**, 2262 (1999).

[12] S. Gama, A. A. Coelho, A. de Campos, A. M. G. Carvalho, F. C. G. Gandra, P. J. von Ranke, and N. A. de Oliveira, *Pressure-induced colossal magnetocaloric effect in MnAs.* Physical Review Letters **93**, 237202 (2004).

[13] P. J. von Ranke, S. Gama, A. A. Coelho, A. de Campos, A. M. G. Carvalho, F. C. G. Gandra, and N. A. de Oliveira, *Theoretical description of the colossal entropic magnetocaloric effect: Application to MnAs,* Physical Review B **73**, 014415 (2006).

[14] N. A. de Oliveira and P. J. von Ranke, *Magnetocaloric effect around a magnetic phase transition,* Physical Review B **77**, 214439 (2008).

[15] L. Tocado, E. Palacios, and R. Burriel, *Entropy determinations and magnetocaloric parameters in systems with first-order transitions: Study of MnAs,* Journal of Applied Physics **105**, 093918 (2009).

[16] L. Caron, Z. Q. Ou, T. T. Nguyen, D. T. Cam Thanh, O. Tegus, and E. Brück, *On the determination of the magnetic entropy change in materials with first-order transitions,* Journal of Magnetism and Magnetic Materials **321**, 3559 (2009).

[17] M. Balli, D. Fruchart, D. Gignoux, and R. Zach, *The "colossal" magnetocaloric effect in $Mn_{1x}Fe_xAs$: What are we really measuring?* Applied Physics Letters **95**, 072509 (2009).

[18] K. A. Gschneider Jr., V. K. Pecharsky, and A. O. Tsokol, *Recent developments in magnetocaloric materials,* Reports on Progress in Physics **68**, 1479 (2005).

[19] Y. Spichkin and R. Gimaev, *Experimental methods of the magnetocaloric effect studies,* International Journal of Refrigeration **37**, 230 (2014).

[20] O. Tegus, N. P. Duong, W. Dagula, L. Zhang, E. Bruck, K. H. J. Buschow, and F. R. de Boer, *Magnetocaloric effect in $GdRu_2Ge_2$,* Journal of Applied Physics **91**, 8528 (2002).

[21] K. A. Gschneidner Jr., V. K. Pecharsky, A. O. Pecharsky, and C. B. Zimm, *Recent Developments in Magnetic Refrigeration,* Materials Science Forum **315-317**, 69 (1999).

[22] S. Y. Dan'kov, A. M. Tishin, V. K. Pecharsky, and K. A. Gschneidner, *Experimental device for studying the magnetocaloric effect in pulse magnetic fields,* Review of Scientific Instruments **68**, 2432 (1997).

[23] B. R. Gopal, R. Chahine, and T. K. Bose, *A sample translatory type insert for automated magnetocaloric effect measurements,* Review of Scientific Instruments **68**, 1818 (1997).

[24] A. K. Patra, *Crystal structure, anisotropy and spin reorientation transition of highly coercive, epitaxial Pr-Co films*, Ph.D. thesis, TU Dresden (2008).

[25] G. C. Papaefthymiou, *Nanoparticle magnetism,* Nano Today **4**, 438 (2009).

[26] W. F. Brown Jr., *Thermal Fluctuations of a Single-Domain Particle,* Physical Review **130**, 1677 (1963).

[27] Q. A. Pankhurst, J. Connolly, S. K. Jones, and J. Dobson, *Applications of magnetic nanoparticles in biomedicine,* Journal of Physics D: Applied Physics **36** (2003).

[28] S. Blügel, *Two-dimensional ferromagnetism of 3d, 4d, and 5d transition metal monolayers on noble metal (001) substrates,* Physical Review Letters **68**, 851 (1992).

[29] R. H. Victora and L. M. Falicov, *Calculated electronic structure of chromium surfaces and chromium monolayers on iron,* Physical Review B **31**, 7335 (1985).

3

EXPERIMENTAL TECHNIQUES

This chapter provides a concise description of the experimental techniques that were used throughout this thesis to prepare and characterize the magnetocaloric materials obtained. In the first part the procedures of sample preparation are described. In the second part a brief description of the characterization techniques such as X-Ray Diffraction (XRD), Neutron Diffraction (ND), magnetic measurements using Superconducting Quantum Interference Device (SQUID) magnetometer, Differential Scanning Calorimetry (DSC) measurements, Scanning Electron Microscopy (SEM), Transmission Electron Microscopy (TEM) and direct temperature change measurements is given.

3.1. SAMPLE PREPARATION

A ball mill, a type of grinder, is used to grind materials into extremely fine powder. There are several types of ball mills: drum ball mills, jet-mills, beat-mills, horizontal rotary ball mills, vibration ball mills and planetary ball mills. Among these types, planetary ball mills are the most commonly used at the laboratory scale for fabricating samples ranging from micro to nano-scale materials. Planetary ball mills exploit the principle of the centrifugal acceleration rather than the gravitational acceleration. In this thesis, the Fritsch Pulverisette planetary ball mill was used to prepare all samples.

3.1.1. HIGH ENERGY BALL MILLING

The materials presented in **Chapter 5, 6, 7 and 8** were prepared by means of high-energy ball milling. Typically, an amount of 15 g of starting materials was put into a tungsten-carbide jar (with a volume of 50 ml) containing 7 tungsten-carbide balls (with a diameter of 10 mm) in an argon (Ar) atmosphere and was ball milled for 10 h with a constant rotation speed of 380 rpm. After that, the fine powders obtained were compacted into small tablets in a hydraulic press with a pressure of 150 $kgfcm^{-2}$. After pressing, the tablets were sealed inside quartz ampoules in an Ar atmosphere of 200 mbar. Except for the materials presented in **Chapter 5**, the commonly used double-step sintering process [1] was applied to sinter all the materials obtained. The samples were sintered at 1373 K for 2 h, annealed at 1123 K for 20 h and then cooled down slowly to room temperature by oven cooling before they were re-sintered at 1373 K for 20 h to enhance their homogeneity. The thermal treatment was completed by direct water quenching of the ampoules from the furnace. The samples were precooled in liquid nitrogen to remove the virgin effect [2], and then crushed by means of a mortar.

3.1.2. SURFACTANT-ASSISTED HIGH-ENERGY BALL MILLING

The materials presented in **Chapter 4** have been produced by a two-stage high-energy ball milling (HEBM) with grinding jars and balls made of tungsten carbide. In the first stage, samples were prepared by the same protocol as described in the section above: first high-energy ball milling followed by a solid-state reaction. The difference is that an amount of 50 g instead of 15 g was placed into a bigger tungsten-carbide jar (with a volume of 250 ml) containing 4 tungsten-carbide balls (with a diameter of 40 mm). Heptane (C_7H_{16}) (99.8 % purity) as the solvent and oleic acid ($C_{18}H_{34}O_2$) (90 %) as surfactant was used for the second stage of the milling process. In the second stage, the powder obtained in the first step was ball-milled again in a protective argon gas atmosphere with the presence of organic solvent heptane and surfactant oleic acid for various milling times. The amount of solvent employed was kept constant at 60 % of the powder

weight, while varying the amount of surfactant between 0 to 30 % of the powder weight. A constant ball-to-powder weight ratio of 10 : 1 and a constant rotation speed of 380 rpm was applied to all samples. The slurry mixture obtained after milling was then dispersed into heptane solvent by ultrasonic vibration and transferred to centrifugal tubes for removing the excess surfactant. This process was repeated at least 3 times before the fine powders obtained were dried in vacuum overnight.

3.2. SAMPLE CHARACTERIZATION

3.2.1. X-RAY POWDER DIFFRACTION

X-ray diffraction (XRD) is a widely used and powerful experimental technique for the characterization of the crystal structure of materials. In this thesis, XRD patterns of the studied polycrystalline samples were collected by means of a PANalytical X-pert Pro diffractometer with Cu-K_α radiation, a secondary-beam flat-crystal monochromator and a multichannel X'celerator detector. An Anton Paar TTK450 Low-Temperature Chamber with a sample holder containing a Pt 100 temperature sensor was employed to perform the temperature-dependent XRD measurements. The short cooling and heating times (80 to 723 K) are guaranteed by the combination of a LNC Liquid Nitrogen Control Unit and a TCU 100 temperature control unit. Measurements may be carried out either under vacuum, air or inert gas. The XRD patterns were recorded in a 2θ range between 20° and 90° at a step of 0.08°. In order to determine the crystal structure, all XRD data were analyzed by the Rietveld refinement method using the Fullprof program [3].

3.2.2. NEUTRON POWDER DIFFRACTION

Due to the limitation of X-ray diffraction with respect to the detection of light elements (e.g., B, C and N), neutron diffraction was employed. Since neutron diffraction is based on the scattering by the nucleus of an atom rather than by the electrons, it is able to detect light elements with a small amount of electrons. Moreover, the ability to distinguish Mn from Fe and P from Si allows for the accurate determination of the crystal structures for the $(Mn,Fe)_2(P,Si)$-based compounds. In addition, due to the spin of neutron the scattering is sensitive to the magnetic moments of Fe and Mn. The neutron diffraction patterns presented in **Chapter 8** were collected on the neutron powder diffraction instrument PEARL at the research reactor of Delft University of Technology. The powder samples of about 8-10 g were put into a thin vanadium can with a diameter of 6 mm and a height of 50 mm [4].

3.2.3. MAGNETIZATION MEASUREMENTS

The magnetization as a function of temperature and applied magnetic field was studied using a superconducting quantum interference device (SQUID) MPMS-XL and MPMS-5S magnetometer, which produces a maximum applied magnetic field of 5 T by a superconducting magnet. The temperature range is between 1.7 and 400 K. The lowest temperature of 1.7 K, which is below the boiling point of liquid helium (4.2 K), can be reached by means of pumping techniques.

For magnetic measurements, 2-3 mg powder samples were inserted in a gelatin capsule and mounted in a plastic straw with diamagnetic contribution of the order of 10^{-8} Am^2 in an external magnetic field of 1 T. The SQUID utilizes an extremely sensitive detection system, which can detect the smallest and largest moments of 10^{-11} Am^2 and 10^{3} Am^2 (with an accuracy of 0.1 %), respectively. Thus, for magnetic materials with a strong magnetic signal, such as ferromagnetic materials, the contribution of the empty sample holder to the total magnetization can be neglectable; for magnetic materials with weak magnetic signal, such as diamagnetic materials, the sample holder is measured separately and its contribution is subtracted from the total magnetization.

To prevent issues related to the so-called "spike" in case of a first-order phase transition [5],[6],[7],[8],[9],[10],[11], in this thesis the isofield $M_B(T)$ curves were used to calculate the isothermal magnetic entropy change (ΔS_m) rather than the isothermal magnetization $M_T(B)$ curves. This approach is expected to avoid the spike because a full transformation from ferromagnetic to paramagnetic phase is recorded for the $M_B(T)$ data. The isofield $M_B(T)$ curves are first measured in field upon cooling and then upon heating with a rate of 2 Kmin^{-1} in the targeted measurement field (Between 2.0 and 0.2 T in 0.2 T increments, and then at a field of 0.05 T).

3.2.4. DIFFERENTIAL SCANNING CALORIMETRY

Differential scanning calorimetry (DSC) is a thermo-analytical technique to measure the differences in Heat Flow Rate between a sample and inert reference as a function of temperature and time. In this thesis, DSC measurements were conducted using a TA-Q2000 DSC instrument equipped with a liquid nitrogen cooling system. Employing the so-called Tzero™ DSC technology, this equipment allows one to measure the heat capacity and latent heat directly with a high precision in a large temperature range from 90 up to 820 K with variable temperature sweep rates. All the measurements in this thesis were carried out with a sweep rate of 10 K/min.

3.2.5. ELECTRON MICROSCOPY

Electron microscopy has been a versatile characterization tool in all the fields of science since Max Knoll and Ernst Ruska built the first electron microscope at Berlin Technische Hoshschule in 1931. The use of a beam of electrons rather than light to form an image in electron microscopes leads to a greater resolution and therefore has a higher magnification (up to 2 million times). The particle size and morphology of the $(Mn,Fe)_2(P,Si)$ nanoparticles obtained in **Chapter 4** were investigated using both JSM-610 LA scanning electron microscope (SEM) and a JEOL JEM1400 transmission electron microscope (TEM). Both SEM and TEM images were taken at several locations for each sample.

3.2.6. DIRECT ADIABATIC TEMPERATURE CHANGE

A home-built experimental setup was used to directly measure the adiabatic temperature change (ΔT_{ad}) by tracking the temperature of the MCE materials during the magnetization/demagnetization processes, while the ambient temperature is slowly scanned between 250 and 325 K and regulated by a climate chamber. For the direct ΔT_{ad} measurements, a small pylon-shaped plastic cup was used as a sample holder. At first, a thermocouple was placed in the center of the sample holder before filling the sample holder with the sample, which is in the form of powder. To enhance the contact of the sample with the thermocouple, the powder was compressed by putting kapok on the top of the sample and then covered with a plastic cap. During the measurement, the sample holder moves in and out a constant magnetic field of 1.1 T generated by two permanent magnets at a frequency of 0.1 Hz, while the surrounding temperature is slowly scanned with a sweep rate of 0.5-1.5 K/min. This setup operates under quasi-adiabatic conditions because of the relatively low temperature-sweeping rate with respect to the dT/dt related to the response time of the thermocouple (about 150 K/min) [12].

REFERENCES

[1] N. H. Dung, L. Zhang, Z. Q. Ou, L. Zhao, L. van Eijck, A. M. Mulders, M. Avdeev, E. Suard, N. H. van Dijk, and E. Brück, *High/low-moment phase transition in hexagonal Mn-Fe-P-Si compounds,* Physical Review B **86**, 045134 (2012).

[2] X. F. Miao, L. Caron, Z. Gercsi, a. Daoud-Aladine, N. H. van Dijk, and E. Brück, *Thermal-history dependent magnetoelastic transition in $(Mn,Fe)_2(P,Si)$,* Applied Physics Letters **107**, 042403 (2015).

[3] J. Rodríguez-Carvajal, *Recent advances in magnetic structure determination by neutron powder diffraction,* Physica B **192**, 55 (1993).

[4] L. van Eijck, L. D. Cussen, G. J. Sykora, E. M. Schooneveld, N. J. Rhodes, A. van Well, and C. Pappas, *Design and performance of a novel neutron powder diffractometer : PEARL at TU Delft,* Journal of Applied Crystallography **49**, 1 (2016).

[5] A. Giguere, M. Foldeaki, B. R. Gopal, R. Chahine, T. K. Bose, A. Frydman, and J. A. Barclay, *Direct measurement of the "giant" adiabatic temperature change in $Gd_5Si_2Ge_2$,* Physical Review Letters **83**, 2262 (1999).

[6] S. Gama, A. A. Coelho, A. De Campos, A. Magnus, G. Carvalho, F. C. G. Gandra, P. J. Von Ranke, and N. A. De Oliveira, *Pressure-induced colossal magnetocaloric effect in MnAs,* Physical Review Letters **93**, 3 (2004).

[7] P. J. Von Ranke, S. Gama, A. A. Coelho, A. De Campos, A. M. G. Carvalho, F. C. G. Gandra, and N. A. De Oliveira, *Theoretical description of the colossal entropic magnetocaloric effect: Application to MnAs,* Physical Review B **73**, 014415 (2006).

[8] G. J. Liu, J. R. Sun, J. Shen, B. Gao, H. W. Zhang, F. X. Hu, and B. G. Shen, *Determination of the entropy changes in the compounds with a first-order magnetic transition,* Applied Physics Letters **90**, 032507 (2007).

[9] M. Balli, D. Fruchart, D. Gignoux, and R. Zach, *The "colossal" magnetocaloric effect in $Mn_{1-x}Fe_xAs$: What are we really measuring?* Applied Physics Letters **95**, 072509 (2009).

[10] L. Caron, Z. Q. Ou, T. T. Nguyen, D. T. Cam Thanh, O. Tegus, and E. Brück, *On the determination of the magnetic entropy change in materials with first-order transitions,* Journal of Magnetism and Magnetic Materials **321**, 3559 (2009).

[11] L. Tocado, E. Palacios, and R. Burriel, *Entropy determinations and magnetocaloric parameters in systems with first-order transitions: Study of MnAs,* Journal of Applied Physics **105**, 2014 (2009).

[12] H. Yibole, *Nature of the first-order magnetic phase transition in giant-magnetocaloric materials*, Ph.D. thesis, TU Delft (2016).

4

EFFECTS OF MILLING CONDITIONS ON NANO-SCALE MNFE(P,SI) PARTICLES BY SURFACTANT-ASSISTED HIGH-ENERGY BALL MILLING

In this chapter, the influence of the milling conditions on the nano-scale MnFe(P,Si) particles obtained by surfactant-assisted high-energy ball milling has been investigated by X-ray diffraction (XRD) and magnetic measurements. The presence of surfactant oleic acid prevents the re-welding of crushed particles and enhances the dispersion of nanoparticles in the solvent during the ball milling. The XRD peak intensities decrease and the peaks broaden with increasing milling time, indicating a decrease in grain size. For increasing milling time, the spontaneous magnetization becomes lower and the thermal hysteresis becomes smaller. The surfactant concentration does not have a strong impact on the magnetic properties of the obtained nanoparticles, which is consistent with the X-ray diffraction data showing the same patterns at different surfactant concentrations.

This chapter is based on the published article: N. V. Thang, N. H. van Dijk, and E. Brück, Physics Procedia, vol. 75, pp. 1104–1111, 2015.

4.1. INTRODUCTION

From both fundamental and practical point of view, the study of the magnetocaloric effect (MCE) in magnetic materials is important because it provides information about the magnetic state and the magnetic phase transition of the MCE material under investigation, but the MCE can also be applied in magnetic refrigeration [1]. Until now, most of the research has focused on the preparation of magnetocaloric materials with micro-scale particles.

In this work, the possibility to produce magnetocaloric nanoparticles is explored. The fabrication of nanoparticles of magnetocaloric materials is of interest from both fundamental and application perspectives [2], [3]. Nanosized MCE materials are predicted to show new magnetic properties compared with bulk materials due to a larger surface-to-volume ratio in nanoparticles, which influences both the magnetic and electronic properties [4], [5]. Moreover, magnetocaloric nanoparticles are more desirable than their bulk counterparts for optimal magnetic refrigeration because the particle size distribution and interparticle interactions have been shown to broaden ΔS_m over a wide temperature range, thus enhancing refrigeration capacity (RC) [6].

Various top-down and bottom-up methods such as surfactant-assisted high-energy ball-milling [7], mechanical alloying [8], sputtering [9], co-precipitation [10], solid-state reaction [11], and sol-gel [12] have been developed to prepare different nanosized materials. In this work, a surfactant-assisted high-energy ball milling technique (top-down) has been used to synthesize $Mn_{1.25}Fe_{0.7}P_{0.6}Si_{0.4}$ nanoparticles because it is a simple, inexpensive, efficient and promising method for the preparation of magnetocaloric nanomaterials. The surfactant acts as lubricant on the particle surfaces to prevent the re-welding of crushed particles during the ball milling and enhances the dispersion of nanoparticles in a solvent [13], [14],[15].

4.2. EXPERIMENTAL

$Mn_{1.25}Fe_{0.70}P_{0.60}Si_{0.40}$ nanoparticles have been produced by a two-stage high-energy ball milling (HEBM) using a planetary ball mill (Fritsch Pulverisette) with the milling vials and balls made of tungsten carbide. Heptane (C_7H_{16}) (99.8 % purity) was used as the solvent and oleic acid ($C_{18}H_{34}O_2$) (90 %) was used as the surfactant for the second stage of the milling process. In the first stage, $Mn_{1.25}Fe_{0.70}P_{0.60}Si_{0.40}$ samples were prepared by the same protocol as described in Refs [16],[17]: first high-energy ball milling and then solid state reaction. In the second stage, the powder obtained in the first step was ball-milled again in a protective argon gas atmosphere with the presence of organic solvent heptane and surfactant oleic acid for milling times vary from 0 to 10 h. The amount of sur-

factant employed was varied from 0 to 30 % of the powder weight while keeping the solvent amount constant at 60 % of the powder weight. The slurry mixture obtained after milling was then dispersed into heptane solvent by ultrasonic vibration and transferred to centrifugal tubes for removing the excess surfactant and dried in vacuum afterwards. The crystalline structures of the particles were characterized by a PANalytical X-pert Pro diffractometer using Cu-K_α radiation at the room temperature. Magnetic measurements were performed using the Reciprocating Sample Option (RSO) mode in a Superconducting Quantum Interference Device (SQUID) magnetometer (Quantum Design MPMS 5XL). Scanning Electron Microscope (SEM) and Transmission Electron Microscope (TEM) have been used to investigate the particle size and morphology of the samples.

4.3. RESULTS AND DISCUSSION

To study the function of the surfactant during the ball milling, the samples were prepared by milling with and without the surfactant. Without the surfactant, the heptane remained clear after milling while it changed color from transparent to brown when the surfactant was added to the milling process (see Fig. 4.1). This indicates that the existence of the surfactant is essential for the dispersion of the nanoparticles in the solvent during the ball milling process.

In order to study the effect of the ball milling time on the structural and magnetic properties, the powder obtained in the first step was ball-milled again in a protective argon gas atmosphere with 60 wt.% of heptane and 10 wt.% of oleic acid for 2.5, 5.0, 7.5 and 10.0 h. The XRD diffraction patterns of the $Mn_{1.25}Fe_{0.70}P_{0.60}Si_{0.40}$ powders obtained before and after milling for different milling times (in the presence of organic solvent heptane and surfactant oleic acid) show that all milled powders exhibit the hexagonal Fe_2P-type structure. In addition, $(Mn,Fe)_3Si$ as an impurity phase is detected (see Fig. 4.2). As shown in Fig. 4.2, the XRD peak intensities decrease while the peaks broaden as the milling times increase, indicating a decrease in particle size. Except for the decrease in the particle size, the strains, induced during milling process, may also attributed to the broadening of the diffraction peaks, which makes it difficult to estimate the particle size from the width of the diffraction peaks [18].

The SEM images of the obtained $Mn_{1.25}Fe_{0.70}P_{0.60}Si_{0.40}$ particles in Fig. 4.3 show irregular shapes and a wide size distribution. It is clearly seen that the sample before ball milling with the surfactant and solvent has a broad size distribution from 1 to 100 μm, while the samples ball milled with the surfactant and solvent are more homogenous. Hence, surfactant-assisted high-energy ball milling is effective in reducing the particle size by varying the ball milling time.

In Fig. 4.4 the TEM images are shown of the $Mn_{1.25}Fe_{0.70}P_{0.60}Si_{0.40}$ nanoparticles synthesized by ball milling for different times (2.5, 5.0, 7.5 and 10.0 h) us-

Figure 4.1: Color of the liquids obtained after milling with and without a surfactant.

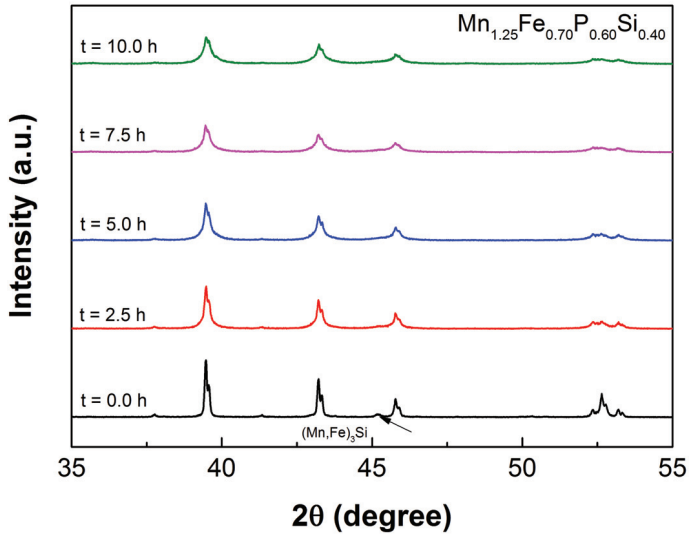

Figure 4.2: X-ray diffraction patterns measured at room temperature for the $Mn_{1.25}Fe_{0.70}P_{0.60}Si_{0.40}$ samples as a function of the ball milling time.

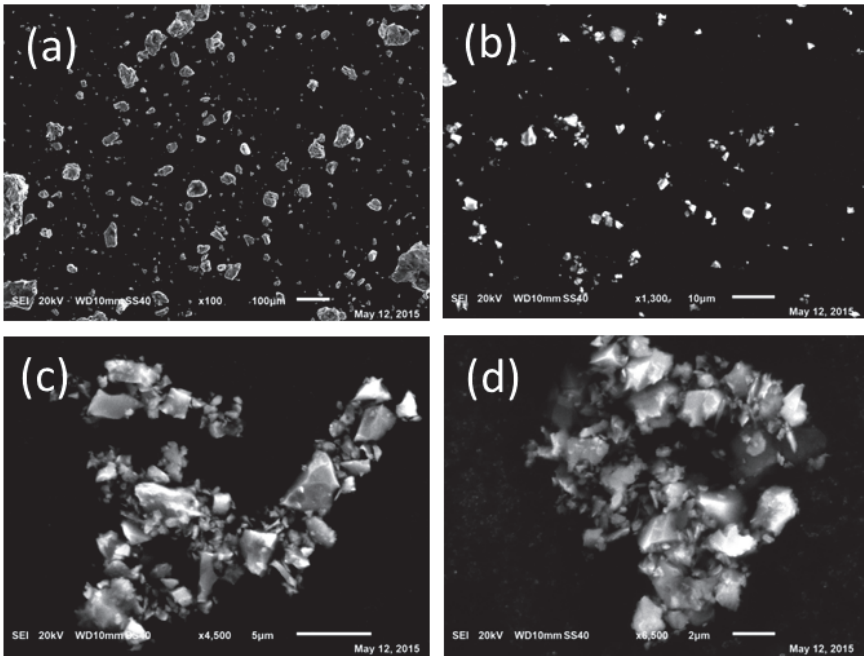

Figure 4.3: SEM images of $Mn_{1.25}Fe_{0.70}P_{0.60}Si_{0.40}$ compounds obtained before (a) and after milling with the solvent and surfactant for 5.0 (b), 7.5 (c) and 10.0 h (d).

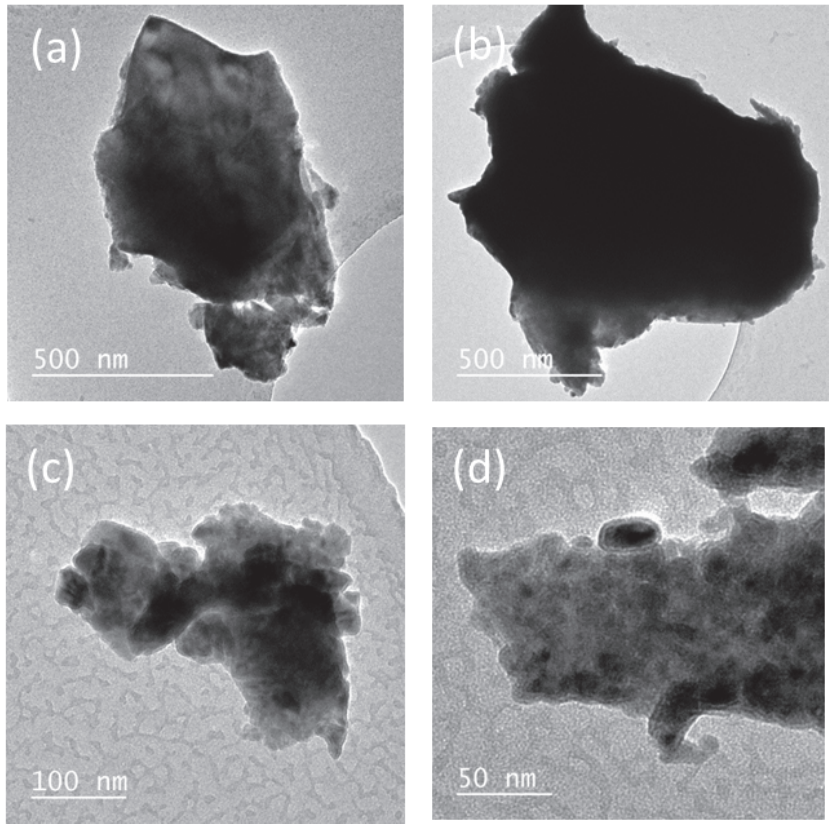

Figure 4.4: TEM images of the nanoparticles prepared by milling $Mn_{1.25}Fe_{0.70}P_{0.60}Si_{0.40}$ for 2.5 (a), 5.0 (b), 7.5 (c) and 10.0 h (d).

ing oleic acid as the surfactant show that there is a decrease in the particle size, but no significant change in morphology of the nanoparticles for increasing ball milling times. Moreover, it is clearly seen that after centrifuge cleaning there remains surfactant covering the surface of nanoparticles.

Table 4.1 compares the results of X ray diffraction and electron microscopy in terms of the average crystallite sizes and the particle sizes, respectively. For X-ray diffraction, the average crystallite size was calculated by applying the Debye-Scherer formula to the maximum intensity (111) peak, which was fitted with the X'Pert High Score Plus software to locate the peak position and the full-width-at-half-maximum (FWHM). It should be noticed that the crystallite size, which is commonly determined by XRD, is the smallest - most likely single crystal in powder form. Particle may be present as a single crystal or an agglomeration of several crystals. Therefore, particle size, which is determined by electron mi-

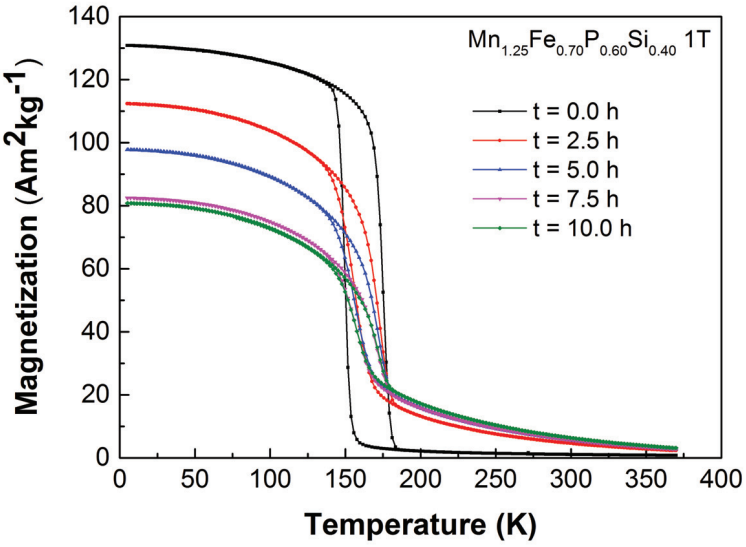

Figure 4.5: Magnetization of the $Mn_{1.25}Fe_{0.70}P_{0.60}Si_{0.40}$ samples as a function of temperature measured in a magnetic field of 1 T upon heating and cooling.

croscopy, is always larger than crystallite size.

Table 4.1: Variation of grain size for samples before and after ball milling with the surfactant at the different ball milling times.

Milling time (h)	Particle size from XRD (nm) (Å)	Particle size from TEM (μm)
0	272	30-50
2.5	58	-
5	38	2-4
7.5	32	0.5-2.0
10	31	0.05-0.50

The temperature dependence of the magnetization for $Mn_{1.25}Fe_{0.70}P_{0.60}Si_{0.40}$ compounds obtained before and after milling with the solvent and surfactant for different milling times is shown in Fig. 4.5. As can be clearly seen, the M-T curve of the $Mn_{1.25}Fe_{0.70}P_{0.60}Si_{0.40}$ powders obtained before ball milling with surfactant and solvent shows a very sharp ferromagnetic to paramagnetic transition and a broad thermal hysteresis, confirming the first-order nature of this transition. When the $Mn_{1.25}Fe_{0.70}P_{0.60}Si_{0.40}$ compounds were milled in heptane with 10 wt.% of oleic acid, the spontaneous magnetization becomes lower, while

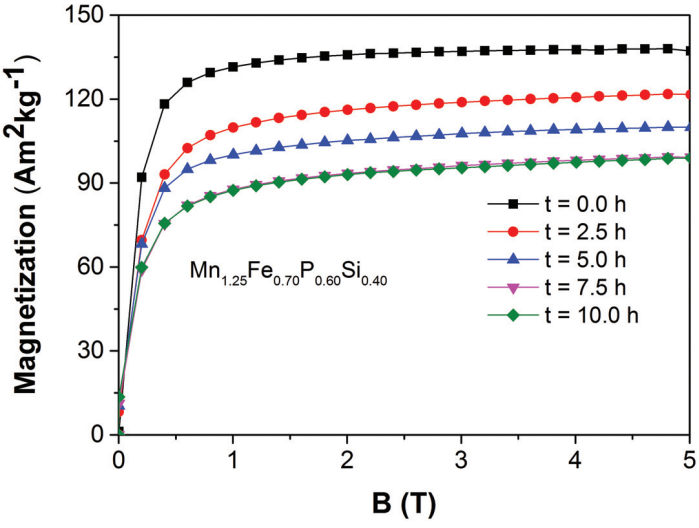

Figure 4.6: Field dependence of the magnetization of $Fe_{0.70}P_{0.60}Si_{0.40}$ samples measured at 5 K.

the thermal hysteresis becomes smaller for increasing milling times. This may be due to (i) a larger contribution of the surface states while the particle size decreases [19],[20] or (ii) the remaining surfactant covering on the surface of nanoparticles, which may lead to an error in the sample mass. The amount of surfactant used is 10% of the powder weight, which causes the potential error in weight. It should be noticed that the structural and magnetic properties of samples milled for 7.5 and 10 h are similar. In other words, the increase in the ball milling time above 7.5 h does not significantly affect the average particle size of the samples.

Fig. 4.6 shows the magnetic field dependence of the magnetization of the $Mn_{1.25}Fe_{0.70}P_{0.60}Si_{0.40}$ samples before and after the second ball milling for 2.5, 5.0, 7.5 and 10.0 h at 5 K. The saturation magnetization decreases with the decrease in the particle size caused by the increase in the ball milling time. As the particle size decreases, atoms near the particle surface may have another electron configuration than internal atoms due to the different chemical and magnetic structures of internal core part and surface shell part of the nano-sized particle [21]. This may lead to a decrease in the exchange interaction for decreasing particle sizes.

Compared to bulk $Mn_{1.25}Fe_{0.70}P_{0.60}Si_{0.40}$ prepared in the first stage, which has $\Delta S_m \sim 8 Jkg^{-1}K^{-1}$ for a field change of 1 T, one found that the MCE of the

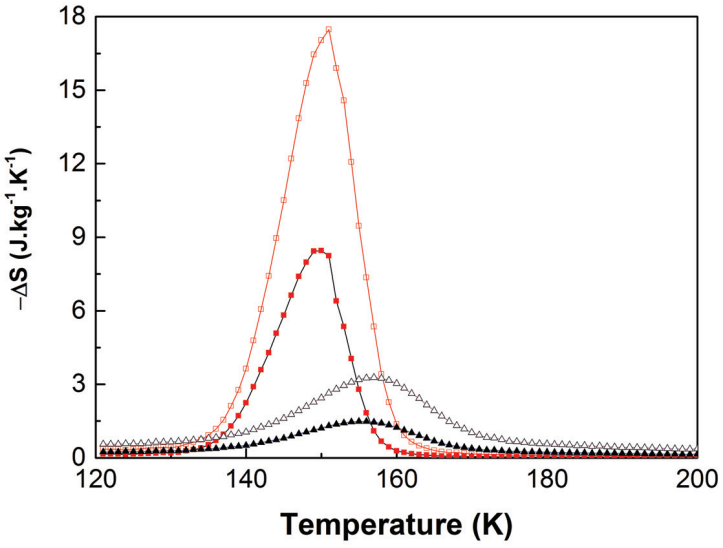

Figure 4.7: Isothermal magnetic entropy change of $Mn_{1.25}Fe_{0.70}P_{0.60}Si_{0.40}$ samples before (red squares) and after 10 h second ball milling (black triangles) for a field change of 1 T (for filled symbols) and 2 T (open symbols).

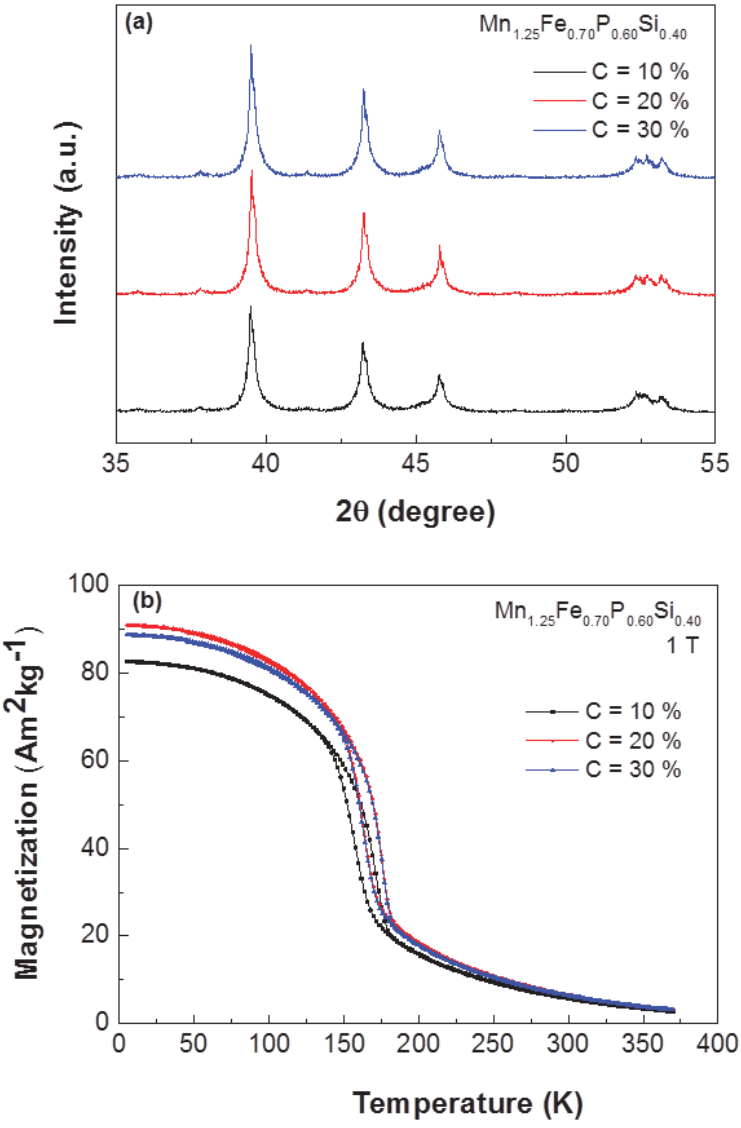

Figure 4.8: The XRD patterns measured at room temperature (a) and the temperature dependence of the magnetization in a field of 1 T upon heating and cooling (b) for $Mn_{1.25}Fe_{0.70}P_{0.60}Si_{0.40}$ samples obtained after 7.5 h milling with different surfactant concentrations.

$Mn_{1.25}Fe_{0.70}P_{0.60}Si_{0.40}$ powders milled for 10 h with the solvent and surfactant was smaller ($\Delta S_m < 2$ Jkg^{-1}K^{-1}) (see Fig. 4.7). This may be due to the decrease in saturation magnetization caused by the decrease in particle size.

Along with the milling time, the effect of the surfactant concentration has also been studied. The XRD diffraction patterns of $Mn_{1.25}Fe_{0.70}P_{0.60}Si_{0.40}$ powders shown in Fig. 4.8(a) are more or less the same for increasing surfactant concentrations, indicating that the surfactant concentration does not have a strong impact on the structural properties. This is consistent with its effect on the magnetic properties of the obtained nano-scale particles.

4.4. CONCLUSION

Magnetocaloric nanoparticles based on the Fe_2P system have been successfully prepared by surfactant-assisted high-energy ball milling. The influence of the milling parameters such as the ball milling time and surfactant concentration on the structural and magnetic properties of nano-scale $Mn_{1.25}Fe_{0.70}P_{0.60}Si_{0.40}$ particles obtained by surfactant-assisted high-energy ball milling has been investigated. While the surfactant concentration does not significantly affect both the structural and magnetic properties, the increase in the ball milling time leads to a decrease in particle size as well as the magnetocaloric effect.

REFERENCES

[1] A. M. Tishin and Y. I. Spichkin, *Recent progress in magnetocaloric effect: Mechanisms and potential applications,* International Journal of Refrigeration **37**, 223 (2014).

[2] J. Gass, H. Srikanth, N. Kislov, S. S. Srinivasan, and Y. Emirov, *Magnetization and magnetocaloric effect in ball-milled zinc ferrite powder,* Journal of Applied Physics **103**, 07B309 (2008).

[3] Q. A. Pankhurst, J. Connolly, S. K. Jones, and J. Dobson, *Applications of magnetic nanoparticles in biomedicine,* Journal of Physics D: Applied Physics **36** (2003).

[4] M. E. Mchenry and D. E. Laughlin, *Nano-scale materials development for future magnetic applications,* Acta Materialia **48** (2000).

[5] V. Franco, K. R. Pirota, V. M. Prida, A. M. J. C. Neto, A. Conde, M. Knobel, B. Hernando, and M. Vazquez, *Tailoring of magnetocaloric response in nanostructured materials: Role of anisotropy,* Physical Review B **77**, 104434 (2008).

[6] P. Gorria, P. Álvarez, J. S. Marcos, J. L. Sánchez Llamazares, M. J. Pérez, and J. A. Blanco, *Crystal structure, magnetocaloric effect and magnetovolume anomalies in nanostructured Pr_2Fe_{17}*, Acta Materialia **57**, 1724 (2009).

[7] V. M. Chakka, B. Altuncevahir, Z. Q. Jin, Y. Li, and J. P. Liu, *Magnetic nanoparticles produced by surfactant-assisted ball milling,* Journal of Applied Physics **99**, 08E912 (2006).

[8] A. Hajalilou, M. Hashim, R. Ebrahimi-Kahrizsangi, H. Mohamed Kamari, and S. Kanagesan, *Parametric optimization of $NiFe_2O_4$ nanoparticles synthesized by mechanical alloying,* Materials Science-Poland **32**, 281 (2014).

[9] P. Shah and A. Gavrin, *Synthesis of nanoparticles using high-pressure sputtering for magnetic domain imaging,* Journal of Magnetism and Magnetic Materials **301**, 118 (2006).

[10] K. Petcharoen and A. Sirivat, *Synthesis and characterization of magnetite nanoparticles via the chemical co-precipitation method,* Materials Science and Engineering: B **177**, 421 (2012).

[11] A. Ceylan, S. Ozcan, C. Ni, and S. Ismat Shah, *Solid state reaction synthesis of $NiFe_2O_4$ nanoparticles,* Journal of Magnetism and Magnetic Materials **320**, 857 (2008).

[12] D.-h. Chen and X.-r. He, *Synthesis of nickel ferrite nanoparticles by sol-gel method,* Materials Research Bulletin **36**, 1369 (2001).

[13] Y. Wang, Y. Li, C. Rong, and J. P. Liu, *Sm-Co hard magnetic nanoparticles prepared by surfactant-assisted ball milling.* Nanotechnology **18**, 465701 (2007).

[14] S. K. Pal, L. Schultz, and O. Gutfleisch, *Effect of milling parameters on $SmCo_5$ nanoflakes prepared by surfactant-assisted high energy ball milling,* Journal of Applied Physics **113**, 013913 (2013).

[15] Y. Shen, M. Q. Huang, A. K. Higgins, S. Liu, J. C. Horwath, and C. H. Chen, *Preparation of $PrCo_5$ bulk magnets using nanograin powders made by surfactant-assisted high energy milling,* Journal of Applied Physics **107**, 09A722 (2010).

[16] N. H. Dung, L. Zhang, Z. Q. Ou, L. Zhao, L. van Eijck, A. M. Mulders, M. Avdeev, E. Suard, N. H. van Dijk, and E. Brück, *High/low-moment phase transition in hexagonal Mn-Fe-P-Si compounds,* Physical Review B **86**, 045134 (2012).

[17] F. Guillou, G. Porcari, H. Yibole, N. van Dijk, and E. Brück, *Taming the first-order transition in giant magnetocaloric materials.* Advanced materials **26**, 2671 (2014).

[18] M. Yue, Y. P. Wang, N. Poudyal, C. B. Rong, and J. P. Liu, *Preparation of Nd–Fe–B nanoparticles by surfactant-assisted ball milling technique,* Journal of Applied Physics **105**, 07A708 (2009).

[19] W. Tang, W. Lu, X. Luo, B. Wang, X. Zhu, W. Song, Z. Yang, and Y. Sun, *Size-induced changes of structural, magnetic and magnetocaloric properties of* $La_{0.7}Ca_{0.2}Ba_{0.1}MnO_3$, Physica B: Condensed Matter **405**, 2733 (2010).

[20] M. Zhang, Z. Zi, Q. Liu, P. Zhang, X. Tang, J. Yang, X. Zhu, Y. Sun, and J. Dai, *Size effects on magnetic properties of* $Ni_{0.5}Zn_{0.5}Fe_2O_4$ *prepared by sol-gel method,* Advances in Materials Science and Engineering **2013** (2013).

[21] D. H. Han, J. P. Wang, and H. L. Luo, *Crystallite size effect on saturation magnetization of fine ferrimagnetic particles,* Journal of Magnetism and Magnetic Materials **136**, 176 (1994).

5

EFFECT OF HEAT TREATMENT CONDITIONS ON MNFE(P,SI,B) COMPOUNDS FOR ROOM TEMPERATURE MAGNETIC REFRIGERATION

$Mn_{1.000}Fe_{0.950}P_{0.595}Si_{0.330}B_{0.075}$ compounds have been synthesized by high-energy ball milling and a subsequent solid-state reaction. The influence of the sintering conditions on the magnetic phase transition of $Mn_{1.000}Fe_{0.950}P_{0.595}Si_{0.330}B_{0.075}$ samples has been systematically investigated using X-ray diffraction and magnetic measurements. The experimental results show that all the samples obtained after different heat treatment conditions crystallize in the Fe_2P-type hexagonal structure. The annealing temperature has a strong influence on the Curie temperature, which can be tuned between 265 and 298 K by sintering the samples at different temperatures between 1273 and 1373 K. The annealing time, however, does not significantly affect the Curie temperature. Both the annealing temperature and the annealing time have a significant effect on the magnetic entropy change. The magnetic entropy change under a magnetic field change of 1 T increases from 2.7 to 6.5 $Jkg^{-1}K^{-1}$ by increasing the annealing temperature from 1273 to 1373 K. By increasing the annealing time, the magnetic entropy change at first increases and then saturates after 20 h of heat treatment at 1373 K.

This chapter is based on the published article: N. V. Thang, H. Yibole, N. H. van Dijk, and E. Brück, Journal of Alloys and Compounds, vol. 699, pp. 633-637, March 2017.

5.1. INTRODUCTION

In recent years, the interest in magnetic materials that show a large magnetocaloric effect (MCE) in a wide temperature range around room temperature under field changes of 1-2 T (generated by permanent magnets) has noticeably increased due to their potential application in room-temperature magnetic refrigeration. Compared to the conventional vapour-compression refrigeration, this cooling technology has more advantages in terms of environmental benefits, energy efficiency and compact devices. Hence, the room-temperature magnetic refrigeration is considered as one of the most promising technologies to replace the vapour-compression refrigeration in the near future [1],[2], [3], [4].

From a practical point of view, an ideal MCE material for magnetic refrigeration should have the following properties [5]: (i) a large isothermal magnetic entropy change (ΔS_m) and adiabatic temperature change (ΔT_{ad}) in low applied magnetic fields, (ii) allow operation in a wide range of temperatures, (iii) limited thermal hysteresis (should be smaller than $\frac{dT_C}{dB}$), (iv) mechanical and chemical stability during operation, (v) readily available starting materials and (vi) low impact on environment. In this respect, among the reported candidates as solid magnetic refrigerants like $Gd_5(Si,Ge)_4$ [6]; Mn(As,Sb) [7],[8]; NiMn-based Heusler alloys [9], $(Mn,Fe)_2(P,X)$ with X = As, Ge, Si [10], [11], [12], [13]; $(Mn,Fe)_2(P,Si,N)$ [14]; $LaFe_{13-x}Si_x$ and $LaFe_{13-x}Si_x(H,C)_y$ [15], [16], [17]; and $La(Mn,Fe,Si)_{13}H_z$ [18]; $(Mn,Fe)_2(P,Si,B)$-based materials turn out to be one of the highly promising [19].

Similar to $(Mn,Fe)_2(P,Si)$-based materials, the $(Mn,Fe)_2(P,Si,B)$-based materials are usually prepared by mechanical alloying and solid-state sintering. The double-step sintering, as described in Ref. [20], is often used to synthesize these materials. This process usually takes about three days to achieve a homogeneous composition and consumes a lot of energy. In principle, the melt-spinning technique followed by a short-time heat treatment, which is considered as an energy-saving method, can be employed to prepare the $(Mn,Fe)_2(P,Si,B)$-based materials [21]. Nevertheless, this technique may be unsuitable for fabrication at an industrial scale due to its limited reproducibility. Moreover, the melt-spun ribbons obtained are normally very brittle, which makes it difficult to process them [22]. Hence, in order to make this family of materials more promising for the large scale production of final products, it is necessary to find optimal sintering conditions to either lower the sintering temperature or shorten the annealing time to obtain a uniform phase.

Recently, it has been reported that the Curie temperature of $Mn_{1.15}Fe_{0.85}P_{0.52}Si_{0.45}B_{0.03}$ alloys, which were synthesized by copper-mould casting and subsequent annealing, can be tuned between 205 to 251 K by increasing the annealing temperature from 1123 to 1423 K [22]. However, there are no

systematic investigations on the correlation between the annealing conditions and the magnetic phase transition of $(Mn,Fe)_2(P,Si,B)$-based materials, which are synthesized by high-energy ball milling and solid-state reaction. This work is devoted to systematically investigate the influence of the annealing temperature and time on the structural properties and the magnetic phase transition of $Mn_{1.000}Fe_{0.950}P_{0.595}Si_{0.330}B_{0.075}$ compounds prepared by ball-milling and subsequent annealing. This would allow a tailoring of the properties of the $(Mn,Fe)_2(P,Si,B)$-based materials and may lower the fabrication costs by tuning the heat treatment conditions.

5.2. EXPERIMENTAL

The key reason for choosing the off-stoichiometric $(Mn,Fe)_{1.95}(P,Si)$ is that this stoichiometry results in the smallest amount of impurity phases [23]. Moreover, $Mn_{1.000}Fe_{0.950}P_{0.595}Si_{0.330}B_{0.075}$ has been chosen for this study because it has recently been reported as a top class magnetocaloric material, which shows a large MCE in a small applied magnetic field, limited thermal hysteresis and an enhanced mechanical stability [24].

To synthesize polycrystalline $Mn_{1.000}Fe_{0.950}P_{0.595}Si_{0.330}B_{0.075}$ samples, the starting materials Mn, Fe, red P, Si and B powders were mechanically ball milled for 10 h in an Ar atmosphere with a constant rotation speed of 380 rpm, then pressed into small tablets with a pressure of 150 kgfcm^{-2}, and finally sealed in quartz ampoules under 200 mbar of Ar before employing the various heat treatment conditions.

To investigate the influence of the annealing time on the structural properties and magnetic phase transition of the $Mn_{1.000}Fe_{0.950}P_{0.595}Si_{0.330}B_{0.075}$ compounds, the samples were annealed at 1373 K for 1 h (HT1), 7 h (HT2), 20 h (HT3), and 25 h (HT4). One sample, which was prepared with the double sintering process described in Ref. [20] (HT5), was prepared for comparison. Samples were also annealed for 25 h at 1273 K (HT6), 1323 K (HT7), 1373 K (HT8) and 1423 K (HT9) in order to investigate the influence of the annealing temperature. It should be noted that the temperature was set to the desired temperature (annealing temperature) before putting the quartz ampoules inside for sintering. This approach is expected to eliminate the formation of the impurity phase $(Mn,Fe)_3Si$, which is formed at lower annealing temperatures. In addition, at the end of the heat treatment process all the samples were quenched into water rather than slow cooling to ambient temperature.

Before the measurements, all the samples were put into liquid nitrogen for 10-15 min to completely remove the virgin effect, which is intrinsic to $(Mn,Fe)_2(P,Si)$-based materials [25]. The crystal structure of all the samples was investigated by X-ray diffraction (XRD) using a PANalytical X-pert Pro diffrac-

tometer with Cu-K_α radiation. The XRD measurements for the structural analysis were performed at 150 K, a temperature at which all the samples are in the ferromagnetic state (FM). The XRD data of all the samples are refined using the Fullprof program [26]. Measurements of the temperature dependence of the magnetization were carried out in a commercial superconducting quantum interference device (SQUID) magnetometer (Quantum Design MPMS 5XL) in the reciprocating sample option (RSO) mode. The isothermal magnetic entropy change of all the samples is derived from the isofield magnetization $M_B(T)$ data based on Maxwell's thermodynamic relation [27]:

$$\Delta S_m(T,B) = \sum_i \frac{M_{i+1}(T_{i+1},B) - M_i(T_i,B)}{T_{i+1} - T_i} \Delta B \tag{5.1}$$

where $M_{i+1}(T_{i+1},B)$ and $M_i(T_i,B)$ represent the values of the magnetization in a magnetic field B at temperatures T_{i+1} and T_i, respectively.

5.3. RESULTS AND DISCUSSION

5.3.1. EFFECT OF THE ANNEALING TIME

Fig. 5.1 shows the XRD patterns collected at 150 K for the $Mn_{1.000}Fe_{0.950}P_{0.595}Si_{0.330}B_{0.075}$ compounds that were annealed at 1373 K for times from 1 to 25 h, and together with the sample that was subjected to the double-step sintering. The results indicate that all the annealed samples crystallize in the hexagonal Fe_2P-type structure (space group P-62m) even when the sample was annealed for only 1 h. It is worth mentioning that non-indexed peaks arises from Tungsten depositing on the anode due to the ageing of the X-ray tube. We do not observe any additional reflections for increasing annealing times, indicating that the formation of the Fe_2P-type main phase is not affected by the annealing time. In fact, the longer annealing process just enhances the compositional homogeneity. The lattice parameters and c/a ratio obtained by the Rietveld refinement method are summarized in Table 5.1. The results indicate that there are very small changes in the lattice parameters for increasing annealing times, leading to a very small reduction in the c/a ratio.

In Fig. 5.2 the magnetization as a function of temperature under a field of 1 T is shown for the HT1, HT2, HT3, HT4 and HT5 samples. It is obvious that varying the annealing time does not have a strong influence on both the thermal hysteresis and the Curie temperature. Moreover, the Curie temperature of the double-step annealed sample is almost the same as that of all the samples annealed at 1373 K for different times. The ferro-to-paramagnetic (FM-PM) transition becomes slightly sharper as the annealing time increases, which is due to better the compositional homogeneity obtained by the longer sintering process.

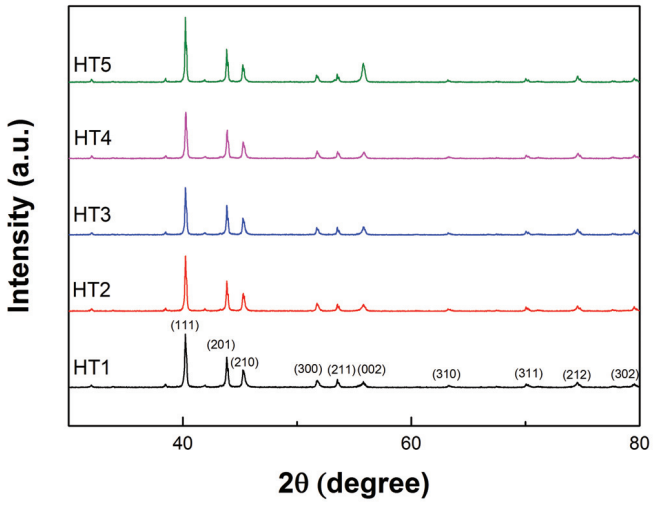

Figure 5.1: XRD patterns measured at 150 K for the HT1, HT2, HT3, HT4 and HT5 samples

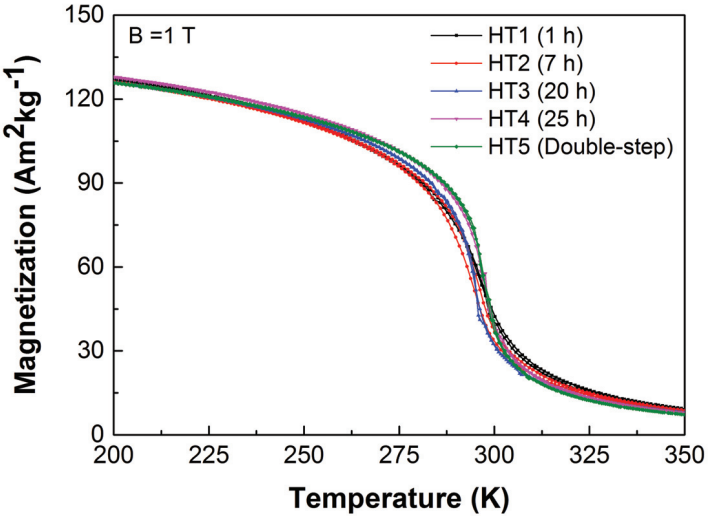

Figure 5.2: Temperature dependence of the magnetization during heating and cooling at a rate of 2 K/min in a magnetic field of 1 T for the HT1, HT2, HT3, HT4 and HT5 samples.

Table 5.1: The crystal lattice parameters a and c, the c/a ratio, and the isothermal magnetic entropy change ΔS_m of the HT1, HT2, HT3, HT4 and HT5 samples.

Samples	a (Å)	c (Å)	c/a	ΔS_m(Jkg^{-1}K^{-1})	
				$\Delta B = 1$ T	$\Delta B = 2$ T
HT1 (1 h)	6.1175(1)	3.29598(8)	0.53878(2)	4.2	6.7
HT2 (7 h)	6.1188(1)	3.29571(8)	0.53862(2)	5.1	8.0
HT3 (20 h)	6.1193(1)	3.29473(8)	0.53842(2)	6.5	9.6
HT4 (25 h)	6.1207(1)	3.29437(8)	0.53829(2)	6.5	9.3
HT5 (Double-step)	6.1207(1)	3.29458(8)	0.53823(2)	7.6	10.3

The temperature dependence of the magnetic entropy change under a magnetic field change of 1 and 2 T for the $Mn_{1.000}Fe_{0.950}P_{0.595}Si_{0.330}B_{0.075}$ compounds annealed at 1373 K is shown in Fig. 5.3 and summarized in Table 5.1. As the annealing time increases the isothermal magnetic entropy change (ΔS_m) at first increases gradually and then saturates after 20 h of heat treatment. The higher values of ΔS_m for increasing annealing time are due to an increase in the sharpness of the FM-PM transition.

5

5.3.2. EFFECT OF THE ANNEALING TEMPERATURE

The XRD patterns of the $Mn_{1.000}Fe_{0.950}P_{0.595}Si_{0.330}B_{0.075}$ compounds sintered for 25 h at different temperatures (1273, 1323, 1373 and 1423 K) are shown in Fig. 5.4. All samples consist of the hexagonal Fe_2P-type main phase. As the annealing temperature increases the diffraction peaks are narrower and exhibit a higher intensity, suggesting an increase in the particle size. Moreover, we observe an extra reflection at $2\theta \approx 22.1^\circ$ for the sample annealed at 1423 K, indicating the formation of a new phase at this annealing temperature.

Table 5.2: The crystal lattice parameters a and c, the c/a ratio, and the isothermal magnetic entropy change ΔS_m of the HT6, HT7, HT8 and HT9 samples.

Samples	a (Å)	c (Å)	c/a	ΔS_m(Jkg^{-1}K^{-1})	
				$\Delta B = 1$ T	$\Delta B = 2$ T
HT6 (1273 K)	6.1070(2)	3.31205(8)	0.54234(2)	2.7	5.0
HT7 (1323 K)	6.1227(1)	3.29873(8)	0.53877(2)	6.2	10.0
HT8 (1373 K)	6.1207(1)	3.29437(8)	0.53823(2)	6.5	9.3
HT9 (1423 K)	6.1209(1)	3.29911(8)	0.53899(2)	9.1	12.7

Fig. 5.5 shows the temperature dependence of the magnetization of the $Mn_{1.000}Fe_{0.950}P_{0.595}Si_{0.330}B_{0.075}$ compounds sintered at different temperatures measured in a field of 1 T upon heating and cooling. The results indicate that the Curie temperature is quite sensitive to the annealing temperature. Hence, along with changing composition, changing the annealing temperature is an additional

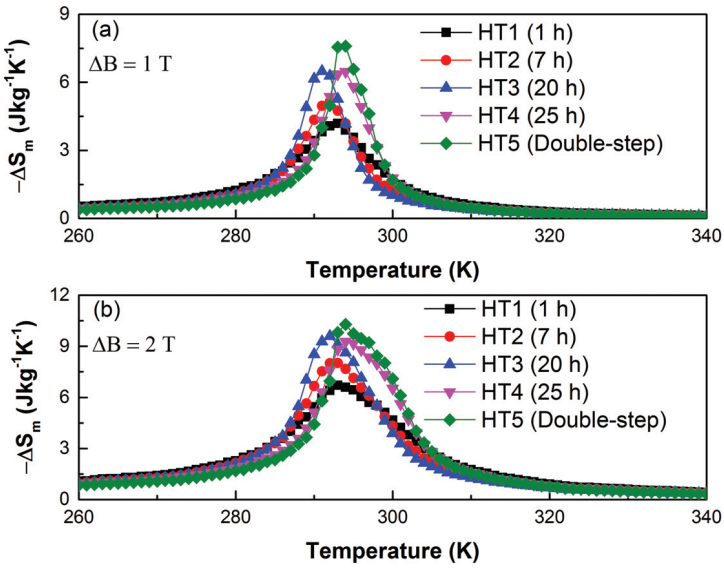

Figure 5.3: Entropy change as a function of temperature for a field change of 1 T (a) and 2 T (b) for the HT1, HT2, HT3, HT4 and HT5 samples.

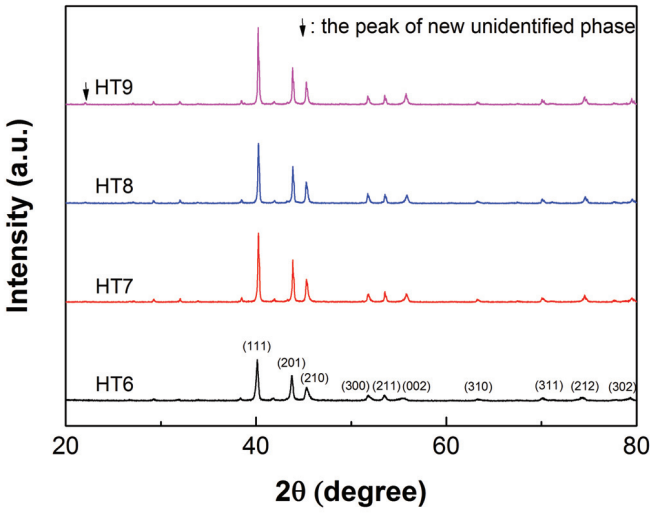

Figure 5.4: XRD patterns measured at 150 K for samples annealed for 25 h at 1273 K (HT6), 1323 K (HT7), 1373 K (HT8) and 1423 K (HT9)

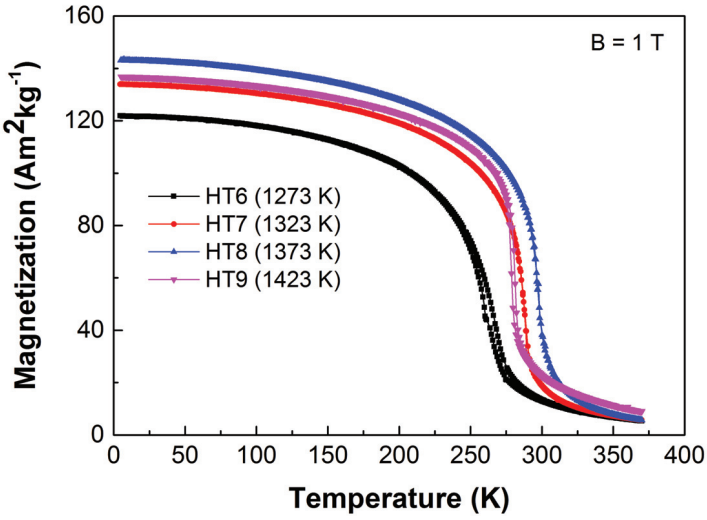

Figure 5.5: Temperature dependence of the magnetization during heating and cooling at a rate of 2 K/min in a magnetic field of 1 T for the HT6, HT7, HT8 and HT9 samples.

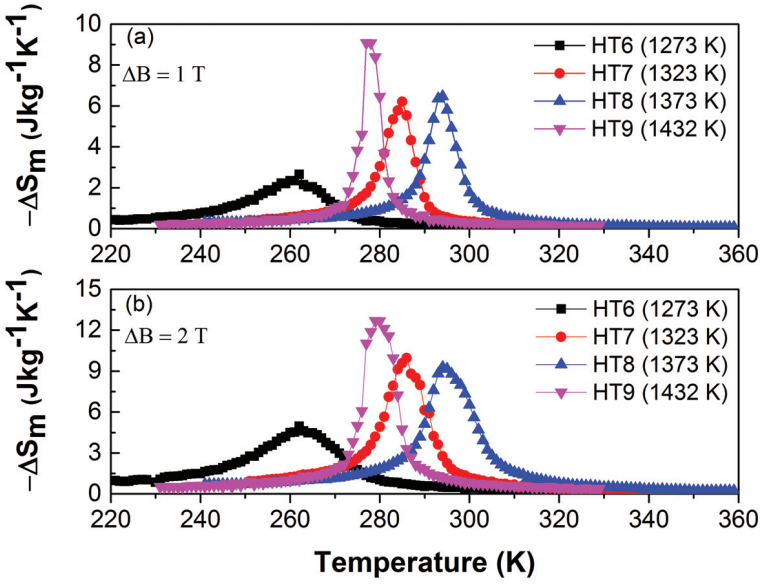

Figure 5.6: Entropy change as a function of temperature under magnetic field changes of 1 T (a) and 2 T (b) for the HT6, HT7, HT8 and HT9 samples

parameter to tune the Curie temperature. In the temperature range from 1223 to 1373 K, the Curie temperature linearly increases with the increasing sintering temperature. However, the Curie temperature decreases from 298 to 279 K as the annealing temperature increases from 1373 to 1423 K. This may be attributed to the formation of a new phase when annealing at higher temperatures, resulting in a slight change in the final composition of the main phase. The change in T_C as a function of annealing temperature is consistent with the change in c/a ratio (see Table 5.2). The experimental results also show that the samples sintered at higher temperatures present relatively sharper FM-PM transitions. The sharper transition, relative higher saturation magnetization and smaller hysteresis with increasing annealing temperature can be attributed to the more homogeneous chemical compositions and larger crystal size.

Fig. 5.6 shows the isothermal magnetic entropy change as a function of temperature for magnetic field changes of 1 and 2 T for the $Mn_{1.000}Fe_{0.950}P_{0.595}Si_{0.330}B_{0.075}$ compounds annealed at different temperatures between 1273 and 1423 K. For the external magnetic field changes of both 1 and 2 T, the ΔS_m increases significantly as the annealing temperature increases from 1273 to 1323 K and then hardly changes on increasing the annealing temperature to 1373 K. However, a further increase in annealing temperature to 1432 K leads to a significant increase in the magnetic entropy change, suggesting that in this case the presence of the additional impurity phase does not have a negative effect on the MCE properties. The higher annealing temperature enhanced the compositional homogeneity, which leads to a sharper first-order magnetic phase transition. The maximum values in magnetic entropy change under a magnetic field change of 1 and 2 T for samples annealed at 1273, 1323, 1373 and 1423 K are summarized in Table 5.2. It should be noted that compared to the sample produced by the double-step sintering, the sample annealed at 1432 K for 25 h has a higher value of ΔS_m. Hence, varying the annealing temperature not only can tune the Curie temperature, but can also enhance the magnetocaloric effect of $(Mn,Fe)_2(P,Si,B)$-based materials. We verified that the changes in ΔS_m solely originate from the heating profile by reproducing one of the heat treatment conditions.

5.4. CONCLUSIONS

In this chapter, we investigated the effect of both annealing temperature and time on the magnetic phase transition of $Mn_{1.000}Fe_{0.950}P_{0.595}Si_{0.330}B_{0.075}$ compounds that were synthesized by ball-milling and subsequent annealing. The experimental results indicate that the Curie temperature can be tuned by annealing at different temperatures, while it hardly changes by varying the annealing time. The maximum value of the magnetic entropy change for the sample annealed at

1423 K for 25 h is higher than that for the double-step annealed sample. Hence, annealing at higher temperature, but for shorter time, is considered as a promising alternative to the conventional double-step sintering process to synthesize Fe_2P-type magnetic refrigerants.

REFERENCES

[1] V. K. Pecharsky and K. A. G. Jr, *Magnetocaloric effect and magnetic refrigeration,* Journal of Magnetism and Magnetic Materials **200**, 44 (1999).

[2] V. Franco, J. Blázquez, B. Ingale, and A. Conde, *The magnetocaloric effect and magnetic refrigeration near room temperature: materials and models,* Annual Review of Materials Research **42**, 305 (2012).

[3] A. Tishin, *Magnetocaloric effect: Current situation and future trends,* Journal of Magnetism and Magnetic Materials **316**, 351 (2007).

[4] F. Scarpa, G. Tagliafico, and L. A. Tagliafico, *A classification methodology applied to existing room temperature magnetic refrigerators up to the year 2014,* Renewable and Sustainable Energy Reviews **50**, 497 (2015).

[5] B. Yu, Q. Gao, B. Zhang, X. Meng, and Z. Chen, *Review on research of room temperature magnetic refrigeration,* International Journal of Refrigeration **26**, 622 (2003).

[6] V. K. Pecharsky and K. A. Gschneidner, *Giant magnetocaloric effect in $Gd_5(Si_2Ge_2)$,* Physical Review Letters **78**, 4494 (1997).

[7] H. Wada, T. Morikawa, K. Taniguchi, T. Shibata, Y. Yamada, and Y. Akishige, *Giant magnetocaloric effect of $MnAs_{1-x}Sb_x$ in the vicinity of first-order magnetic transition,* Physica B: Condensed Matter **328**, 114 (2003).

[8] A. de Campos, M. da Luz, A. de Campos, A. A. Coelho, L. Cardoso, A. O. dos Santos, and S. Gama, *Investigations in $MnAs_{1x}Sb_x$: Experimental validation of a new magnetocaloric composite,* Journal of Magnetism and Magnetic Materials **374**, 342 (2015).

[9] J. Liu, T. Gottschall, K. P. Skokov, J. D. Moore, and O. Gutfleisch, *Giant magnetocaloric effect driven by structural transitions,* Nature Materials , 620 (2012).

[10] O. Tegus, E. Brück, K. H. J. Buschow, and F. R. de Boer, *Transition-metal-based magnetic refrigerants for room-temperature applications.* Nature **415**, 150 (2002).

[11] N. T. Trung, Z. Q. Ou, T. J. Gortenmulder, O. Tegus, K. H. J. Buschow, and E. Brück, *Tunable thermal hysteresis in MnFe(P,Ge) compounds,* Applied Physics Letters **94**, 102513 (2009).

[12] D. T. Cam Thanh, E. Brück, N. T. Trung, J. C. P. Klaasse, K. H. J. Buschow, Z. Q. Ou, O. Tegus, and L. Caron, *Structure, magnetism, and magnetocaloric properties of $MnFeP_{1-x}Si_x$ compounds,* Journal of Applied Physics **103**, 07B318 (2008).

[13] H. Yibole, F. Guillou, L. Zhang, N. H. van Dijk, and E. Brück, *Direct measurement of the magnetocaloric effect in MnFe(P, X) (X = As, Ge, Si) materials,* Journal of Physics D: Applied Physics **47**, 075002 (2014).

[14] N. Thang, X. Miao, N. van Dijk, and E. Brück, *Structural and magnetocaloric properties of $(Mn,Fe)_2(P,Si)$ materials with added nitrogen,* Journal of Alloys and Compounds **670**, 123 (2016).

[15] A. Fujita, S. Fujieda, Y. Hasegawa, and K. Fukamichi, *Itinerant-electron metamagnetic transition and large magnetocaloric effects in $La(Fe_xSi_{1-x})_{13}$ compounds and their hydrides,* Physical Review B **67**, 104416 (2003).

[16] M. Phejar, V. Paul-Boncour, and L. Bessais, *Investigation on structural and magnetocaloric properties of $LaFe_{13-x}Si_x(H,C)_y$ compounds,* Journal of Solid State Chemistry **233**, 95 (2016).

[17] M. Krautz, K. Skokov, T. Gottschall, C. S. Teixeira, A. Waske, J. Liu, L. Schultz, and O. Gutfleisch, *Systematic investigation of Mn substituted $La(Fe,Si)_{13}$ alloys and their hydrides for room-temperature magnetocaloric application,* Journal of Alloys and Compounds **598**, 27 (2014).

[18] A. Barcza, M. Katter, V. Zellmann, S. Russek, S. Jacobs, and C. Zimm, *Stability and magnetocaloric properties of sintered $La(Fe,Mn,Si)_{13}H_z$ alloys,* IEEE Transactions on Magnetics **47**, 3391 (2011).

[19] F. Guillou, H. Yibole, G. Porcari, L. Zhang, N. H. van Dijk, and E. Brück, *Magnetocaloric effect, cyclability and coefficient of refrigerant performance in the MnFe(P,Si,B) system,* Journal of Applied Physics **116**, 063903 (2014).

[20] N. H. Dung, L. Zhang, Z. Q. Ou, L. Zhao, L. van Eijck, A. M. Mulders, M. Avdeev, E. Suard, N. H. van Dijk, and E. Brück, *High/low-moment phase transition in hexagonal Mn-Fe-P-Si compounds,* Physical Review B **86**, 045134 (2012).

[21] Y. Shao, M. Zhang, Y. Zhang, A. Yan, and J. Liu, *Effect of annealing on the structure and magnetic entropy change of $Mn_{1.1}Fe_{0.9}P_{0.8}Ge_{0.2}$ ribbons,* Journal of Magnetism and Magnetic Materials **362**, 90 (2014).

[22] H. Yu, Z. Zhu, J. Lai, Z. Zheng, D. Zeng, and J. Zhang, *Enhance magnetocaloric effects in $Mn_{1.15}Fe_{0.85}P_{0.52}Si_{0.45}B_{0.03}$ alloy achieved by copper-mould casting and annealing treatments,* Journal of Alloys and Compounds **649**, 1043 (2015).

[23] N. Dung, *Moment formation and giant magnetocaloric effects in hexagonal Mn-Fe-P-Si compounds*, Ph.D. thesis, TU Delft (2012).

[24] F. Guillou, G. Porcari, H. Yibole, N. van Dijk, and E. Brück, *Taming the first-order transition in giant magnetocaloric materials.* Advanced materials **26**, 2671 (2014).

[25] X. F. Miao, L. Caron, Z. Gercsi, A. Daoud-Aladine, N. H. van Dijk, and E. Brück, *Thermal-history dependent magnetoelastic transition in $(Mn,Fe)_2(P,Si)$,* Applied Physics Letters **107**, 042403 (2015).

[26] J. Rodríguez-Carvajal, *Recent advances in magnetic structure determination by neutron powder diffraction,* Physica B: Condensed Matter **192**, 55 (1993).

[27] E. Brück, *Developments in magnetocaloric refrigeration,* Journal of Physics D: Applied Physics **38**, R381 (2005).

6

STRUCTURAL AND MAGNETOCALORIC PROPERTIES OF $(Mn,Fe)_2(P,Si)$ MATERIALS WITH ADDED NITROGEN

Amongst magnetic materials that exhibit a giant magnetocaloric effect near room temperature, the $(Mn,Fe)_2(P,Si)$ system is one of the most promising candidates for magnetic refrigeration. Although the $(Mn,Fe)_2(P,Si)$ materials hold many advantages, controlling the magnetic entropy change ΔS_m, the adiabatic temperature change ΔT_{ad}, the thermal hysteresis and the mechanical stability across the ferromagnetic transition requires a delicate tuning of the composition. This work investigates the addition of nitrogen, as an interstitial or substitutional element, as a new parameter to tune the properties of $(Mn,Fe)_2(P,Si)$ materials. We found that the nitrogen addition results in a decrease of the Curie temperature, consistent with the observed increase in the c/a ratio. The introduction of nitrogen in $(Mn,Fe)_2(P,Si)$ materials also results in a strong enhancement of the mechanical stability.

This chapter is based on the published article: N. V. Thang, X. F. Miao, N. H. van Dijk, and E. Brück, Journal of Alloys and Compounds, vol. 670, pp. 123–127, Jun. 2016.

6.1. INTRODUCTION

Recently, magnetocaloric materials have been studied intensively because of their potential application in magnetic refrigeration. Compared to the commonly used vapour-compression refrigeration, magnetic refrigeration, which is based on magnetocaloric effect (MCE), has many advantages. For example, the cooling efficiency of magnetic refrigeration, can reach up to 60 % of the Carnot efficiency. This efficiency gain will result in a reduced CO_2 release. In addition, magnetic refrigerators can be built more compactly as the refrigerants are magnetic solids rather than gases. Moreover, magnetic refrigeration generates much less noise due to the absence of an energy-consuming compressor and fewer moving parts. This is also an environmentally friendly technology because of the absence of dangerous and environmentally unfriendly refrigerants such as ozone depleting chemicals (e.g. chlorofluorocarbons), hazardous chemicals (e.g. NH_3) and greenhouse gases (e.g. hydrochlorofluorocarbons and hydrofluorocarbons). Therefore, magnetic refrigeration is a promising technology with the potential to replace the conventional gas-compression technology [1], [2], [3].

Magnetic materials that display a large MCE near room temperature are a key requirement to realize magnetic refrigeration. In recent years, many novel materials with large MCE have been developed, such as $Gd_5(Si,Ge)_4$ [4], Mn(As,Sb) [5], [6], $(Mn,Fe)_2(P,X)$ (X = As, Ge, Si) [7], [8], [9], $LaFe_{13-x}Si_x$ and their related compounds [10], [11], [12], $(Mn,Fe)_2(P,Si,B)$ [13] and NiMn-based Heusler alloys [14]. Among the presently known MCE materials with a first-order magnetic transition (FOMT) the $(Mn,Fe)_2(P,Si)$ compounds fulfill most of the requirements for practical applications of magnetic refrigeration [15]. First, it has a limited thermal hysteresis at the FOMT. Second, the Curie temperatures are in the vicinity of the required working temperature. Third, it has a large MCE at moderate magnetic field. In addition, it is easy to tune the operating temperature by varying the Mn/Fe and/or P/Si ratio. Furthermore, the composition of these compounds does not contain any toxic or expensive elements such as arsenic and germanium, respectively.

Several different approaches have been developed to tailor the properties of the $(Mn,Fe)_2(P,Si)$-based materials. It has recently been reported that the introduction of B results into a tunable high-performance MCE material system. In the $(Mn,Fe)_2(P,Si,B)$ materials, B acts as a substitutional element [15], whereas it is an interstitial element in the $(Mn,Fe)_2(P,As,B)$ materials [16]. It is well known that the magnetocaloric properties of magnetic materials can be influenced by the application of physical pressure [17],[18]. However, applying physical pressure is an impractical approach for applications. Thus, chemical pressure is commonly employed instead by the introduction of interstitial elements. The introduction of an interstitial element is expected to provide a relatively simple tun-

ing parameter to provide a gradual displacement of the phase transition without a strong impact on the magnetocaloric properties [16]. Interstitial elements may also provide a useful tool to investigate the role of the magneto-elastic coupling in the FOMT [15]. Nitrogen is an ideal candidate as it has a smaller atomic radius than boron and the same electron configuration as phosphorous. This work reports on a new approach to tune the magnetocaloric properties of the $(Mn,Fe)_2(P,Si)$ compounds by adding nitrogen. We demonstrate that N atoms occupy both substitutional and interstitial sites of the hexagonal Fe_2P-type crystal structure. The introduction of nitrogen provides the possibility to tune the Curie temperature, while the magnetocaloric properties are preserved and the mechanical stability is improved.

6.2. EXPERIMENTAL DETAILS

All samples were prepared following the same protocol: first high-energy ball milling and then a solid-state reaction was applied. The nitrogen source was introduced in solid form using $Fe_{2-4}N$ iron nitride powder. Stoichiometric mixtures of the starting materials Mn, Fe, $Fe_{2-4}N$, red P and Si powders were ball milled for 10 h with a constant rotation speed of 380 rpm at room temperature. After milling, the mixture was compacted into small tablets (with a diameter of 12 mm and a height of 5-10 mm) in a hydraulic pressing system. After pressing, the tablets were sealed inside quartz ampoules with 200 mbar of Ar. Then, the samples were sintered at 1373 K for 2 h and annealed at 1123 K for 20 h. The samples were slowly cooled to room temperature before they were re-sintered at 1373 K for 20 h to achieve a homogeneous composition. The thermal treatment was completed by rapidly quenching to room temperature by directly dipping the ampoules into water. The samples were precooled in liquid nitrogen to remove the virgin effect [19], and then crushed using a mortar.

The crystalline structure of the samples was characterized by X-ray diffraction (XRD) using a PANalytical X-pert Pro diffractometer with Cu-K_α radiation. The refinements were done using the Fullprof program [20]. A differential scanning calorimeter (DSC) equipped with a liquid nitrogen cooling system was used to measure the specific heat. Magnetic measurements were performed using the Reciprocating Sample Option (RSO) mode in a Superconducting Quantum Interference Device (SQUID) magnetometer (Quantum Design MPMS 5XL). The magnetic entropy change, one of the characteristic parameters for MCE, was derived from the isofield magnetization measurements using the Maxwell relation.

6.3. RESULTS AND DISCUSSIONS

6.3.1. INTERSTITIAL NITROGEN ADDITION

Fig. 6.1 shows the XRD patterns of $Mn_{1.25}Fe_{0.70}P_{0.50}Si_{0.50}N_z$ compounds measured at 150 K (a) and 500 K (b) (in the ferromagnetic and paramagnetic state, respectively), for samples with a nominal nitrogen composition of z = 0.00, 0.01, 0.03, 0.05 and 0.07. All samples exhibit the hexagonal Fe_2P-type crystal structure and, as commonly observed in this material family, display a small amount of $(Mn,Fe)_3Si$ impurity phase. The XRD pattern gradually changes with an increase in nitrogen content, as the a and c lattice parameters evolve. We do not observe any additional reflections, indicating that the nitrogen is fully accommodated in the Fe_2P-type structure.

The XRD data were analyzed by the Rietveld refinement method [21] using the Fullprof program. The lattice parameters and unit-cell volume are summarized in Table 6.1. The results indicate that for an increase in N concentration, the lattice parameter a decreases, the lattice parameter c increases, whereas the unit-cell volume hardly changes between 150 and 500 K. A small difference of only 1.3 % in volume between these temperatures was observed, which originates from the FOMT and the thermal expansion.

Table 6.1: Lattice parameters and unit-cell volume of the $Mn_{1.25}Fe_{0.7}P_{0.5}Si_{0.5}N_z$ compounds with z = 0.00, 0.01, 0.03, 0.05 and 0.07 at 150 K and 500 K.

Compound	a (Å)	c (Å)	V (Å^3)	c/a
$Mn_{1.25}Fe_{0.7}P_{0.5}Si_{0.5}N_z$	(150/500 K)	(150/500 K)	(150/500 K)	(150/500 K)
z = 0	6.18812/6.10262	3.31082/3.4617	109.795/111.649	0.53503/0.56725
z = 0.01	6.17579/6.08798	3.31471/3.46045	109.486/111.0.73	0.53673/0.56841
z = 0.03	6.16894/6.08753	3.31819/3.46299	109.359/111.138	0.53789/0.56887
z = 0.05	6.16551/6.08563	3.32517/3.46859	109.467/111.249	0.53932/0.56996
z = 0.07	6.15434/6.07985	3.33346/3.47014	109.342/111.087	0.54164/0.57076

Fig. 6.2 shows the evolution of the unit-cell volume V and the c/a ratio in the ferromagnetic state (150 K) and paramagnetic state (500 K) for the $Mn_{1.25}Fe_{0.70}P_{0.50}Si_{0.50}N_z$ compounds. The addition of nitrogen as an interstitial element leads to two main features. First, there is a gradual increase in the c/a ratio when z increases. Second, the unit-cell volume slightly decreases when the N concentration is increased to 1%. A further increase in N concentration up to 7% only causes a slight variation in unit-cell volume in both the paramagnetic and ferromagnetic state (Fig. 6.2(a)). It is expected that the unit-cell volume increases when the nitrogen atoms enter the structure as an interstitial element. The addition of nitrogen as a substitutional element should lead to a larger decrease in the unit-cell volume compared to the boron addition, as the radius of a nitrogen atom is smaller than that of boron. The slight variation in unit-cell vol-

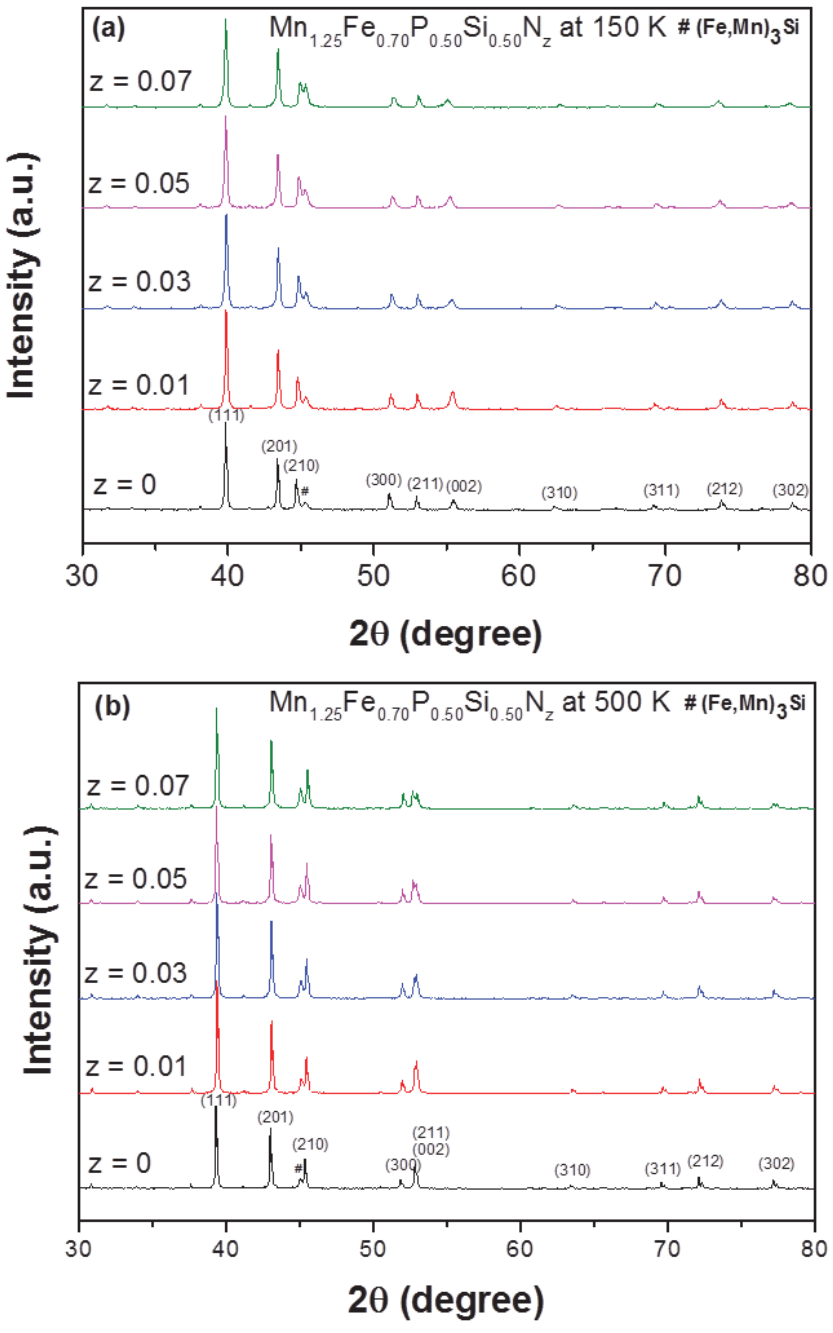

Figure 6.1: X-ray diffraction patterns measured at 150 K (left) and 500 K (right) for $Mn_{1.25}Fe_{0.70}P_{0.50}Si_{0.50}N_z$ compounds.

ume for increasing nitrogen doping suggests that in this case the nitrogen atoms enter the structure partly as substitutional and partly as interstitial element.

In Fig. 6.3 the temperature dependence of the magnetization is shown for the $Mn_{1.25}Fe_{0.70}P_{0.50}Si_{0.50}N_z$ compounds measured during cooling and heating in a magnetic field of 1 T. Two main features were observed. First, the Curie temperature decreases as a function of the nitrogen content, which is consistent with the increase in the c/a ratio observed in Fig. 6.2(b). Second, the increase in nitrogen concentration leads to a gradual decrease in the spontaneous magnetization and a slight increase in thermal hysteresis. The presence of thermal hysteresis (ΔT_{hys}) reveals the first-order nature of the transitions, which usually results in a large MCE [1].

Table 6.2: Curie temperature T_C in zero-field derived from the DSC data measured on heating; the isothermal entropy change derived from the isofield magnetization curves in a field change of 1 T, thermal hysteresis derived from the DSC data measured in zero field upon cooling and heating and the relative changes in lattice parameter and at the transition for the $Mn_{1.25}Fe_{0.70}P_{0.50}Si_{0.50}N_z$ compounds.

$Mn_{1.25}Fe_{0.70}P_{0.50}Si_{0.50}N_z$	T_C (K)	ΔS_m (Jkg^{-1})	ΔT_{hys} (K)	$\Delta a/a$(%)	$\Delta c/c$(%)
z = 0.00	260	13.75	4.80	0.97	1.98
z = 0.01	245	14.59	5.40	1.04	2.04
z = 0.03	232	13.80	5.60	1.08	2.15

Dung and coworkers [22] have pointed out that there is a correlation between the magnitude of the hysteresis and the relative changes in lattice parameters $\Delta a/a$ and $\Delta c/c$ at T_C. Hence, the XRD patterns as a function of temperature were collected in zero field to investigate the origin of the increase in thermal hysteresis for increasing z. Fig. 6.4 shows the temperature dependence of the lattice parameters a and c for the $Mn_{1.25}Fe_{0.70}P_{0.50}Si_{0.50}N_z$ compounds with z = 0.00, 0.01, 0.03. As shown in Fig. 6.4, the same trend in the thermal evolution of the lattice parameters a and c has been observed for all samples. Specifically, the lattice parameter a decreases while the lattice parameter c increases for increasing temperature. We note that the volume change at T_C is very small due to the opposite change in the a and c parameters. This may contribute to an improvement in mechanical stability for the N-doped materials. In our experiments, we observed that the N-doped materials remain in their physical forms when precooled in liquid nitrogen, whereas the pristine (Mn,Fe)$_2$(P,Si) materials are easily fragmented. As presented in Table 6.2, larger $\Delta a/a$ and $\Delta c/c$ ratios result in a larger ΔT_{hys}. This increase in ΔT_{hys} is expected to be due to a higher energy barrier to nucleate the new phase. This is in good agreement with the previous report on (Mn,Fe)$_2$(P,Si) compounds [22].

We note that the sharp first-order magnetic transition of the

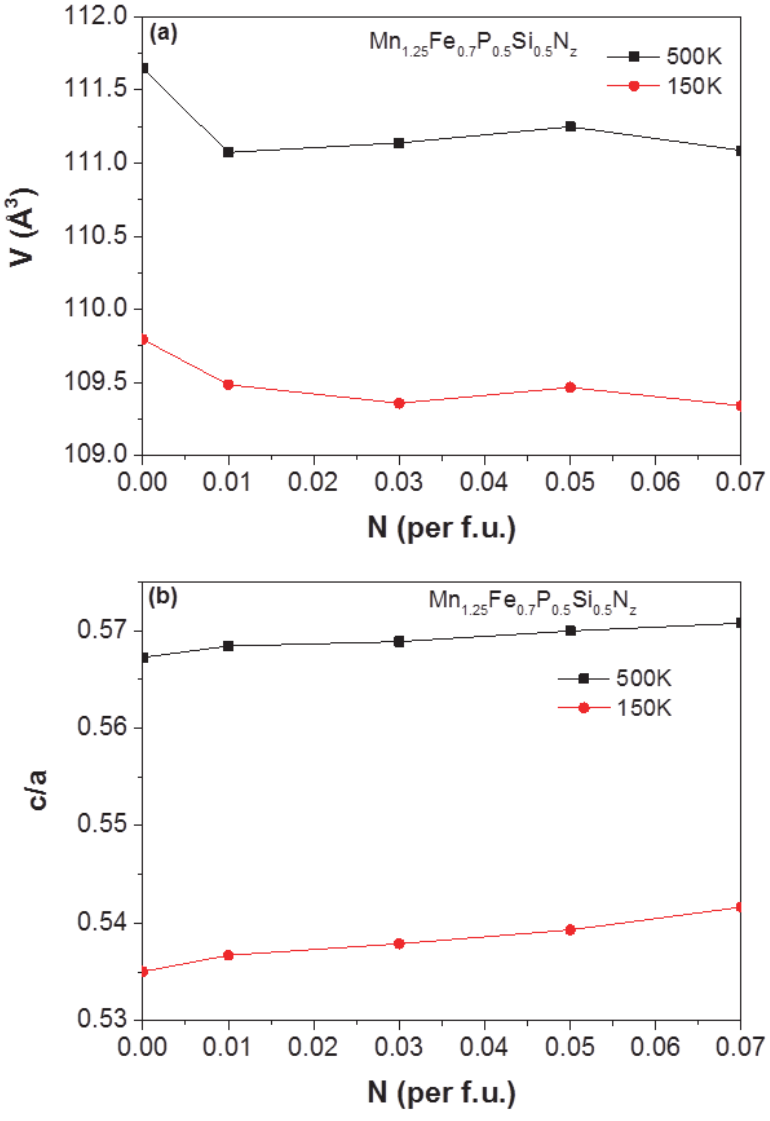

Figure 6.2: Unit-cell volume V (a) and c/a ratio (b) of the $Mn_{1.25}Fe_{0.70}P_{0.50}Si_{0.50}N_z$ compounds in the paramagnetic (500 K) and ferromagnetic state (150 K) as function of the nitrogen content.

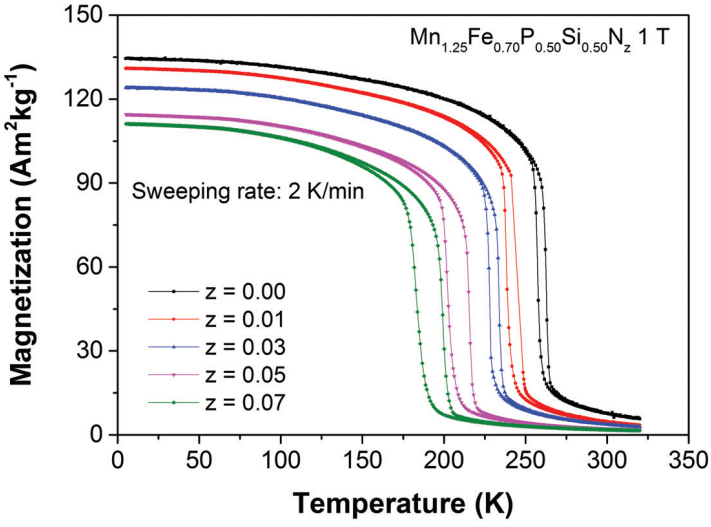

Figure 6.3: Magnetization curves measured on heating and cooling in a magnetic field of 1 T for the $Mn_{1.25}Fe_{0.70}P_{0.50}Si_{0.50}N_z$ compounds.

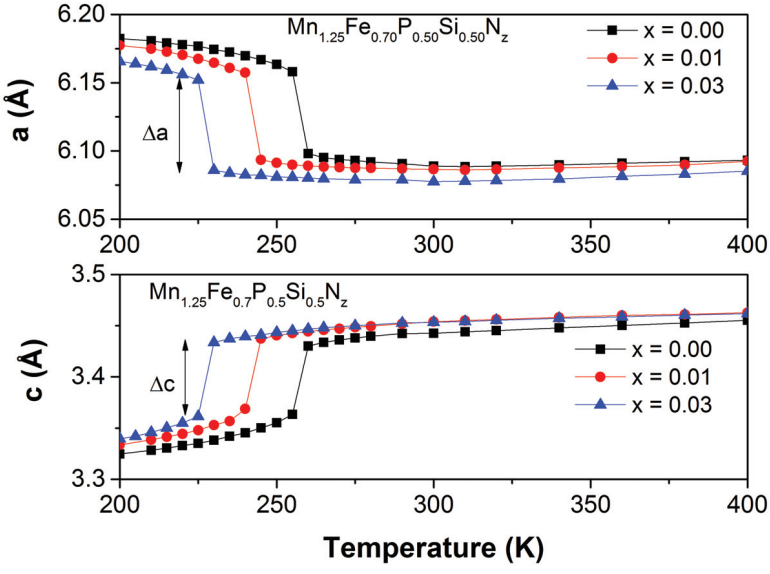

Figure 6.4: Lattice parameters a and c as a function of temperature derived from the XRD patterns measured in zero field upon heating for the $Mn_{1.25}Fe_{0.70}P_{0.50}Si_{0.50}N_z$ (z = 0.00, 0.01, 0.03) compounds

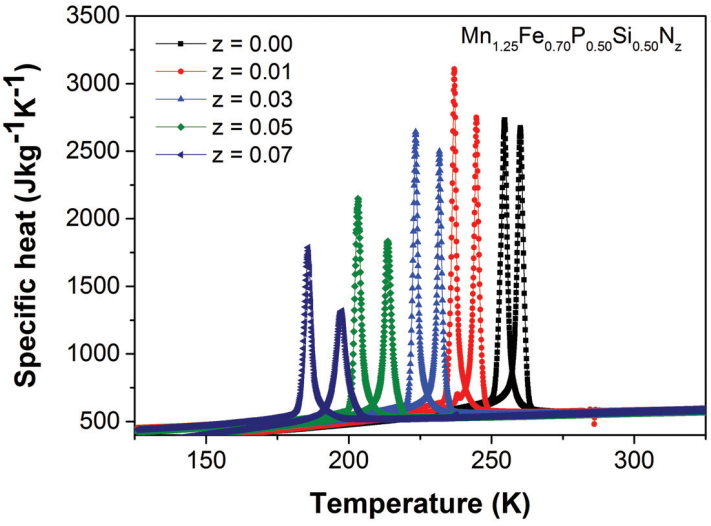

Figure 6.5: Specific heat of the $Mn_{1.25}Fe_{0.70}P_{0.50}Si_{0.50}N_z$ compounds measured in zero-field upon cooling and heating.

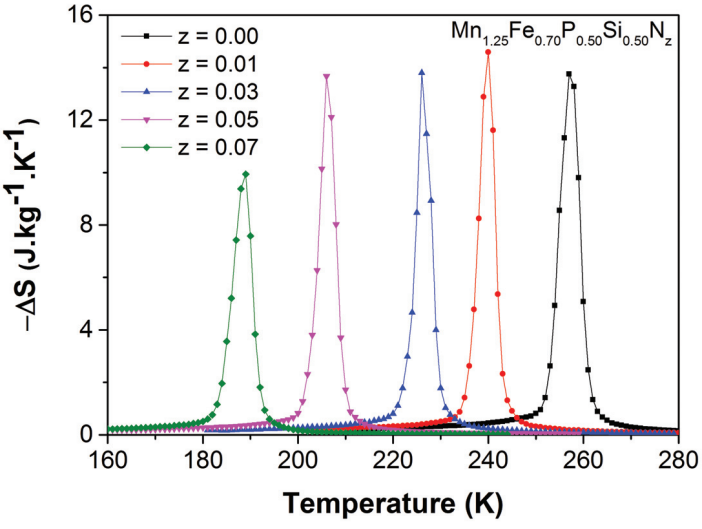

Figure 6.6: Entropy change for the $Mn_{1.25}Fe_{0.70}P_{0.50}Si_{0.50}N_z$ compounds as a function of temperature for a field change of 1 T.

$Mn_{1.25}Fe_{0.70}P_{0.50}Si_{0.50}N_z$ compounds becomes weaker for increasing N concentrations. This is indicated by the lower and broader peak at T_C in the specific heat curves of Fig. 6.5. Fig. 6.6 shows the isothermal entropy change for the $Mn_{1.25}Fe_{0.70}P_{0.50}Si_{0.50}N_z$ compounds as a function of temperature for a field change of 1 T. The ΔS_m values of the $Mn_{1.25}Fe_{0.70}P_{0.50}Si_{0.50}N_z$ compounds are comparable to those observed for many well-known magnetocaloric materials, such as $Gd_5Si_2Ge_2$, Heusler alloys and $La(Fe,Si)_{13}H_y$ [2]. The results indicate that a small nitrogen addition offers a new control parameter to tune the Curie temperature, while it hardly influences the magnetic entropy change.

6.3.2. SUBSTITUTIONAL NITROGEN ADDITION

Table 6.3: Lattice parameters and unit-cell volume of the $Mn_{1.25}Fe_{0.70}P_{0.5-z}Si_{0.5}N_z$ and $Mn_{1.25}Fe_{0.70}P_{0.5}Si_{0.5-z}N_z$ compounds with z = 0.00, 0.01, 0.03, 0.05 and 0.07 at room temperature.

Compound	a (Å)	c (Å)	V (Å^3)
$Mn_{1.25}Fe_{0.70}P_{0.5-z}Si_{0.5}N_z$			
z = 0.00	6.09032	3.44543	110.676
z = 0.01	6.08425	3.45370	110.721
z = 0.03	6.07954	3.46159	110.802
z = 0.07	6.06300	3.46996	110.466
$Mn_{1.25}Fe_{0.70}P_{0.50}Si_{0.5-z}N_z$			
z = 0.00	6.08688	3.46211	111.090
z = 0.01	6.06911	3.47201	110.755
z = 0.03	6.05927	3.47648	110.538
z = 0.05			

In Fig. 6.7, the X-ray diffraction patterns are shown for the $Mn_{1.25}Fe_{0.70}P_{0.5-z}Si_{0.5}N_z$ and $Mn_{1.25}Fe_{0.70}P_{0.5}Si_{0.5-z}N_z$ compounds, where N respectively substitutes P and Si. It is clear that the substitution of P, as well as Si, by N does not result in a structure change for z = 0.01. However, for z ≥ 0.03 *a* $Fe_{2-4}N$ impurity phase is observed. The lattice parameters and unit-cell volume of these compounds are summarized in Table 6.3.

In Fig. 6.8, the temperature dependence of the magnetization, recorded on cooling and heating in a magnetic field of 1 T, is shown for the $Mn_{1.25}Fe_{0.70}P_{0.5-z}Si_{0.5}N_z$ (a) and $Mn_{1.25}Fe_{0.70}P_{0.5}Si_{0.5-z}N_z$ (b) compounds. It is obvious that similar to the interstitial nitrogen addition, N substitutions for either P or Si lead to a decrease in T_C and an increase in thermal hysteresis for an increasing nitrogen content. However, the changes in T_C and ΔT_{hys} are more pronounced when N substitutes Si rather than P. Interestingly, the spontaneous magnetization of the samples with a substitutional formulation is a little lower than for samples with interstitial formulations at the same nitrogen concentration.

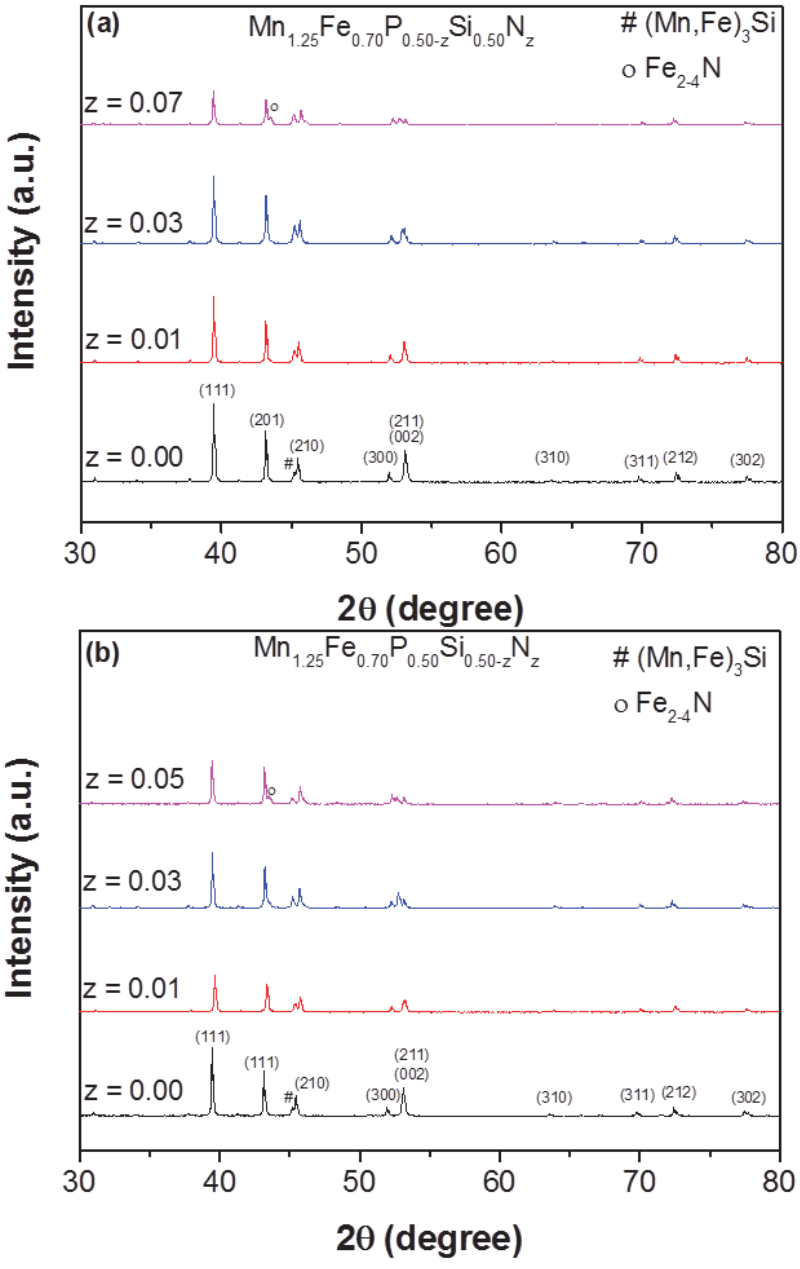

Figure 6.7: X-ray diffraction patterns measured at room temperature for $Mn_{1.25}Fe_{0.70}P_{0.5-z}Si_{0.5}N_z$ compounds (a) and for $Mn_{1.25}Fe_{0.70}P_{0.5}Si_{0.5-z}N_z$ compounds (b).

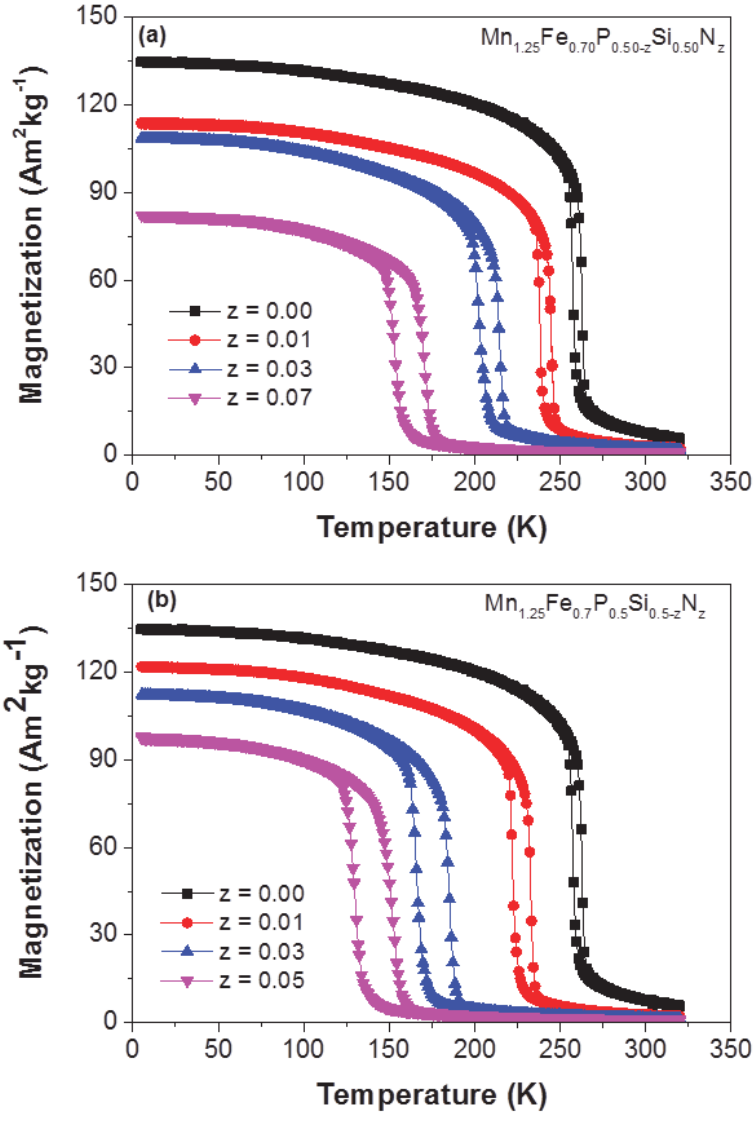

Figure 6.8: Magnetization curves measured on heating and cooling in a magnetic field of 1 T for the $Mn_{1.25}Fe_{0.70}P_{0.5-z}Si_{0.5}N_z$ (a) and $Mn_{1.25}Fe_{0.70}P_{0.5}Si_{0.5-z}N_z$ (b) compounds.

6.4. CONCLUSIONS

The influence of nitrogen additions on the crystal structure and the magnetocaloric properties of $(Mn,Fe)_2(P,Si)$ compounds has been discussed in detail. The addition of nitrogen leads to a slight variation in the unit-cell volume, indicating that nitrogen atoms enter the structure both as a substitutional and as an interstitial element. The addition of nitrogen leads to a moderate decrease in Curie temperature, while it preserves the magnetocaloric properties and improves the mechanical stability. It is found that the nitrogen addition provides a new control parameter to tune the Curie temperature and improves the mechanical properties of $(Mn,Fe)_2(P,Si)$ materials.

REFERENCES

[1] A. M. Tishin and Y. I. Spichkin, *The magnetocaloric effect and its applications* (Institue of Physics Publishing, Bristol, 2003).

[2] K. A. GschneidnerJr, V. K. Pecharsky, and A. O. Tsokol, *Recent developments in magnetocaloric materials,* Reports on Progress in Physics **68**, 1479 (2005).

[3] A. Smith, C. R. Bahl, R. Bjørk, K. Engelbrecht, K. K. Nielsen, and N. Pryds, *Materials Challenges for High Performance Magnetocaloric Refrigeration Devices,* Advanced Energy Materials **2**, 1288 (2012).

[4] V. K. Pecharsky and K. A. Gschneidner, *Giant magnetocaloric effect in $Gd_5(Si_2Ge_2)$,* Physical Review Letters **78**, 4494 (1997).

[5] H. Wada and Y. Tanabe, *Giant magnetocaloric effect of $MnAs_{1-x}Sb_x$,* Applied Physics Letters **79**, 3302 (2001).

[6] H. Wada, T. Morikawa, K. Taniguchi, T. Shibata, Y. Yamada, and Y. Akishige, *Giant magnetocaloric effect of $MnAs_{1-x}Sb_x$ in the vicinity of first-order magnetic transition,* Physica B: Condensed Matter **328**, 114 (2003).

[7] O. Tegus, E. Brück, K. H. J. Buschow, and F. R. de Boer, *Transition-metal-based magnetic refrigerants for room-temperature applications.* Nature **415**, 150 (2002).

[8] N. T. Trung, Z. Q. Ou, T. J. Gortenmulder, O. Tegus, K. H. J. Buschow, and E. Bruck, *Tunable thermal hysteresis in MnFe(P,Ge) compounds,* Applied Physics Letters **94**, 102513 (2009).

[9] D. T. Cam Thanh, E. Brück, N. T. Trung, J. C. P. Klaasse, K. H. J. Buschow, Z. Q. Ou, O. Tegus, and L. Caron, *Structure, magnetism, and magne-*

tocaloric properties of $MnFeP_{1-x}Si_x$ compounds, Journal of Applied Physics **103**, 07B318 (2008).

[10] F. Hu, B. Shen, J. Sun, Z. Cheng, G. Rao, and X. Zhang, *Influence of negative lattice expansion and metamagnetic transition on magnetic entropy change in the compound $LaFe_{11.4}Si_{1.6}$,* Applied Physics Letters **78**, 3675 (2001).

[11] F. X. Hu, M. Ilyn, A. M. Tishin, J. R. Sun, G. J. Wang, Y. F. Chen, F. Wang, Z. H. Cheng, and B. G. Shen, *Direct measurements of magnetocaloric effect in the first-order system $LaFe_{11.7}Si_{1.3}$,* Journal of Applied Physics **93**, 5503 (2003).

[12] A. Fujita, S. Fujieda, Y. Hasegawa, and K. Fukamichi, *Itinerant-electron metamagnetic transition and large magnetocaloric effects in $La(Fe_xSi_{1-x})_{13}$ compounds and their hydrides,* Physical Review B **67**, 104416 (2003).

[13] F. Guillou, H. Yibole, G. Porcari, L. Zhang, N. H. van Dijk, and E. Brück, *Magnetocaloric effect, cyclability and coefficient of refrigerant performance in the MnFe(P,Si,B) system,* Journal of Applied Physics **116**, 063903 (2014).

[14] J. Liu, T. Gottschall, K. P. Skokov, J. D. Moore, and O. Gutfleisch, *Giant magnetocaloric effect driven by structural transitions,* Nature Materials , 620 (2012).

[15] F. Guillou, H. Yibole, G. Porcari, and E. Brück, *Boron addition in MnFe(P,Si) magnetocaloric materials: interstitial vs substitutional scenarii,* Physica Status Solidi (C) **11**, 1007 (2014).

[16] Z. Ou, L. Caron, N. Dung, L. Zhang, and E. Brück, *Interstitial boron in MnFe(P,As) giant-magnetocaloric alloy,* Results in Physics **2**, 110 (2012).

[17] E. Brück, J. Kamarad, V. Sechovsky, Z. Arnold, O. Tegus, and F. de Boer, *Pressure effects on the magnetocaloric properties of $MnFeP_{1-x}As_x$,* Journal of Magnetism and Magnetic Materials **310**, e1008 (2007).

[18] H. Yabuta, K. Umeo, T. Takabatake, L. Chen, and Y. Uwatoko, *Pressure effects on the first order transition in MnFe(P,As) and MnFe(P,Ge),* Journal of Magnetism and Magnetic Materials **310**, 1826 (2007).

[19] X. F. Miao, L. Caron, Z. Gercsi, A. Daoud-Aladine, N. H. van Dijk, and E. Brück, *Thermal-history dependent magnetoelastic transition in $(Mn,Fe)_2(P,Si)$,* Applied Physics Letters **107**, 042403 (2015).

[20] *See http://www.ill.eu/sites/fullprof/index.html,* .

[21] H. M. Rietveld, *A profile refinement method for nuclear and magnetic structures,* Journal of Applied Crystallography **2**, 65 (1969).

[22] N. H. Dung, L. Zhang, Z. Q. Ou, and E. Brück, *Magnetoelastic coupling and magnetocaloric effect in hexagonal Mn–Fe–P–Si compounds,* Scripta Materialia **67**, 975 (2012).

7

TUNEABLE GIANT MAGNETOCALORIC EFFECT IN $(MN,FE)_2(P,SI)$ MATERIALS BY CO-B AND NI-B CO-DOPING

The influence of Co (Ni) and B co-doping on the structural, magnetic and magnetocaloric properties of $(Mn,Fe)_2(P,Si)$ compounds is investigated by X-ray diffraction, differential scanning calorimetry, magnetic and direct temperature change measurements. It is found that Co (Ni) and B co-doping is an effective approach to tune both the Curie temperature and the thermal hysteresis of $(Mn,Fe)_2(P,Si)$ materials without losing either the giant magnetocaloric effect or the positive effect of the B substitution on the mechanical stability. An increase in B concentration leads to a rapid decrease in thermal hysteresis, while an increase in the Co or Ni concentration hardly changes the thermal hysteresis of the $(Mn,Fe)_2(P,Si)$ compounds. However, the Curie temperature decreases slowly as a function of the Co or Ni content, while it increases dramatically for increasing B concentration. Hence, the co-substitution of Fe and P by Co (Ni) and B, respectively, offers a new control parameter to adjust the Curie temperature and reduce the thermal hysteresis of the $(Mn,Fe)_2(P,Si)$ materials.

This chapter is based on the published article: N. V. Thang, N. H. van Dijk and E. Brück, Materials, 2017, 10, 14.

7.1. INTRODUCTION

The magnetocaloric effect (MCE), which was first described in 1917 by Weiss and Piccard [1], [2], corresponds to the change in temperature when a magnetic field is changed under adiabatic conditions or the change in entropy when the field is changed under isothermal conditions. From a thermodynamic point of view, the isothermal magnetic entropy change ΔS_m and the adiabatic temperature change ΔT_{ad} are two characteristic parameters to evaluate the MCE of a magnetic material. ΔS_m is a measure of how much heat can be transported (at a given temperature) by magnetic means, while ΔT_{ad}, is a measure of how big the temperature difference is that can be achieved in the transfer of the heat to and from the heat transfer fluid [3]. In other words, ΔS_m determines the cooling capacity, and ΔT_{ad} is directly associated with the driving force of heat transfer and thus determines the cycle frequency. Hence, to evaluate the MCE adequately, both ΔS_m and ΔT_{ad} needs to be taken into account.

Magnetic materials that show a giant MCE have drawn widespread attention in the recent past due to their potential applications for room-temperature magnetic refrigeration [3], [4]. Compared to the conventional vapour-compression refrigeration, this cooling technology promises a 25 % higher energy efficiency and does not use dangerous and environmentally unfriendly refrigerants such as ozone depleting chemicals (e.g., chlorofluorocarbons (CFCs)), hazardous chemicals (e.g., ammonia (NH_3)) or greenhouse gases (e.g., hydrofluorocarbons (HFCs) and hydrochlorofluorocarbons (HCFCs)) [3], [5], [6]. This makes magnetic refrigeration one of the most promising technologies to replace vapour-compression refrigeration in the near future.

Materials displaying a first-order magnetic transition (FOMT) near room temperature are promising candidates for magnetic refrigeration because these materials show a larger magnetocaloric effect (MCE) than those showing a second-order magnetic transition. In second order magnetic phase transitions, the existence of short-range order and spin fluctuations above the Curie temperature (T_C) brings about a reduction in the maximum possible $\left|\left(\frac{\partial M}{\partial T}\right)_B\right|$ value, and the maximum MCE is thus reduced accordingly. In contrast, a first-order magnetic phase transition ideally occurs at a certain temperature (the transition temperature, T_t) and then the $\left|\left(\frac{\partial M}{\partial T}\right)_B\right|$ value should be theoretically infinitely large. Until now, the reported materials with a large MCE near room temperature are: $Gd_5(Si,Ge)_4$ [7]; Mn(As,Sb) [8], [9]; $(Mn,Fe)_2(P,X)$ with X = As, Ge, Si [10], [11], [12]; $LaFe_{13-x}Si_x$ and its hydrides [13], [14], [15]; $(Mn,Fe)_2(P,Si,B)$ [16]; $(Mn,Fe)_2(P,Si,N)$ [17]; NiMn-based Heusler alloys [18]; FeRh [19]; $MnCoGeB_x$ [20]; $MnCoGe_{1-x}Ga_x$ [21]; $MnCo_{1-x}Fe_xSi$ [22]. Among all above candidates for solid-state refrigerants, the $(Mn,Fe)_2(P,Si)$-based materials are one of the most promising because they

provide optimal conditions for practical applications (large MCE, low cost starting materials, and environmental benefits). $(Mn,Fe)_2(P,Si)$-based materials crystallize in the hexagonal Fe_2P-type structure (space group P-62m). In this structure, there are two specific metallic and non-metallic sites. For $3d$ transition metals, Mn preferentially occupies the $3g$ site at the pyramidal (x_2, 0, ½) position, while Fe preferentially occupies the $3f$ site at the tetrahedral (x_1, 0, 0) position. The non-metal elements P and Si occupy the $1b$ site at the (0, 0, ½) position and the $2c$ site at the (1/3, 1/3, 0) position with weakly preferred occupation of Si on the $2c$ site [23].

From an application point of view, $(Mn,Fe)_2(P,Si)$-based materials need to have a very small hysteresis that should at least be smaller than their adiabatic temperature change (ΔT_{ad}) and have a continuously tunable T_C close to the working temperature, so that they can be used as a feasible magnetic refrigerant material. Since the discovery of the $(Mn,Fe)_2(P,Si)$ system, much effort has been put into tuning the Curie temperature (T_C) and reducing the thermal hysteresis (ΔT_{hys}) without losing the giant MCE by varying the Mn/Fe and/or P/Si ratio [24]; by substituting Mn and Fe by other transition metal and rare earths [25] or by substituting P or Si by B [26], [27]. It has been found that boron substitution leads to an enhanced mechanical stability and a significant decrease in thermal hysteresis without losing the giant MCE [27], [28]. The substitution of either P or Si by B leads to a strong increase in T_C, which complicates tuning T_C by varying the boron content. In principle, one can keep the boron content constant and vary the Mn/Fe and/or P/Si ratio to tune T_C. However, the adjustment of the Mn/Fe and/or P/Si ratio often leads to either a decrease in the magnetization or an increase in the ΔT_{hys} , which is undesired for magnetic refrigeration. Hence, tuning T_C, while maintaining a thermal hysteresis as small as possible, is an essential step to practical magnetic refrigeration applications. It has recently been reported that the Co (Ni) substitution for either Mn or Fe lowers the Curie temperature and potentially reduces the thermal hysteresis [25], [29], [30]. Thus, co-doping of Co (Ni) and B in the $(Mn,Fe)_2(P,Si)$ system is expected to combine the positive effect of B substitution on improving the mechanical stability and reducing the thermal hysteresis, while T_C can be tuned more easily than for sole B doping.

In this work, we show that it is possible to reduce the thermal hysteresis and tune T_C, while keeping a large MCE and good mechanical stability in $(Mn,Fe)_2(P,Si)$ compounds by Co(Ni) and B co-doping.

7.2. EXPERIMENTAL

Three series of samples were prepared in the same way: first high-energy ball milling followed by solid-state sintering. In the first series, a variation of the

boron (B) content was applied for $Mn_{1.00}Fe_{0.85}Co_{0.10}P_{0.55-z}Si_{0.45}B_z$. In the second series a variation of the cobalt (Co) content was applied for $Mn_{1.00}Fe_{0.95-z}Co_zP_{0.51}Si_{0.45}B_{0.04}$. In the last series a variation of the nickel (Ni) content was applied for $Mn_{1.00}Fe_{0.95-z}Ni_zP_{0.51}Si_{0.45}B_{0.04}$. Stoichiometric quantities of the starting materials Mn, Fe, Co, red P, B and Si powders were ground in a planetary ball mill for 10 h with a constant rotation speed of 380 rpm. The planetary ball mill Fritsch Pulverisette with the grinding jars and ball made of tungsten carbide (7 balls with a diameter of 10 mm per jar) has been used to prepared all samples. The milled powders were compacted to small tablets (with a diameter of 12 mm and a height of 5-10 mm) with a pressure of 150 kgfcm^{-2}. After pressing, the tablets were sealed in quartz ampoules under 200 mbar of Ar before employing the double-step sintering described in Ref. [31] and quenching into water. It is worth noting that all samples have good mechanical stability, which was supported by the absence of cracking after cooling the samples in liquid nitrogen.

The X-ray diffraction (XRD) data of all samples were collected at various temperatures in a PANalytical X-pert Pro diffractometer equipped with an Anton Paar TTK450 low-temperature chamber using Cu-K_α radiation and were refined using the Fullprof program [32]. A differential scanning calorimeter (DSC) equipped with a liquid nitrogen cooling system was used to measure the specific heat. Magnetic measurements were carried out in a Superconducting Quantum Interference Device (SQUID) magnetometer (Quantum Design MPMS 5XL).

Direct measurements of the adiabatic temperature change ΔT_{ad} for powder samples were performed in a home-built experimental setup, which is designed to track the temperature of the magnetocaloric materials during magnetization and demagnetization processes while the surrounding temperature is slowly scanned over the temperature range of interest. For the direct measurements, a thermocouple was put in the middle of the sample holder, which is a small pylon-shaped plastic cup. Then, the sample holder was filled with the sample. Kapok was put on top of the powder to compress the powder, which helps increase the heat contact of the sample with the thermocouple. Finally, the sample holder was covered by a plastic cap. During the measurements, the sample holders move in and out a magnetic field generated by two permanent magnets at a frequency of 0.1 Hz. The temperature sweep rate of a climate chamber, which regulates the surrounding temperature, is about 0.5-1.5 K/min. This is relatively low with respect to the dT/dt related to the response time of the thermocouple (about 150 K/min). Hence, this set up can be considered operating under quasi-adiabatic conditions [33].

To ensure the reproducibility of the measurements, the measurements were carried out upon warming and cooling three times. Only the last warming and

cooling ΔT_{ad}(T) curves are presented in this work.

7.3. RESULTS AND DISCUSSION

7.3.1. $Mn_{1.00}Fe_{0.85}Co_{0.10}P_{0.55-z}Si_{0.45}B_z$ COMPOUNDS

The influence of Co and B co-doping on the (Mn,Fe)$_2$(P,Si)-based materials was first investigated in a batch of samples with a fixed Co concentration. Fig. 7.1 shows the XRD patterns measured at 400 K (a temperature at which all the compounds are in the paramagnetic state) of $Mn_{1.00}Fe_{0.85}Co_{0.10}P_{0.55-z}Si_{0.45}B_z$ compounds, with a nominal composition of z = 0.00, 0.02, 0.04 and 0.06. All samples were found to crystallize in the hexagonal Fe_2P-type structure (space group P-62m), indicating that the Co and B co-doping do not affect the Fe_2P phase formation. A small amount of (Mn,Fe)$_3$Si impurity phases, as often observed in this material system, is detected. The unit-cell volume decreases linearly for increasing B concentrations (about -0.23 Å^3/at.% B), which is in good agreement with the results reported by Guillou et al. [27] for the (Mn,Fe)$_2$(P,Si,B) system. Similar to the (Mn,Fe)$_2$(P,Si,B) system, the lattice parameter a decreases, while the lattice parameter c increases, leading to a decrease in the c/a ratio with increasing B content, as shown in Fig. 7.2.

The temperature dependence of the magnetization (M-T curve) measured in a magnetic field of 1 T for the $Mn_{1.00}Fe_{0.85}Co_{0.10}P_{0.55-z}Si_{0.45}B_z$ series is shown in Fig. 7.3. It is found that the Curie temperature (T_C) of the $Mn_{1.00}Fe_{0.85}Co_{0.10}P_{0.55-z}Si_{0.45}B_z$ compounds increases rapidly for increasing B concentrations, which is consistent with the evolution of the c/a ratio. Strikingly, there is a significant decrease in the thermal hysteresis when z increases. For the z = 0.00 and 0.02 samples, the magnetic transitions display a large thermal hysteresis, which is a clear signal for a first-order magnetic transition. Nevertheless, for the z = 0.04 and 0.06 samples, the magnetic transitions are close to the border between a first-order and a second-order magnetic transition, which is supported by a broad transition and a very small (or even not experimentally observable) thermal hysteresis. The corresponding values of the thermal hysteresis for z = 0.00, 0.02, 0.04 and 0.06 are ΔT_{hys} = 30.0, 17.0, 1.5, and 0.0 K, respectively. The average decrease in thermal hysteresis by B substitution is about 7 K/at.% B.

As can be seen in Fig. 7.4, the lower and broader peak in the specific heat curves at T_C indicate that the magnetic transition of the $Mn_{1.00}Fe_{0.85}Co_{0.10}P_{0.55-z}Si_{0.45}B_z$ compounds changes gradually from a first-order to a second-order magnetic transition for increasing z. Moreover, there is a decrease in the latent heat as a function of the boron content. The corresponding latent heat values obtained by the integration of the curves in zero field for z = 0.00, 0.02, 0.04 and 0.06 are 10.1, 8.0, 5.4 and 3.5 kJkg^{-1}, respectively. From

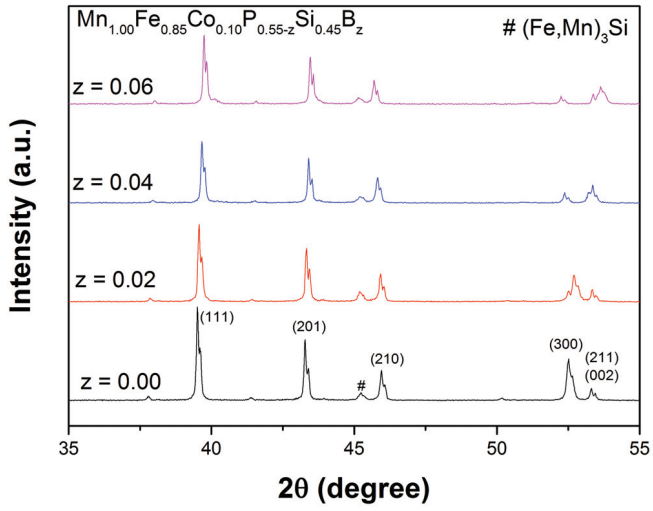

Figure 7.1: X-ray diffraction patterns measured at 400 K ($T > T_C$) for the $Mn_{1.00}Fe_{0.85}Co_{0.10}P_{0.55-z}Si_{0.45}B_z$ compounds

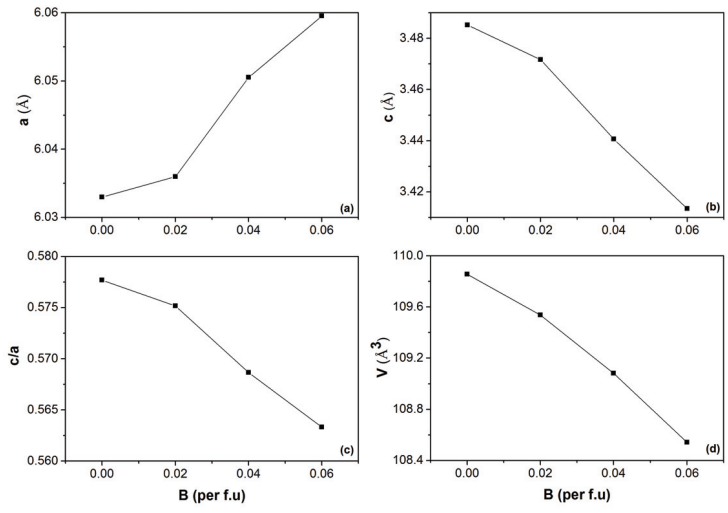

Figure 7.2: Lattice parameters a (a) and c (b), the c/a ratio (c) and the unit-cell volume V (d) obtained from XRD measurements at 400 K as a function of the B content for the $Mn_{1.00}Fe_{0.85}Co_{0.10}P_{0.55-z}Si_{0.45}B_z$ compounds.

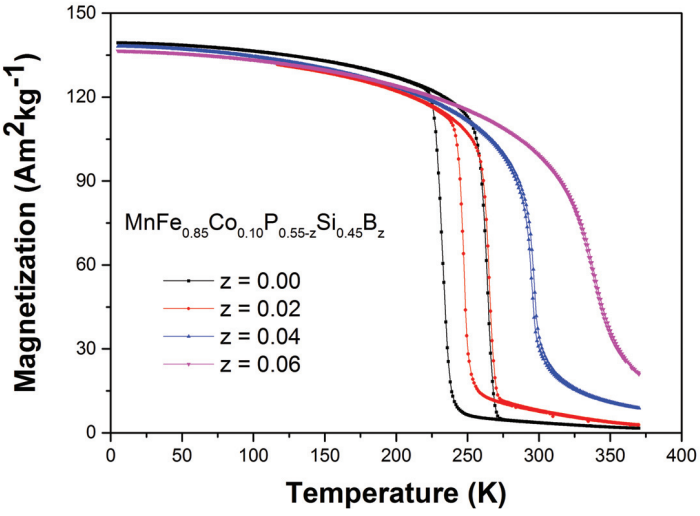

Figure 7.3: Magnetization as a function of temperature measured on heating and cooling in a magnetic field of 1 T for the $Mn_{1.00}Fe_{0.85}Co_{0.10}P_{0.55-z}Si_{0.45}B_z$ compounds. The temperature sweep rate is 2 K/min.

the above behavior, it is clear that an increase in the boron content weakens the first-order magnetic transition.

To evaluate the MCE of the $Mn_{1.00}Fe_{0.85}Co_{0.10}P_{0.51}Si_{0.45}B_{0.04}$ compound, the isofield magnetization M_B(T) curves are measured in the vicinity of T_C. The M_B(T) curves have been used (instead of the isothermal magnetization M_T(B) curves) to calculate the isothermal magnetic entropy change (ΔS_m) because the application of the Maxwell equation on the M_B(T) curves is expected to prevent the so-called "spike" caused by a phase co-existence [34], [35]. The isofield M_B(T) curves are first measured in field upon cooling and then upon heating with a rate of 2 Kmin^{-1}. For the calculation of ΔS_m only the data recorded upon cooling are used. Fig. 7.5(a) shows ΔS_m as a function of temperature in a field change of 1 and 2 T for the $Mn_{1.00}Fe_{0.85}Co_{0.10}P_{0.51}Si_{0.45}B_{0.04}$ compound. The absolute values of ΔS_m are 7.3 and 10.7 Jkg^{-1}K^{-1} for a field change of 1 and 2 T, respectively. The low value of the latent heat positively contributes to the large field dependence of the Curie temperature of $\frac{dT_C}{dB} = 5.18$ KT^{-1} found in the $Mn_{1.00}Fe_{0.85}Co_{0.10}P_{0.51}Si_{0.45}B_{0.04}$ compound.

To obtain additional information on the nature of the phase transition, an Arrot plot (see Fig. 7.5(b)) has been derived from the magnetic measurements in

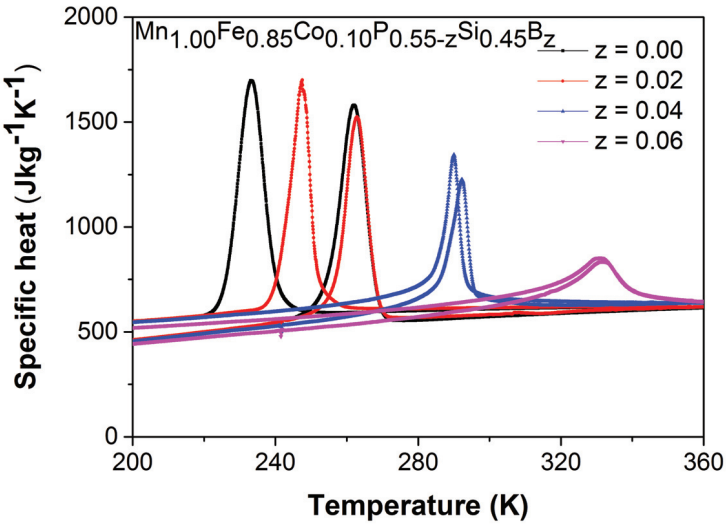

Figure 7.4: Specific heat derived from DSC measurements for the $Mn_{1.00}Fe_{0.85}Co_{0.10}P_{0.55-z}Si_{0.45}B_z$ compounds measured in zero field upon cooling and heating.

the vicinity of T_C. The S-shaped magnetization curve confirms the presence of a first-order magnetic transition for this sample.

The magnetic field dependence of the magnetization of the $Mn_{1.00}Fe_{0.85}Co_{0.10}P_{0.55-z}Si_{0.45}B_z$ compounds with z = 0.00, 0.02, 0.04 and 0.06 at T = 5 K is shown in Fig. 7.6. It is found that there is a slight decrease in the saturation magnetization (M_s) for increasing z.

7.3.2. $Mn_{1.00}Fe_{0.95-z}Co_zP_{0.51}Si_{0.45}B_{0.04}$

The results in Section 7.3.1 indicate that the $Mn_{1.00}Fe_{0.85}Co_{0.10}P_{0.51}Si_{0.45}B_{0.04}$ compound, which shows a large isothermal entropy change and a small thermal hysteresis, is a very promising candidate for room-temperature magnetic refrigeration. Hence, a batch of samples based on a variation in the cobalt content $Mn_{1.00}Fe_{0.95-z}Co_zP_{0.51}Si_{0.45}B_{0.04}$ was prepared with the aim of tuning T_C without losing the giant MCE or increasing (ΔT_{hys}) in the (Mn,Fe)$_2$(P,Si) system.

The evolution of the lattice parameters and unit-cell volume as a function of temperature for the $Mn_{1.00}Fe_{0.95-z}Co_zP_{0.51}Si_{0.45}B_{0.04}$ is presented in Fig. 7.7. The most prominent feature is the abrupt jump in the lattice parameters at the ferro to paramagnetic phase transition. This confirms the existence of a first-

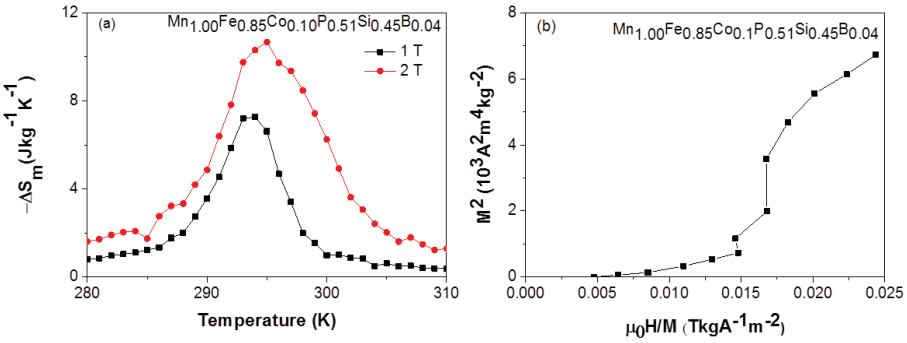

Figure 7.5: (a) Magnetic entropy change (ΔS_m) as a function of temperature for a field change of 1 T (black markers) and 2 T (red markers) (b) Arrot plots derived from isofield M_B(T) curves measured upon cooling in the vicinity of T_C for the $Mn_{1.00}Fe_{0.85}Co_{0.10}P_{0.51}Si_{0.45}B_{0.04}$ compound.

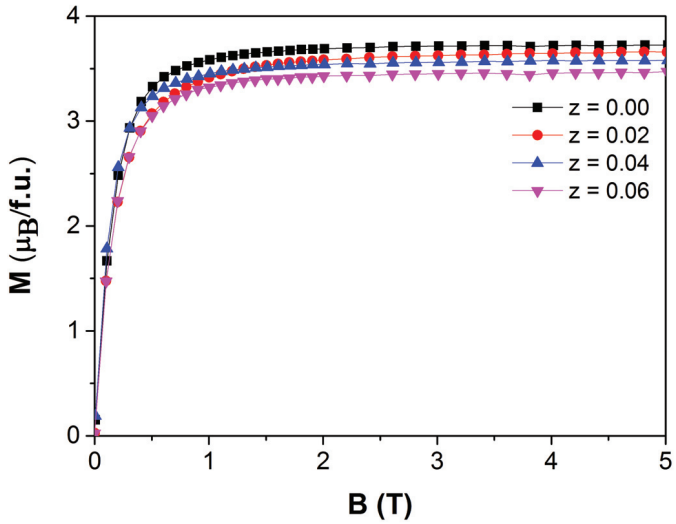

Figure 7.6: Field dependence of the magnetization of $Mn_{1.00}Fe_{0.85}Co_{0.10}P_{0.55-z}Si_{0.45}B_z$ compounds measured at a temperature of 5 K.

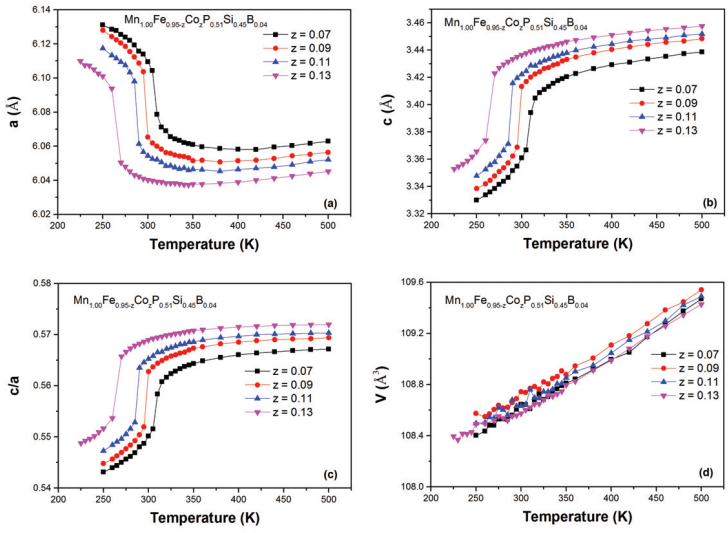

Figure 7.7: Temperature dependence of the lattice parameters a (a) and c (b), the c/a ratio (c) and the unit-cell volume V (d) for the $Mn_{1.00}Fe_{0.95-z}Co_zP_{0.51}Si_{0.45}B_{0.04}$ compounds with z = 0.07, 0.09, 0.11 and 0.13, derived from X-ray diffraction patterns measured upon heating.

7

order magneto-elastic transition (FOMET). Three main features can be noticed for the influence of Co and B co-doping. First, the lattice parameter a decreases, while c increases, both in the ferromagnetic (FM) state and in the paramagnetic (PM) state for an increasing Co content. Second, the combined evolution of a and c results in an increase in the c/a ratio, both in the FM state and in the PM state. Finally, there is a very small volume change at the magnetic transition for these samples because the a and c parameters change in opposite direction. It is worth noting that, similar to $(Mn,Fe)_2(P,Si,B)$ system, there is no noticeable ΔV at the FOMET ($\Delta V/V < 0.05$ %). Guillou et al. [26] established that the absence of a unit-cell volume change at the transition improves the mechanical stability in the $(Mn,Fe)_2(P,Si,B)$ system in comparison to the $(Mn,Fe)_2(P,Si)$ compounds. The Co and B co-doping still takes advantage of the strong impact of the B substitution to provide an enhanced mechanical stability.

Fig. 7.8 shows the M-T curves measured in a magnetic field of 1 T for the $Mn_{1.00}Fe_{0.95-z}Co_zP_{0.51}Si_{0.45}B_{0.04}$ series. Consistent with the results reported by Huliyageqi et al. [30], it is found that an increase in the Co concentration lowers the Curie temperature, while the ΔT_{hys} value is retained to be very small (ΔT_{hys} = 1-2 K) with a sharp transition at T_C. The corresponding values of T_C obtained

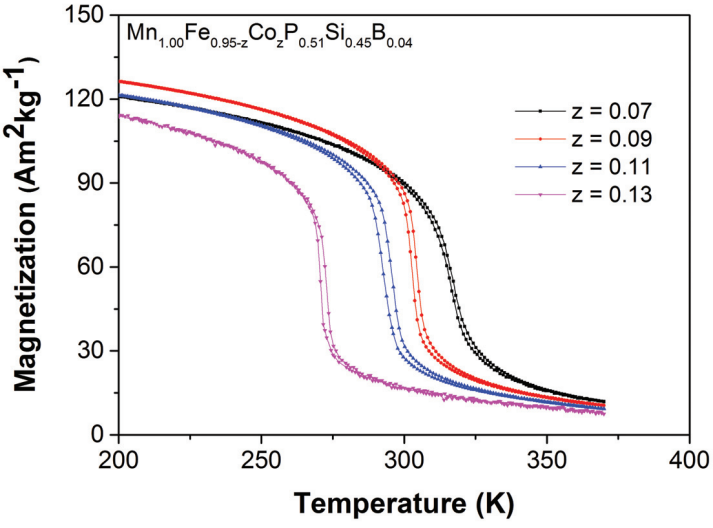

Figure 7.8: Magnetization as a function of temperature measured on heating and cooling in a magnetic field of 1 T for the $Mn_{1.00}Fe_{0.95-z}Co_zP_{0.51}Si_{0.45}B_{0.04}$ compounds. The temperature sweep rate is 2 K/min

from the heating curves for z = 0.07, 0.09, 0.11 and 0.13 are 316, 304, 295 and 272 K, respectively. Hence, keeping the B content constant and varying the Co content provides a handle to tune T_C in a broad range around room temperature, while maintaining a very small thermal hysteresis. The variations in T_C, ΔS_m, ΔT_{hys} as a function of Co content for the $Mn_{1.00}Fe_{0.95-z}Co_zP_{0.51}Si_{0.45}B_{0.04}$ compounds are summarized in Table 7.1.

Table 7.1: Curie temperature (T_C) derived from the magnetization curves measured on heating, the isothermal entropy change (ΔS_m) derived from the isofield magnetization curves in a field change of 0.5, 1.0, 1.5 and 2.0 T, thermal hysteresis (ΔT_{hys}) derived from the magnetization curves measured in 1 T upon cooling and heating for the $Mn_{1.00}Fe_{0.95-z}Co_zP_{0.51}Si_{0.45}B_{0.04}$ compounds.

z	T_C	ΔS_m (JK^{-1}kg^{-1})				ΔT_{hys} (K)
		ΔB = 0.5 T	ΔB = 1.0 T	ΔB = 1.5T	ΔB = 2.0 T	
0.07	316	2.7	5.3	6.8	8.1	1.3
0.09	304	5.0	9.1	10.7	11.9	1.7
0.11	295	3.7	7.7	10.0	11.4	2.5
0.13	272	7.7	9.2	10.6	11.5	1.9

Although Co and B co-doping leads to a partial loss of magnetic transition sharpness compared to (Mn,Fe)$_2$(P,Si)-based materials, the ΔS_m derived from

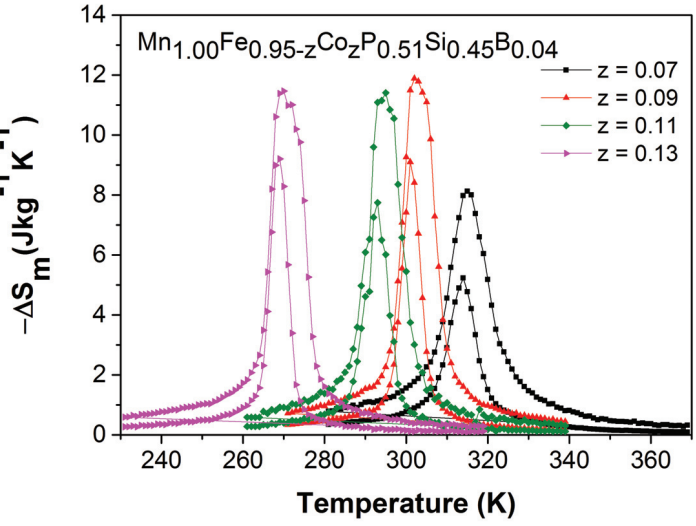

Figure 7.9: Magnetic entropy change as a function of temperature for a field change of 1 T (lower curve) and 2 T (upper curve) derived from isofield M_B(T) curves measured upon cooling in the vicinity of T_C for the $Mn_{1.00}Fe_{0.95-z}Co_zP_{0.51}Si_{0.45}B_{0.04}$ compounds

the isofield magnetization curves, presented in Fig. 7.9, is still comparable to those reported for giant-MCE materials like (Mn,Fe)$_2$(P,Si,B) [26], $Gd_5Si_2Ge_2$, Heusler alloys and La(Fe,Si)$_{13}H_y$ [6]. The peak values, which are weakly depending on the Co content, are in the range of 5-9 and 9-12 $JK^{-1}kg^{-1}$ for a field change of 1 and 2 T, respectively.

The adiabatic temperature change obtained from the direct measurements on the $Mn_{1.00}Fe_{0.95-z}Co_zP_{0.51}Si_{0.45}B_{0.04}$ compounds is shown in Fig. 7.10. For a field change of 1.1 T, the ΔT_{ad} of the $Mn_{1.00}Fe_{0.95-z}Co_zP_{0.51}Si_{0.45}B_{0.04}$ powder samples varies from 1.8 to 2.0 K, which is comparable or slightly higher than those of the (Mn,Fe)$_2$(P,Si)-based materials [36]. It should be noted that we used powder samples rather than bulk samples for these direct measurements, which leads to a potential underestimation of the adiabatic temperature change due to lower thermal conductance between the sample and the thermocouple. In other words, the real ΔT_{hys} values of $Mn_{1.00}Fe_{0.95-z}Co_zP_{0.51}Si_{0.45}B_{0.04}$ compounds should be higher.

In Fig. 7.11, the magnetic field dependence of the magnetization for the $Mn_{1.00}Fe_{0.95-z}Co_zP_{0.51}Si_{0.45}B_{0.04}$ samples with z = 0.07, 0.09, 0.11 and 0.13 at 5 K is shown. Interestingly, there is hardly any change in the saturation mag-

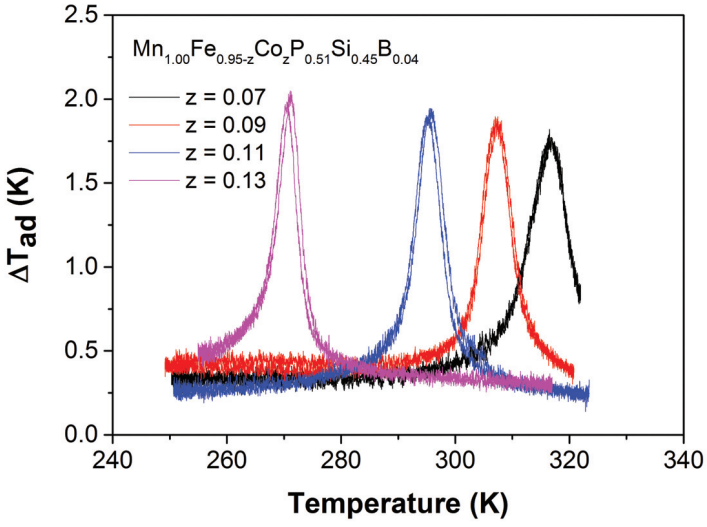

Figure 7.10: Temperature dependence of the adiabatic temperature change obtained by direct measurements for the $Mn_{1.00}Fe_{0.95-z}Co_zP_{0.51}Si_{0.45}B_{0.04}$ compounds in a magnetic field change of ΔB = 1.1 T.

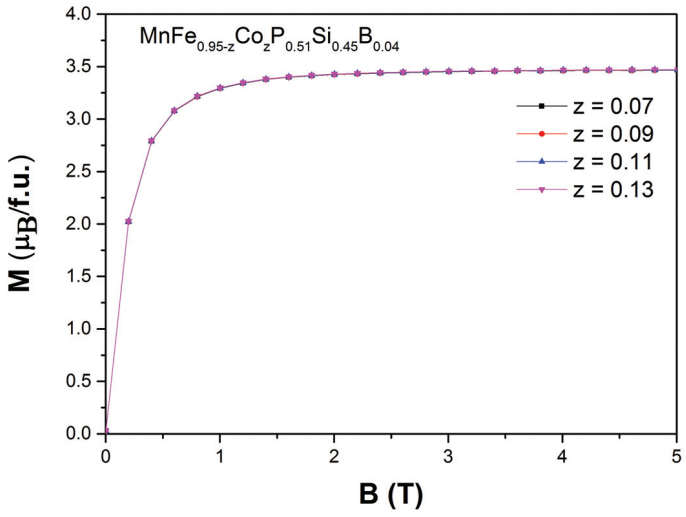

Figure 7.11: Magnetization of the $Mn_{1.00}Fe_{0.95-z}Co_zP_{0.51}Si_{0.45}B_{0.04}$ compounds as a function of the applied magnetic field measured at a temperature of 5 K.

netization (M_s) for increasing Co content. Therefore, when combining a fixed B concentration with varying the Co content, the size of the magnetic moments and the thermal hysteresis of (Mn,Fe,Co)$_2$(P,Si,B)-based materials are retained, while keeping a large MCE in a wide range of working temperatures.

7.3.3. $Mn_{1.00}Fe_{0.95-z}Ni_zP_{0.51}Si_{0.45}B_{0.04}$

The experimental results in section 7.3.2 show that co-doping of Co and B in the (Mn,Fe)$_2$(P,Si) system offers a new control parameter to tune T_C while keeping a small thermal hysteresis and preserving the positive effect of boron addition on the mechanical stability. However, Co is quite expensive, which affects fabrication costs, one of the most important factors for commercial applications. Hence, it is desirable to find another element that can replace Co, without any significant effect on both MCE and mechanical properties in (Mn,Fe,Co)$_2$(P,Si,B) compounds, to lower fabrication costs. The experimental results from Wada et al. [25] show that the substitution of Fe by Ni in the (Mn,Fe)$_2$(P,Si) system has the same effect as Co substitution on both the Curie temperature and the thermal hysteresis. Moreover, Ni is three times cheaper than Co [37]. This suggests that Ni is an ideal choice to replace Co in the (Mn,Fe,Co)$_2$(P,Si,B) system.

The XRD patterns of $Mn_{1.00}Fe_{0.95-z}Ni_zP_{0.51}Si_{0.45}B_{0.04}$ compounds with z = 0.06, 0.08, 0.10 and 0.12 shown in Fig. 7.12 indicate that the co-substitution of Fe by Ni and P by B does not change the crystal structure. All the samples crystallize in the hexagonal Fe_2P-type structure (space group P-62m). The structure refinement results show that an increase in the Ni content leads to an increase in the c/a ratio resulting in a lower T_C.

The magnetization versus temperature curves of the $Mn_{1.00}Fe_{0.95-z}Ni_zP_{0.51}Si_{0.45}B_{0.04}$ compounds upon cooling and heating in an applied field of 1 T shown in Fig. 7.13 indicate that all the samples have a sharp first-order magnetic transitions around T_C. Similar to Co doping, an increase in Ni concentration leads to a decrease in T_C, which is consistent with the results reported by Wada et al. [25]. It is worth noting that the change in Ni content does not significantly affect the thermal hysteresis. While T_C amounts to 308, 298, 289 and 265 K for the samples with z = 0.06, 0.08, 0.10 and 0.12, respectively, the thermal hysteresis remains constant at 1-2 K.

Fig. 7.14 shows ΔS_m of the $Mn_{1.00}Fe_{0.95-z}Ni_zP_{0.51}Si_{0.45}B_{0.04}$ compounds in a field change of 1 and 2 T. The ΔS_m was derived from the isofield magnetization curves using the Maxwell relation. The peak values, which are weakly depending on the Ni content, are in the range of 6-8 and 9-13 $JK^{-1}kg^{-1}$ for a field change of 1 and 2 T, respectively. Compared to the Co and B co-doping system, the isothermal magnetic entropy change of Ni and B co-doping system is slightly lower.

The adiabatic temperature change ΔT_{ad} derived from the direct measure-

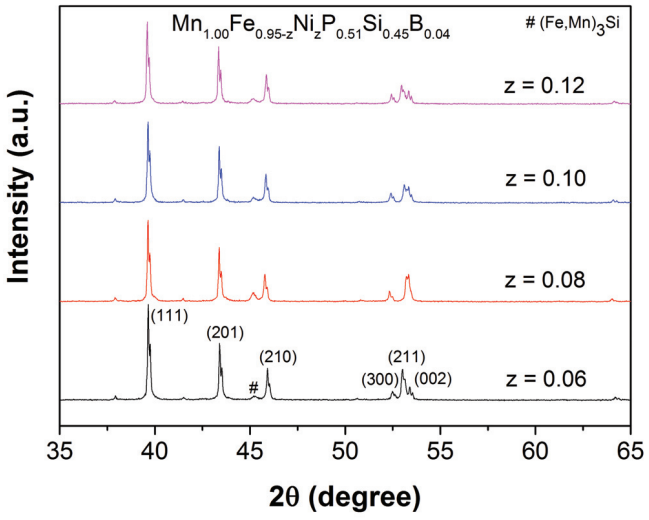

Figure 7.12: X-ray diffraction patterns measured at 400 K for the $Mn_{1.00}Fe_{0.95-z}Ni_zP_{0.51}Si_{0.45}B_{0.04}$ compounds.

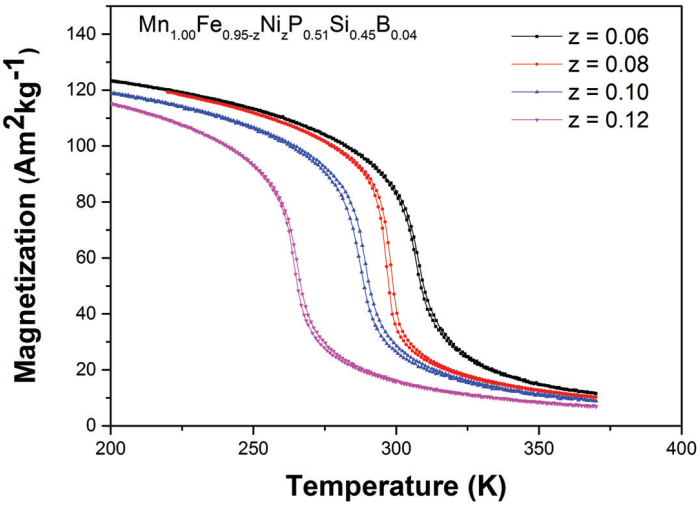

Figure 7.13: Magnetization as a function of temperature measured on heating and cooling in a magnetic field of 1 T for the $Mn_{1.00}Fe_{0.95-z}Ni_zP_{0.51}Si_{0.45}B_{0.04}$ compounds. The applied sweep rate is 2 K/min.

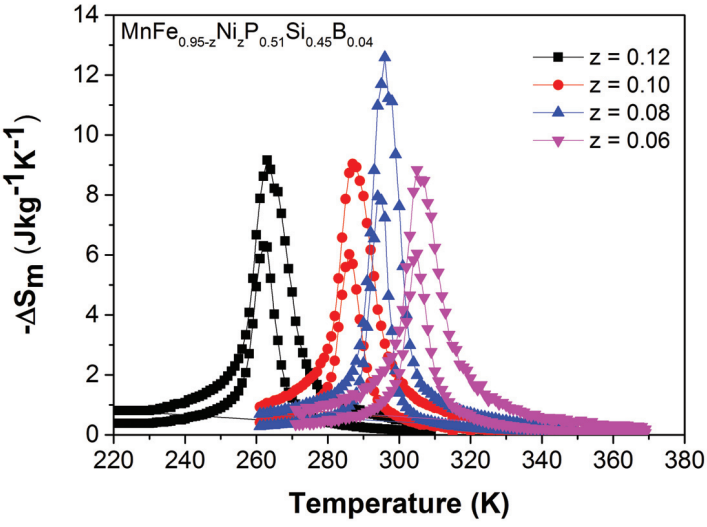

Figure 7.14: Magnetic entropy change as a function of temperature for a field change of 1 T (lower curve) and 2 T (upper curve) derived from isofield M_B(T) curves measured upon cooling in the vicinity of TC for the $Mn_{1.00}Fe_{0.95-z}Ni_zP_{0.51}Si_{0.45}B_{0.04}$ compounds

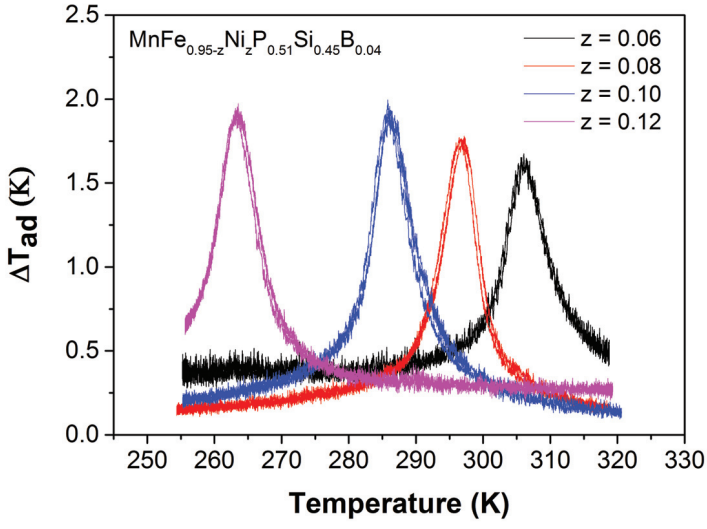

Figure 7.15: Temperature dependence of the adiabatic temperature change obtained by direct measurements for a magnetic field change of ΔB = 1.1 T.

ments is shown in Fig. 7.15. For a field change of 1.1 T, the ΔT_{ad} varies from 1.7 to 1.9 K. The ΔT_{ad}(T) of $Mn_{1.00}Fe_{0.95-z}Ni_zP_{0.51}Si_{0.45}B_{0.04}$ powder is comparable or slightly lower than that of Co and B co-doping samples. Hence, along with Co and B co doping, co-doping of Ni and B also offers an additional control parameter to tune T_C and adjust the thermal hysteresis while maintaining a large MCE and improving mechanical properties in $(Mn,Fe)_2(P,Si)$ compounds. This makes the $Mn_{1.00}Fe_{0.95-z}Ni_zP_{0.51}Si_{0.45}B_{0.04}$ compounds also very promising for room-temperature magnetic refrigeration.

7.4. CONCLUSIONS

$(Mn,Fe,Co)_2(P,Si,B)$-based and $(Mn,Fe,Ni)_2(P,Si,B)$-based materials have been prepared by high-energy ball milling and solid-state reaction. The effect of the co-substitution of Fe by Co or Ni and P by B on T_C, ΔT_{hys} and the MCE has been studied systematically by X-ray diffraction (XRD), differential scanning calorimetry (DSC), magnetic and direct temperature change measurements. The experimental results show that by Co (Ni) and B co-doping, the thermal hysteresis is tunable to very small values (or even not experimentally observable), while maintaining a large MCE in a wide temperature range around room temperature. T_C can be tuned from 272 to 316 K and from 265 to 308 K by varying Co content and Ni content, respectively. Therefore, co-substitution of Fe by Co (Ni) and P by B is found to be a promising approach to tune the Curie temperature, while keeping the thermal hysteresis as small as possible, maintaining a giant MCE and improving the mechanical stability in the $(MnFe)_2(P,Si)$ system. This makes $(Mn,Fe,Co)_2(P,Si,B)$ and $(Mn,Fe,Ni)_2(P,Si,B)$ compounds highly promising for near room-temperature magnetic refrigeration. In other words, Co-B and Ni-B co-doping offers new control parameters to bring practical magnetic cooling near room temperature a step closer.

REFERENCES

[1] P. Weiss and A. Picard, *Le phènomène magnètocalorique,* Journal de Physique Théorique et Appliquée **7**, 103 (1917).

[2] A. Smith, *Who discovered the magnetocaloric effect?* The European Physical Journal H **38**, 507 (2013).

[3] A. Smith, C. R. Bahl, R. Bjørk, K. Engelbrecht, K. K. Nielsen, and N. Pryds, *Materials Challenges for High Performance Magnetocaloric Refrigeration Devices,* Advanced Energy Materials **2**, 1288 (2012).

[4] V. Franco, J. Blázquez, B. Ingale, and A. Conde, *The Magnetocaloric Effect*

and Magnetic Refrigeration Near Room Temperature: Materials and Models, Annual Review of Materials Research **42**, 305 (2012).

[5] A. M. Tishin and Y. I. Spichkin, *The magnetocaloric effect and its applications* (Institue of Physics Publishing, Bristol, 2003).

[6] K. GschneidnerJr, V. Pecharsky, and A. Tsokol, *Recent developments in magnetocaloric materials,* Reports on Progress in Physics **68**, 1479 (2005).

[7] V. K. Pecharsky and K. A. Gschneidner, *Giant Magnetocaloric Effect in $Gd_5(Si_2Ge_2)$,* Physical Review Letters **78**, 4494 (1997).

[8] H. Wada and Y. Tanabe, *Giant magnetocaloric effect of $MnAs_{1-x}Sb_x$,* Applied Physics Letters **79**, 3302 (2001).

[9] H. Wada, T. Morikawa, K. Taniguchi, T. Shibata, Y. Yamada, and Y. Akishige, *Giant magnetocaloric effect of $MnAs_{1-x}$ Sb_x in the vicinity of first-order magnetic transition,* Physica B: Condensed Matter **328**, 114 (2003).

[10] O. Tegus, E. Brück, K. H. J. Buschow, and F. R. de Boer, *Transition-metal-based magnetic refrigerants for room-temperature applications.* Nature **415**, 150 (2002).

[11] N. T. Trung, Z. Q. Ou, T. J. Gortenmulder, O. Tegus, K. H. J. Buschow, and E. Brück, *Tunable thermal hysteresis in MnFe(P,Ge) compounds,* Applied Physics Letters **94**, 102513 (2009).

[12] D. T. Cam Thanh, E. Brück, N. T. Trung, J. C. P. Klaasse, K. H. J. Buschow, Z. Q. Ou, O. Tegus, and L. Caron, *Structure, magnetism, and magnetocaloric properties of $MnFeP_{1-x}Si_x$ compounds,* Journal of Applied Physics **103**, 07B318 (2008).

[13] F. Hu, B. Shen, J. Sun, Z. Cheng, G. Rao, and X. Zhang, *Influence of negative lattice expansion and metamagnetic transition on magnetic entropy change in the compound $LaFe_{11.4}Si_{1.6}$,* Applied Physics Letters **78**, 3675 (2001).

[14] F. X. Hu, M. Ilyn, A. M. Tishin, J. R. Sun, G. J. Wang, Y. F. Chen, F. Wang, Z. H. Cheng, and B. G. Shen, *Direct measurements of magnetocaloric effect in the first-order system $LaFe_{11.7}Si_{1.3}$,* Journal of Applied Physics **93**, 5503 (2003).

[15] A. Fujita, S. Fujieda, Y. Hasegawa, and K. Fukamichi, *Itinerant-electron metamagnetic transition and large magnetocaloric effects in $La(Fe_xSi_{1-x})_{13}$ compounds and their hydrides,* Physical Review B **67**, 104416 (2003).

[16] F. Guillou, H. Yibole, G. Porcari, L. Zhang, N. H. van Dijk, and E. Brück, *Magnetocaloric effect, cyclability and coefficient of refrigerant performance in the MnFe(P,Si,B) system,* Journal of Applied Physics **116**, 063903 (2014).

[17] N. Thang, X. Miao, N. van Dijk, and E. Brück, *Structural and magnetocaloric properties of (Mn,Fe)$_2$(P,Si) materials with added nitrogen,* Journal of Alloys and Compounds **670**, 123 (2016).

[18] J. Liu, T. Gottschall, K. P. Skokov, J. D. Moore, and O. Gutfleisch, *Giant magnetocaloric effect driven by structural transitions,* Nature Materials **11**, 620 (2012).

[19] S. A. Nikitin, G. Myalikgulyev, A. M. Tishin, M. P. Annaorazov, K. A. Asatryan, and A. L. Tyurin, *The magnetocaloric effect in $Fe_{49}Rh_{51}$ compound,* Physical Letters A **148**, 363 (1990).

[20] A. Quintana-Nedelcos, J. Sánchez Llamazares, and H. Flores-Zuñiga, *On the magnetostructural transition in $MnCoGeB_x$ alloy ribbons,* Journal of Alloys and Compounds **644**, 1003 (2015).

[21] D. Zhang, Z. Nie, Z. Wang, L. Huang, Q. Zhang, and Y. D. Wang, *Giant magnetocaloric effect in MnCoGe with minimal Ga substitution,* Journal of Magnetism and Magnetic Materials **387**, 107 (2015).

[22] J. Chen, Z. Wei, E. Liu, X. Qi, W. Wang, and G. Wu, *Structural and magnetic properties of $MnCo_{1-x}Fe_xSi$ alloys,* Journal of Magnetism and Magnetic Materials **387**, 159 (2015).

[23] X. F. Miao, L. Caron, P. Roy, N. H. Dung, L. Zhang, W. A. Kockelmann, R. A. de Groot, N. H. van Dijk, and E. Brück, *Tuning the phase transition in transition-metal-based magnetocaloric compounds,* Physical Review B **89**, 174429 (2014).

[24] N. Dung, *Moment formation and giant magnetocaloric effects in hexagonal Mn-Fe-P-Si compounds*, Ph.D. thesis, TU Delft (2012).

[25] H. Wada, T. Takahara, K. Katagiri, T. Ohnishi, K. Soejima, and K. Yamashita, *Recent progress of magnetocaloric effect and magnetic refrigerant materials of Mn compounds (invited),* Journal of Applied Physics **117**, 172606 (2015).

[26] F. Guillou, G. Porcari, H. Yibole, N. van Dijk, and E. Brück, *Taming the first-order transition in giant magnetocaloric materials.* Advanced materials (Deerfield Beach, Fla.) **26**, 2671 (2014).

[27] F. Guillou, H. Yibole, N. van Dijk, and E. Brück, *Effect of boron substitution on the ferromagnetic transition of $MnFe_{0.95}P_{2/3}Si_{1/3}$*, Journal of Alloys and Compounds **632**, 717 (2015).

[28] F. Guillou, H. Yibole, N. van Dijk, L. Zhang, V. Hardy, and E. Brück, *About the mechanical stability of MnFe(P,Si,B) giant-magnetocaloric materials,* Journal of Alloys and Compounds **617**, 569 (2014).

[29] Z. Ou, *Magnetic structure and phase formation of magnetocaloric Mn-Fe-P-X compounds*, Ph.D. thesis, TU Delft (2013).

[30] B. Huliyageqi, Y.-x. Geng, Y.-j. Li, and O. Tegus, *A significant reduction of hysteresis in MnFe(P,Si) compounds,* Journal of the Korean Physical Society **63**, 525 (2013).

[31] N. H. Dung, L. Zhang, Z. Q. Ou, L. Zhao, L. van Eijck, A. M. Mulders, M. Avdeev, E. Suard, N. H. van Dijk, and E. Brück, *High/low-moment phase transition in hexagonal Mn-Fe-P-Si compounds,* Physical Review B **86**, 045134 (2012).

[32] *Available online: http://www.ill.eu/sites/fullprof/index.html,* .

[33] H. Yibole, *Nature of the first-order magnetic phase transition in giant-magnetocaloric materials*, Ph.D. thesis, TU Delft (2016).

[34] L. Tocado, E. Palacios, and R. Burriel, *Entropy determinations and magnetocaloric parameters in systems with first-order transitions: Study of MnAs,* Journal of Applied Physics **105**, 093918 (2009).

[35] A. M. G. Carvalho, A. Coelho, P. von Ranke, and C. Alves, *The isothermal variation of the entropy (ΔS_T) may be miscalculated from magnetization isotherms in some cases: MnAs and $Gd_5Ge_2Si_2$ compounds as examples,* Journal of Alloys and Compounds **509**, 3452 (2011).

[36] H. Yibole, F. Guillou, L. Zhang, N. H. van Dijk, and E. Brück, *Direct measurement of the magnetocaloric effect in MnFe(P, X) (X = As, Ge, Si) materials,* Journal of Physics D: Applied Physics **47**, 075002 (2014).

[37] *Available online: http://www.infomine.com/investment/metal-prices/,* .

8

EFFECT OF CARBON DOPING ON THE STRUCTURE AND MAGNETIC PHASE TRANSITION IN $(Mn,Fe)_2(P,Si)$

Given the potential applications of $(Mn,Fe)_2(P,Si)$-based materials for room-temperature magnetic refrigeration, several research groups have carried out fundamental studies aimed at understanding the role of the magneto-elastic coupling in the first-order magnetic transition and further optimizing this system. Inspired by the beneficial effect of the addition of boron on the magnetocaloric effect of $(Mn,Fe)_2(P,Si)$-based materials, we have investigated the effect of carbon (C) addition on the structural properties and the magnetic phase transition of $Mn_{1.25}Fe_{0.70}P_{0.50}Si_{0.50}C_z$ and $Mn_{1.25}Fe_{0.70}P_{0.55}Si_{0.45}C_z$ compounds by X-ray diffraction, neutron diffraction and magnetic measurements in order to find an additional control parameter to further optimize the performance of these materials. All samples crystallize in the hexagonal Fe_2P-type structure (space group P-62m), suggesting that C doping does not affect the phase formation. It is found that the Curie temperature increases, while the thermal hysteresis and the isothermal magnetic entropy change decrease by adding carbon. Room-temperature neutron diffraction experiments on $Mn_{1.25}Fe_{0.70}P_{0.55}Si_{0.45}C_z$ compounds reveal that the added C substitutes P/Si on the 2c site and/or occupies the 6k interstitial site of the hexagonal Fe_2P-type structure.

8.1. INTRODUCTION

Room-temperature magnetic refrigeration exploiting the magnetocaloric effect (MCE) of magnetic materials has the potential to address the disadvantages of conventional vapor-compression refrigeration when it comes to the environmental impact, energy efficiency and device volume [1],[2],[3]. Magnetic marterials, which show large low-field magnetocaloric effect in the vicinity of the Curie temperature close to the working temperature, have been attracting increasing attention over the past few decades due to their potential applications for room-temperature magnetic refrigeration. During the past decades, a large MCE in the room-temperature range has been observed in several classes of materials including $Gd_5(Si,Ge)_4$ [4]; MnAs and Mn(As,Sb) [5],[6]; $(Mn,Fe)_2(P,X)$ with X = As, Ge, Si [7],[8],[9]; $(Mn,Fe)_2(P,Si,B)$ [10]; $MnCoGeB_x$ [11]; $MnCoGe_{1-x}Ga_x$ [12]; $MnCo_{1-x}Fe_xSi$ [13]; $La(Fe,Si)_{13}$ and their hydrides [14],[15]; $La(Mn,Fe,Si)_{13}H_z$ [16]; $Fe_{49}Rh_{51}$ [17] and Heusler alloys [18],[19]. A combination of a large MCE, tuneable Curie temperature, limited thermal hysteresis, non-toxic and abundant ingredients makes $(Mn,Fe)_2(P,Si)$-based compounds one of the most attractive candidate materials for commercial room-temperature magnetic refrigeration.

In order to cover a wide range of temperatures, different magnetocaloric materials with the desired variation in T_C are required, while having both a large MCE and a small thermal hysteresis. With the aim to tune the Curie temperature and reduce the thermal hysteresis, while improving the mechanical stability and maintaining an acceptable MCE in the $(Mn,Fe)_2(P,Si)$ system, a lot of work has recently been done by balancing the Mn:Fe ratio and P:Si ratios [20],[21], by the introduction of nitrogen [22], [23], by varying the duration and temperature of the heat treatment [24] and by Co-B and Ni-B co-doping [25]. Miao and coworkers [23] have recently shown that the magnetic transition of $(Mn,Fe)_2(P,Si)$ can be tailored by adding C. The C atoms were found to occupy the interstitial $6k$ and $6j$ sites in the hexagonal structure. The aim of the present study is to obtain the complementary information on the influence of C additions on the magnetocaloric properties, which is key information that needs to be taken into account for practical applications. Based on the earlier studies by Miao and coworkers [23] the C atoms were expected to be introduced interstitially and therefore the C was added to the composition (rather than substituted for another element).

To study the influence of C on the structural and magnetocaloric properties of $(Mn,Fe)_2(P,Si)$-based materials, in this work, C was added to the $Mn_{1.25}Fe_{0.70}P_{0.50}Si_{0.50}$ and $Mn_{1.25}Fe_{0.70}P_{0.55}Si_{0.45}$ compounds. These two compounds have been chosen for this work due to their different magnitude of the latent heat. In fact, an increase in P/Si ratio leads to a stronger first-order magnetic transition. The influence of C addition on the structural, magnetic and

magnetocaloric properties of the compounds obtained was systematically investigated by X-ray diffraction and magnetic measurements. In order to determine the occupancy of C added in the crystal structure, room-temperature neutron diffraction was employed for $Mn_{1.25}Fe_{0.70}P_{0.55}Si_{0.45}C_z$ compounds. This may allow understanding the relation between the changes in crystal structure and in the magnetic phase transition.

8.2. EXPERIMENTAL

To investigate the influence of carbon addition on the structural properties and magnetic phase transition, two series of samples, $Mn_{1.25}Fe_{0.70}P_{0.50}Si_{0.50}C_z$ and $Mn_{1.25}Fe_{0.70}P_{0.55}Si_{0.45}C_z$, were prepared by high-energy ball milling followed by a conventional double-step annealing process [26]. The mixtures of 15 g starting materials, namely Fe, Mn, red-P, Si and C (graphite), were ball milled for 10 h with a constant rotation speed of 380 rpm in tungsten-carbide jars with 7 tungsten-carbide balls under argon atmosphere. The fine powders obtained were compacted into small tablets and were then sealed into quartz ampoules with 200 mbar argon before the heat treatment was performed.

Magnetic properties were characterized using a commercial superconducting quantum interference device (SQUID) magnetometer (Quantum Design MPMS XL) in the reciprocating sample option (RSO) mode. X-ray powder diffraction experiments using a PANalytical X-pert Pro diffractometer with Cu-K_α radiation were carried out at room temperature. The room temperature neutron diffraction data were collected on the neutron powder diffraction instrument PEARL [27] at the research reactor of Delft University of Technology. For neutron measurements, 8-10 g powder samples were put into a vanadium can with a diameter of 6 mm and a height of 50 mm. Structure refinement of the X-ray and neutron diffraction data was done by using the Rietveld method implemented in the Fullprof program [28].

8.3. RESULTS AND DISCUSSION

8.3.1. $Mn_{1.25}Fe_{0.70}P_{0.50}Si_{0.50}C_z$ COMPOUNDS

The room-temperature XRD patterns of the $Mn_{1.25}Fe_{0.70}P_{0.50}Si_{0.50}C_z$ (z = 0.00, 0.05, 0.10 and 0.15) compounds indicate that all samples exhibit the hexagonal Fe_2P-type main phase. The temperature dependence of the magnetization for the $Mn_{1.25}Fe_{0.70}P_{0.50}Si_{0.50}C_z$ compounds was measured during cooling and heating after removing "virgin effect" [29] under an applied magnetic field of 1 T and is shown in Fig. 8.1. All samples show sharp ferro-to-paramagnetic phase transitions accompanied by a small thermal hysteresis. The Curie temperature (T_C) increases while the thermal hysteresis

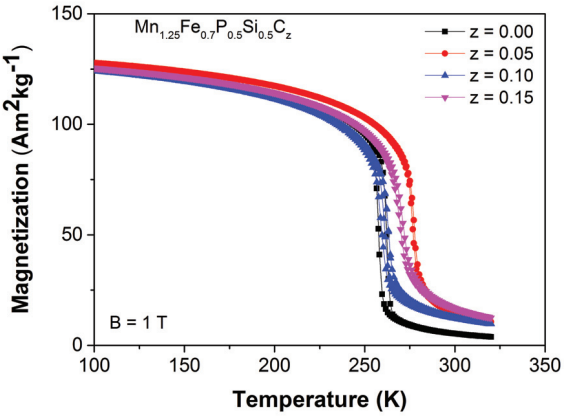

Figure 8.1: Magnetization of the $Mn_{1.25}Fe_{0.70}P_{0.50}Si_{0.50}C_z$ compounds as a function of temperature during heating and cooling at a rate of 2 K/min in a magnetic field of 1 T.

(ΔT_{hys}) decreases as carbon is added. However, the change in T_C is not linear as a function of the carbon content. Compared to B doping [30], the influence of C doping on both T_C and ΔT_{hys} is less pronounced.

Table 8.1: Curie temperature (T_C) derived from the magnetization curves measured on cooling, the isothermal entropy change (ΔS_m) derived from the isofield magnetization curves in a field change of 0.5, 1.0, 1.5 and 2.0 T, thermal hysteresis (ΔT_{hys}) derived from the magnetization curves measured in 1 T upon cooling and heating for the $Mn_{1.25}Fe_{0.70}P_{0.50}Si_{0.50}C_z$ compounds.

z	T_C (K)	ΔS_m (JK^{-1}kg^{-1})				ΔT_{hys} (K)
		ΔB = 0.5 T	ΔB = 1.0 T	ΔB = 1.5T	ΔB = 2.0 T	
0.00	256	6.97	14.43	18.56	21.01	4.6
0.05	275	5.88	9.79	11.65	13.02	0.5
0.10	260	3.46	7.12	9.60	11.19	3.5
0.15	270	3.05	5.61	7.53	9.21	1.3

The isothermal entropy change (ΔS_m) of the $Mn_{1.25}Fe_{0.70}P_{0.50}Si_{0.50}C_z$ compounds in a field change of 0.5, 1.0, 1.5 and 2.0 T derived from the isofield magnetization curves using the Maxwell relation is shown in Fig. 8.2 and summarized in Table. 8.1. It is noticeable that for magnetic field changes of between 0.5 and 2.0 T, ΔS_m decreases as a function of C concentration although T_C does not show a systematic change for increasing C concentration. Moreover, the $Mn_{1.25}Fe_{0.70}P_{0.50}Si_{0.50}C_{0.05}$ compound shows nice magnetocaloric properties in low field (0.5 T) accompanied by a very small (neglectable) thermal hysteresis. An acceptable magnetocaloric effect at lower magnetic field strength would be a sig-

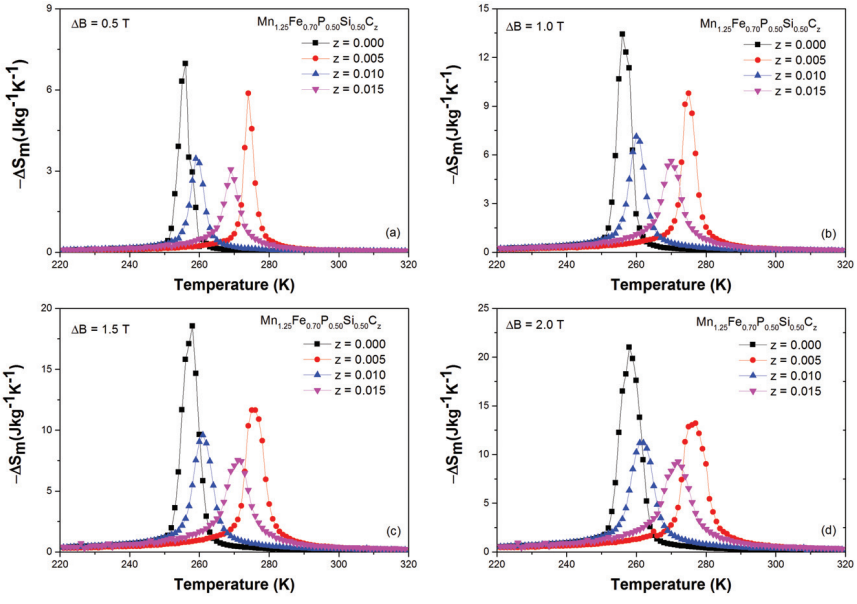

Figure 8.2: Isothermal magnetic entropy change of the $Mn_{1.25}Fe_{0.70}P_{0.50}Si_{0.50}C_z$ compounds as a function of temperature for a field change of 0.5 (a), 1.0 (b), 1.5 (c) and 2.0 T (d).

nificant advantage for practical applications since it allows reducing the mass of permanent magnets needed to generate the magnetic field. Thus, it is highly desirable to verify the effect of C doping on the thermal hysteresis, magnetic phase transition and magnetocaloric properties of $(Mn,Fe)_2(P,Si)$-based compounds.

8.3.2. $Mn_{1.25}Fe_{0.70}P_{0.55}Si_{0.45}C_z$ COMPOUNDS

To verify the influence of C added on the magnetic phase transition and the thermal hysteresis of $(Mn,Fe)_2(P,Si)$-based compounds, another series of samples with the parent compound was prepared. Room-temperature XRD patterns of $Mn_{1.25}Fe_{0.70}P_{0.55}Si_{0.45}C_z$ compounds indicate that the hexagonal Fe_2P-type structure remains unchanged by adding C. This confirms that the C addition preserved the crystal structure of $(Mn,Fe)_2(P,Si)$.

Table 8.2: Curie temperature (T_C) derived from the magnetization curves measured on cooling, the isothermal entropy change (ΔS_m) derived from the isofield magnetization curves in a field change of 0.5, 1.0, 1.5 and 2.0 T, thermal hysteresis (ΔT_{hys}) derived from the magnetization curves measured in 1 T upon cooling and heating for the $Mn_{1.25}Fe_{0.70}P_{0.55}Si_{0.45}C_z$ compounds.

z	$T_C(K)$	$\Delta S_m(JK^{-1}kg^{-1})$				ΔT_{hys} (K)
		ΔB = 0.5 T	ΔB = 1.0 T	ΔB = 1.5T	ΔB = 2.0 T	
0.000	202	5.27	12.36	18.53	24.64	13.4
0.025	229	5.70	12.55	16.98	20.99	5.4
0.050	224	5.79	11.83	15.82	19.28	7.4
0.075	226	5.71	11.53	14.86	18.38	7.3

Fig. 8.3 shows the temperature dependence of the magnetization for the $Mn_{1.25}Fe_{0.70}P_{0.55}Si_{0.45}C_z$ compounds. A remarkable thermal hysteresis confirms that the nature of the phase transitions in the parent and doped compounds is first order. It is noticeable that the Curie temperature can be tuned between 202 and 226 K, while maintaining the sharp magnetic phase transition and reducing the thermal hysteresis by the introduction of C in the parent $Mn_{1.25}Fe_{0.70}P_{0.55}Si_{0.45}$ compound. The Curie temperature of all the C-doped compounds is higher than that of the parent compound. Similar to the $Mn_{1.25}Fe_{0.70}P_{0.55}Si_{0.45}C_z$ series, the change in the Curie temperature of the $Mn_{1.25}Fe_{0.70}P_{0.55}Si_{0.45}C_z$ compounds does not linearly increase as a function of C doping concentration. It is worth mentioning that the introduction of interstitial C atoms in other well known MCE materials like $LaFe_{11.5}Si_{1.5}C_x$ [31] leads to an increase in the Curie temperature, while the Curie temperature decreases with increasing the carbon concentration for $MnAsC_x$ [32], $Ni_{43}Mn_{46}Sn_{11}C_x$ [33], and $Mn_{38}Fe_{22}Al_{40}C_x$ [34] . However, no further investigation has been done on these compounds to resolve the occupancy of C in the crystal structure.

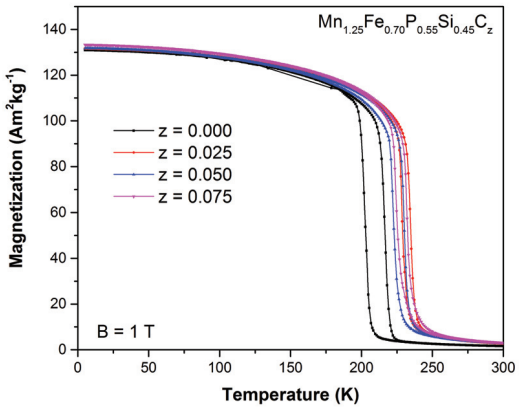

Figure 8.3: Magnetization of $Mn_{1.25}Fe_{0.70}P_{0.55}Si_{0.45}C_z$ compounds as a function of temperature during heating and cooling at a rate of 2 K/min in a magnetic field of 1 T.

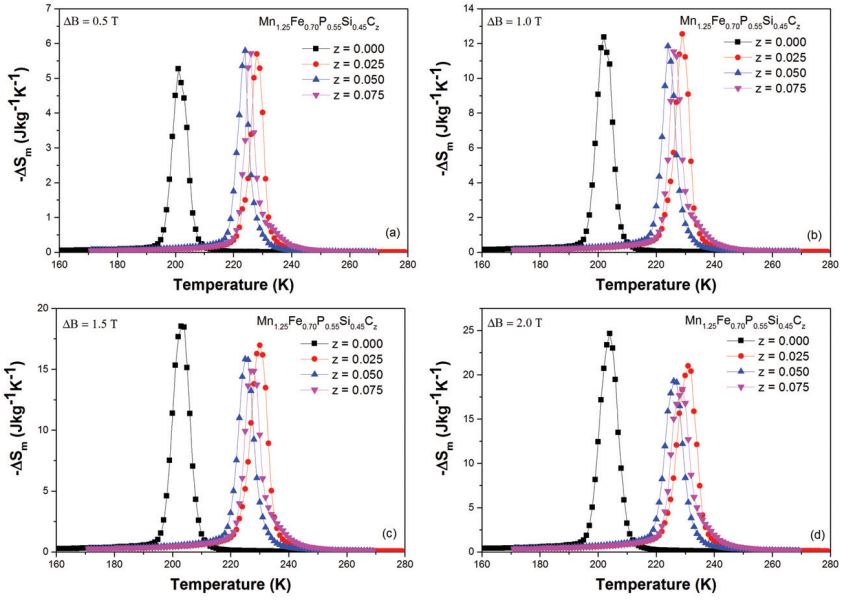

Figure 8.4: Isothermal magnetic entropy change of the $Mn_{1.25}Fe_{0.70}P_{0.55}Si_{0.45}C_z$ compounds as a function of temperature for a field change of 0.5 (a), 1.0 (b), 1.5 (c) and 2 T (d).

Table 8.3: The C concentrations in $Mn_{1.25}Fe_{0.70}P_{0.55}Si_{0.45}C_z$ compounds.

Nominal composition	Nominal w.t. % C	Measured w.t. % C
$Mn_{1.25}Fe_{0.70}P_{0.55}Si_{0.45}$	0.00	0.06
$Mn_{1.25}Fe_{0.70}P_{0.55}Si_{0.45}C_{0.025}$	0.22	0.24
$Mn_{1.25}Fe_{0.70}P_{0.55}Si_{0.45}C_{0.050}$	0.43	0.43
$Mn_{1.25}Fe_{0.70}P_{0.55}Si_{0.45}C_{0.075}$	0.65	0.64

Table 8.4: Structural parameters obtained from neutron diffraction data of $Mn_{1.25}Fe_{0.70}P_{0.55}Si_{0.45}C_z$ (z = 0.000, 0.025, 0.050, 0.075) in the paramagnetic state. Space group: $P-62m$. Atomic positions: 3f (x_1,0,1/2); 3g (x_2,0,1/2); 2c (1/3,2/3,0) and 1b (0,0,1/2)

	Parameters	z = 0.000	z = 0.0250	z = 0.050	z = 0.075
Unit cell	a (Å)	6.0609(1)	6.0690(1)	6.0691(1)	6.0696(1)
	c (Å)	3.4578(1)	3.4398(1)	3.4405(1)	3.4391(1)
	V (Å^3)	109.996(6)	109.721(5)	109.751 (5)	109.722(5)
3f	x_1	0.2552(3)	0.2557(3)	0.2558(3)	0.2550(3)
	n(Fe)/n(Mn)	0.176/0.074(1)	0.181/0.069(1)	0.182/0.068(1)	0.184/0.066(1)
3g	x_2	0.5912(5)	0.5909(4)	0.5908(4)	0.5908(4)
	n(Mn)/n(Fe)	0.25/0.00	0.25/0.00	0.25/0.00	0.25/0.00
2c	n(P)/n(Si)	0.099/0.068 (2)	0.080/0.087(1)	0.078/0.089(1)	0.077/0.090(1)
	n(C)	-	0.011(1)	0.012(1)	0.014(1)
1b	n(P)/n(Si)	0.039/0.046(2)	0.050/0.026(1)	0.060/0.024(1)	0.061/0.023(1)
	R_p (%)	5.13	4.65	4.46	4.56
	ωR_p (%)	6.68	5.84	5.79	5.85
	χ^2	5.97	4.89	6.65	7.00

The ΔS_m of the $Mn_{1.25}Fe_{0.70}P_{0.55}Si_{0.45}C_z$ compounds in a field change of 0.5, 1.0, 1.5 and 2.0 T derived from the isofield magnetization data is shown in Fig. 8.4 and summarized in Table. 8.2. As shown in Fig. 8.4, the ΔS_m for a field change of both 0.5 and 1.0 T hardly changes as C is added. However, there is a slight decrease in the ΔS_m for a field change of 1.5 and 2.0 T with carbon addition. Hence, a certain amount of C can be added to (Mn,Fe)$_2$(P,Si) compounds in order to tune the magnetic phase transition and reduce the thermal hysteresis, while preserving an acceptable magnetocaloric effect for practical applications.

To quantify the concentration of C in the obtained samples, the combustion method using a LECO element analyzer was employed. The results obtained from the elemental analysis are in good agreement with the nominal compositions and are summarized in Table 8.3. However, it is necessary to investigate how much and where the C atoms have entered the structure. This is not possible with X-rays as C is hardly visible for X-rays. Hence, neutron diffraction experiments were performed at room temperature to resolve the occupancy of C atoms in the crystal structure of the doped compounds.

In Fig. 8.5, the room-temperature neutron diffraction patterns for the

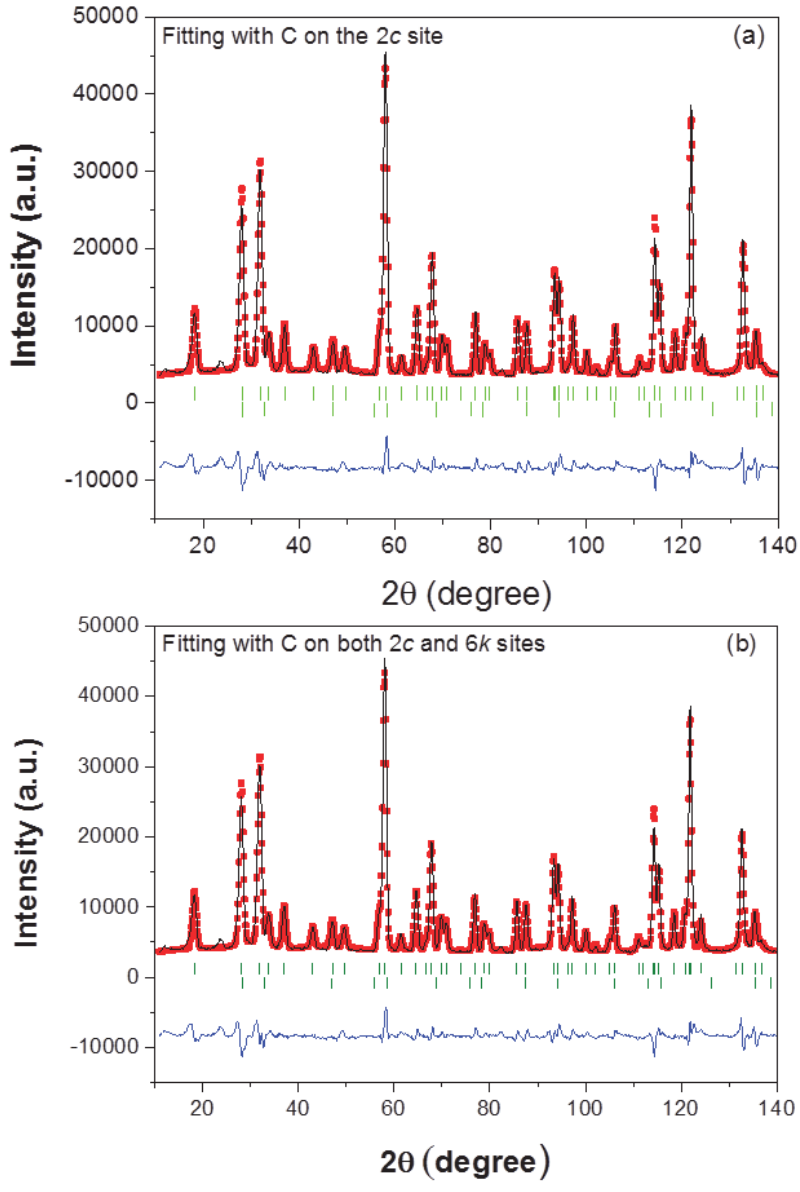

Figure 8.5: Powder neutron diffraction patterns for $Mn_{1.25}Fe_{0.70}P_{0.55}Si_{0.45}C_{0.025}$, fitting with C on the 2*c* site (a) and C on both 2*c* and 6*k* sites (b). Vertical lines indicate the Bragg peak positions for the main phase Fe_2P-type (top) and the impurity phase $(Mn,Fe)_3Si$ (bottom). Black line indicates observed profile; red squares indicate calculated data points; blue line indicates the difference between the observed and calculated profile.

Table 8.5: Structural parameters obtained from neutron diffraction data of $Mn_{1.25}Fe_{0.70}P_{0.55}Si_{0.45}C_z$ (z = 0.000, 0.025, 0.050, 0.075) in the paramagnetic state. Space group: $P-62m$. Atomic positions: $3f$ (x_1,0,1/2); $3g$ (x_2,0,1/2); $2c$ (1/3,2/3,0), $1b$ (0,0,1/2) and $6k$ (x_3, y_3,1/2)

	Parameters	z = 0.000	z = 0.0250	z = 0.050	z = 0.075
Unit cell	a (Å)	6.0609(1)	6.0690(1)	6.0691(1)	6.0696(1)
	c (Å)	3.4578(1)	3.4398(1)	3.4405(1)	3.4391(1)
	V (Å^3)	109.996(6)	109.722(5)	109.751 (5)	109.722(5)
$3f$	x_1	0.2552(3)	0.2555(3)	0.2556(3)	0.2560(3)
	n(Fe)/n(Mn)	0.176/0.074(1)	0.184/0.066(1)	0.185/0.065(1)	0.183/0.067(1)
$3g$	x_2	0.5912(5)	0.5910(5)	0.5911(5)	0.5915(7)
	n(Mn)/n(Fe)	0.25/0.00	0.25/0.00	0.25/0.00	0.25/0.00
$2c$	n(P)/n(Si)	0.099/0.068 (2)	0.067/0.100(4)	0.069/0.098(4)	0.079/0.088(6)
	n(C)	-	0.016(1)	0.016(1)	0.011(1)
$1b$	n(P)/n(Si)	0.039/0.046(2)	0.071/0.013(4)	0.069/0.015(4)	0.059/0.025(6)
$6k$	x_3	-	4.92(1)	4.93(1)	4.33(1)
	y_3	-	0.23(1)	0.24(2)	0.43(2)
	n(C)	-	0.07(1)	0.006(1)	0.010(1)
	R_p (%)	5.13	4.69	4.53	4.59
	ωR_p (%)	6.68	5.78	5.81	5.89
	χ^2	5.97	4.81	6.70	7.09

$Mn_{1.25}Fe_{0.70}P_{0.55}Si_{0.45}C_z$ compounds in the paramagnetic state are shown as an example. The Rietveld refinement using the FullProf package for all samples confirms the Fe_2P-type hexagonal structure (space group P-62m) with two specific metallic and non-metallic sites. It is worth mentioning that less than 2 wt.% of the $(Mn,Fe)_3Si$ impurity phase is detected in these samples. The unit-cell volume is expected to increase if C atoms enter the structure as an interstitial element. However, the initial reduction in the unit-cell volume when carbon is added suggests that in this case C atoms substitute non-metal atoms on the $2c/1b$ sites, since C has a smaller atomic radius than both P and Si. Moreover, the unit-cell volume hardly changes after further C doping, indicating that part of C added may also enter the interstitial sites. Hence, two different atomic models with C substituting P/Si on the $2c$ site and/or occupies the $6k$ interstitial sites have been used to resolve the occupancy of C atoms in the crystal structure. The structural parameters derived from the Rietveld refinement for the $Mn_{1.25}Fe_{0.70}P_{0.55}Si_{0.45}C_z$ compounds are summarized in Table. 8.4 and Table. 8.5. It is found that in both cases the total C occupation is not strongly influenced by the amount of C added and the Rietveld refinements are not sensitive enough to distinguish the C atom occupancy at the substitutional and/or interstitial sites. However, the unit-cell volume decreases as C is added and hardly changes after further C doping, indicating that C atoms may enter the crystal structure both as an interstitial and a substitutional element rather than only occupy the substitu-

tional sites. Note that Miao and coworkers [23] observed an increase in the unit-cell volume as a function of the C concentration instead and pointed out that C occupies the $6k$ and $6j$ interstitial sites. This differece may come from different preparation methods since the samples of Miao and coworkers are prepared by melt spinning.

8.4. CONCLUSIONS

The influence of C addition on the structure and the magnetic phase transition of $Mn_{1.25}Fe_{0.70}P_{0.50}Si_{0.50}C_z$ and $Mn_{1.25}Fe_{0.70}P_{0.55}Si_{0.45}C_z$ compounds fabricated by high-energy ball milling and a solid-state reaction has been investigated. The experimental results indicate that C doping allows to tune the Curie temperature of the parent alloys and to reduce the thermal hysteresis. The magnetic softness of the C doped compounds results in large MCE even in lower magnetic fields compared to the parent compounds. The refinements based on the room-temperature neutron diffraction data indicate that C substitutes P/Si on the $2c$ site and/or occupies the $6k$ interstitial site of the hexagonal Fe_2P-type structure.

REFERENCES

[1] E. Brück, *Developments in magnetocaloric refrigeration,* Journal of Physics D: Applied Physics **38**, R381 (2005).

[2] K. Gschneidner and V. Pecharsky, *Thirty years of near room temperature magnetic cooling: Where we are today and future prospects,* International Journal of Refrigeration **31**, 945 (2008).

[3] B. Yu, M. Liu, P. W. Egolf, and A. Kitanovski, *A review of magnetic refrigerator and heat pump prototypes built before the year 2010,* International Journal of Refrigeration **33**, 1029 (2010).

[4] V. K. Pecharsky and K. A. Gschneidner, *Giant magnetocaloric effect in $Gd_5(Si_2Ge_2)$,* Physical Review Letters **78**, 4494 (1997).

[5] H. Wada and Y. Tanabe, *Giant magnetocaloric effect of $MnAs_{1-x}Sb_x$,* Applied Physics Letters **79**, 3302 (2001).

[6] H. Wada, T. Morikawa, K. Taniguchi, T. Shibata, Y. Yamada, and Y. Akishige, *Giant magnetocaloric effect of $MnAs_{1-x}Sb_x$ in the vicinity of first-order magnetic transition,* Physica B: Condensed Matter **328**, 114 (2003).

[7] O. Tegus, E. Brück, K. H. J. Buschow, and F. R. de Boer, *Transition-metal-based magnetic refrigerants for room-temperature applications.* Nature **415**, 150 (2002).

[8] N. T. Trung, Z. Q. Ou, T. J. Gortenmulder, O. Tegus, K. H. J. Buschow, and E. Brück, *Tunable thermal hysteresis in MnFe(P,Ge) compounds,* Applied Physics Letters **94**, 102513 (2009).

[9] D. T. Cam Thanh, E. Brück, N. T. Trung, J. C. P. Klaasse, K. H. J. Buschow, Z. Q. Ou, O. Tegus, and L. Caron, *Structure, magnetism, and magnetocaloric properties of $MnFeP_{1-x}Si_x$ compounds,* Journal of Applied Physics **103**, 07B318 (2008).

[10] F. Guillou, H. Yibole, G. Porcari, L. Zhang, N. H. van Dijk, and E. Brück, *Magnetocaloric effect, cyclability and coefficient of refrigerant performance in the MnFe(P,Si,B) system,* Journal of Applied Physics **116**, 063903 (2014).

[11] N. Trung, L. Zhang, L. Caron, K. Buschow, and E. Brück, *Giant magnetocaloric effects by tailoring the phase transitions,* Applied Physics Letters **96**, 172504 (2010).

[12] D. Zhang, Z. Nie, Z. Wang, L. Huang, Q. Zhang, and Y. D. Wang, *Giant magnetocaloric effect in MnCoGe with minimal Ga substitution,* Journal of Magnetism and Magnetic Materials **387**, 107 (2015).

[13] J. Chen, Z. Wei, E. Liu, X. Qi, W. Wang, and G. Wu, *Structural and magnetic properties of $MnCo_{1-x}Fe_xSi$ alloys,* Journal of Magnetism and Magnetic Materials **387**, 159 (2015).

[14] F. X. Hu, M. Ilyn, A. M. Tishin, J. R. Sun, G. J. Wang, Y. F. Chen, F. Wang, Z. H. Cheng, and B. G. Shen, *Direct measurements of magnetocaloric effect in the first-order system $LaFe_{11.7}Si_{1.3}$,* Journal of Applied Physics **93**, 5503 (2003).

[15] A. Fujita, S. Fujieda, Y. Hasegawa, and K. Fukamichi, *Itinerant-electron metamagnetic transition and large magnetocaloric effects in $La(Fe_xSi_{1-x})_{13}$ compounds and their hydrides,* Physical Review B **67**, 104416 (2003).

[16] A. Barcza, M. Katter, V. Zellmann, S. Russek, S. Jacobs, and C. Zimm, *Stability and magnetocaloric properties of sintered $La(Fe,Mn,Si)_{13}H_z$ alloys,* IEEE Transactions on Magnetics **47**, 3391 (2011).

[17] M. P. Annaorazov, K. A. Asatryan, G. Myalikgulyev, S. A. Nikitin, A. M. Tishin, and A. L. Tyurin, *Alloys of the Fe-Rh system as a new class of working material for magnetic refrigerators,* Renewable and Sustainable Energy Reviews **32**, 867 (1992).

[18] F. Hu, B. Shen, J. Sun, and G. Wu, *Large magnetic entropy change in a Heusler alloy $Ni_{52.6}Mn_{23.1}Ga_{24.3}$ single crystal,* Physical Review B **64**, 132412 (2001).

[19] J. Liu, T. Gottschall, K. P. Skokov, J. D. Moore, and O. Gutfleisch, *Giant magnetocaloric effect driven by structural transitions,* Nature Materials **11**, 620 (2012).

[20] X. F. Miao, L. Caron, P. Roy, N. H. Dung, L. Zhang, W. A. Kockelmann, R. A. de Groot, N. H. van Dijk, and E. Brück, *Tuning the phase transition in transition-metal-based magnetocaloric compounds,* Physical Review B **89**, 174429 (2014).

[21] N. H. Dung, Z. Q. Ou, L. Caron, L. Zhang, D. T. C. Thanh, G. A. De Wijs, R. A. De Groot, K. H. J. Buschow, and E. Brück, *Mixed magnetism for refrigeration and energy conversion,* Advanced Energy Materials **1**, 1215 (2011).

[22] N. Thang, X. Miao, N. van Dijk, and E. Brück, *Structural and magnetocaloric properties of $(Mn,Fe)_2(P,Si)$ materials with added nitrogen,* Journal of Alloys and Compounds **670**, 123 (2016).

[23] X. F. Miao, N. V. Thang, L. Caron, H. Yibole, R. I. Smith, N. H. van Dijk, and E. Brück, *Tuning the magnetoelastic transition in $(Mn,Fe)_2(P,Si)$ by B, C, and N doping,* Scripta Materialia **124**, 129 (2016).

[24] N. Thang, H. Yibole, N. van Dijk, and E. Brück, *Effect of heat treatment conditions on MnFe(P,Si,B) compounds for room-temperature magnetic refrigeration,* Journal of Alloys and Compounds **699**, 633 (2017).

[25] N. Thang, N. Dijk, and E. Brück, *Tuneable giant magnetocaloric effect in $(Mn,Fe)_2(P,Si)$ materials by Co-B and Ni-B co-doping,* Materials **10**, 14 (2017).

[26] N. H. Dung, L. Zhang, Z. Q. Ou, L. Zhao, L. van Eijck, A. M. Mulders, M. Avdeev, E. Suard, N. H. van Dijk, and E. Brück, *High/low-moment phase transition in hexagonal Mn-Fe-P-Si compounds,* Physical Review B **86**, 045134 (2012).

[27] L. van Eijck, L. D. Cussen, G. J. Sykora, E. M. Schooneveld, N. J. Rhodes, A. van Well, and C. Pappas, *Design and performance of a novel neutron powder diffractometer : PEARL at TU Delft,* Journal of Applied Crystallography **49**, 1 (2016).

[28] J. Rodríguez-Carvajal, *Recent advances in magnetic structure determination by neutron powder diffraction,* Physica B: Condensed Matter **192**, 55 (1993).

[29] X. F. Miao, L. Caron, Z. Gercsi, A. Daoud-Aladine, N. H. van Dijk, and E. Brück, *Thermal-history dependent magnetoelastic transition in $(Mn,Fe)_2(P,Si)$,* Applied Physics Letters **107**, 042403 (2015).

[30] F. Guillou, H. Yibole, N. van Dijk, and E. Brück, *Effect of boron substitution on the ferromagnetic transition of* $MnFe_{0.95}P_{2/3}Si_{1/3}$, Journal of Alloys and Compounds **632**, 717 (2015).

[31] S. Li, R. Huang, Y. Zhao, W. Wang, and L. Li, *Cryogenic abnormal thermal expansion properties of carbon-doped* $La(Fe,Si)_{13}$ *compounds,* Physical Chemistry Chemical Physics **17**, 30999 (2015).

[32] W. B. Cui, W. Liu, Q. Zhang, B. Li, X. H. Liu, F. Yang, X. G. Zhao, and Z. D. Zhang, *Carbon-doping effects on the metamagnetic transition and magnetocaloric effect in* $MnAsC_x$, Journal of Magnetism and Magnetic Materials **322**, 2223 (2010).

[33] Y. Zhang, J. Liu, Q. Zheng, J. Zhang, W. Xia, J. Du, and A. Yan, *Large magnetic entropy change and enhanced mechanical properties of Ni-Mn-Sn-C alloys,* Scripta Materialia **75**, 26 (2014).

[34] Q. Guo, Z. Ou, R. Han, W. Wei, S. Ebisu, and O. Tegus, *Carbon doping effect on structural and magnetocaloric effect in* $Mn_{38}Fe_{22}Al_{40}C_x$ *alloys,* Chemical Physics Letters **640**, 137 (2015).

SUMMARY

During the last several years, $(Mn,Fe)_2(P,Si)$-based materials have gained much attention for room-temperature cooling and heat pump applications due to their large magnetocaloric effect in a small applied magnetic field, low cost starting materials, tunable Curie temperature and tailorable thermal hysteresis. This thesis intends to explore the influence of the particle size, heat treatment conditions and compositions on the structural properties and giant magnetocaloric effect in $(Mn,Fe)_2(P,Si)$-based compounds, which allows optimizing their performance for magnetic cooling and heat pumping applications.

To explore the possibility to produce magnetocaloric nanoparticles, in **Chapter 4** $Mn_{1.25}Fe_{0.70}P_{0.60}Si_{0.40}$ nanoparticles were prepared by surfactant-assisted high-energy ball milling. The influence of the ball milling time and surfactant concentration on the structural and magnetic properties of the nano-scale $Mn_{1.25}Fe_{0.70}P_{0.60}Si_{0.40}$ particles obtained was investigated by X-ray diffraction (XRD) and magnetic measurements. The function of the surfactant is to prevent the re-welding of crushed particles and to enhance the dispersion of nanoparticles in the solvent during the ball milling process. It is found that the ball milling time does have a significant effect on the particle size and magnetic properties, but the surfactant concentration does not. Particularly, the spontaneous magnetization and the thermal hysteresis become smaller as the particle size decreases for an increase in the ball milling time.

In order to find optimal annealing conditions for the $(Mn,Fe)_2(P,Si,B)$-based materials, in **Chapter 5**, the influence of both the annealing temperature and time on the structural properties and magnetic phase transition of $Mn_{1.000}Fe_{0.950}P_{0.595}Si_{0.330}B_{0.075}$ compounds was investigated. It is found that the Curie temperature can be tuned between 265 and 298 K by sintering the samples at different temperatures between 1273 and 1373 K, while it hardly changes by varying the duration of the heat treatment. Furthermore, both the annealing time and the annealing temperature have a significant influence on the isothermal magnetic entropy change. The magnetic entropy change increases as a function of both the annealing time and temperature due to the enhanced compositional homogeneity of materials obtained after a longer annealing time and/or higher annealing temperature. Hence, tuning the heat treatment conditions offers an additional control parameter to tailor the properties of the $(Mn,Fe)_2(P,Si,B)$-based materials.

In **Chapter 6**, the influence of nitrogen addition on the structural and magnetocaloric properties was studied for the $Mn_{1.25}Fe_{0.70}P_{0.50}Si_{0.50}N_z$, $Mn_{1.25}Fe_{0.70}P_{0.50-z}Si_{0.50}N_z$ and $Mn_{1.25}Fe_{0.70}P_{0.50}Si_{0.50-z}N_z$ compounds. The evolution of the unit-cell volume as a function of nitrogen concentration obtained from X-ray diffraction data indicates that nitrogen atoms occupy both substitutional and interstitial sites of the hexagonal Fe_2P-type crystal structure. Moreover, the addition of nitrogen leads to a moderate decrease in the Curie temperature and a slight increase in the thermal hysteresis, while it preserves the magnetocaloric properties and improves the mechanical stability. Thus, the nitrogen addition provides a new control parameter to both tune the Curie temperature and improve the mechanical properties of $(Mn,Fe)_2(P,Si)$ materials while maintaining acceptable magnetocaloric properties.

In **Chapter 7**, the influence of Co-B and Ni-B co-doping on the structural, magnetic and magnetocaloric properties was investigated in three series of samples $Mn_{1.00}Fe_{0.85}Co_{0.10}P_{0.55-z}Si_{0.45}B_z$, $Mn_{1.00}Fe_{0.95-z}Co_zP_{0.51}Si_{0.45}B_{0.04}$ and $Mn_{1.00}Fe_{0.95-z}Ni_zP_{0.51}Si_{0.45}B_{0.04}$ using X-ray diffraction, differential scanning calorimetry, magnetic and direct temperature change measurements. X-ray diffraction data imply that the co-substitution of Fe by Co(Ni) and P by B does not affect the formation of the Fe_2P-type phase. It is found that an increase in B concentration leads to a dramatic increase in the Curie temperature and a rapid decrease in the thermal hysteresis. In contrast, an increase in Co or Ni concentration leads to a slow decrease in the Curie temperature, while the thermal hysteresis hardly changes. By keeping the B concentration constant and varying the Co(Ni) concentration, the Curie temperature can easily be tuned between 272 and 316 K for Co substitution (between 265 and 308 K for Ni substitution), while maintaining a small thermal hysteresis and a large magnetocaloric effect in the $(Mn,Fe)_2(P,Si)$ system. Hence, $(Mn,Fe,Co)_2(P,Si,B)$-based and $(Mn,Fe,Ni)_2(P,Si,B)$-based materials can be considered as one of the most promising candidates for near room-temperature magnetic refrigeration.

In **Chapter 8**, a systematic study of the effect of carbon addition on the structural, magnetic and magnetocaloric properties of $(Mn,Fe)_2(P,Si)$-based materials was done. It is found that the Curie temperature can be tuned by adding a certain amount of carbon, while reducing the thermal hysteresis and keeping an acceptable magnetocaloric effect. The site occupation of C added is resolved by room-temperature neutron diffraction. The refined results suggest that C substitutes P/Si on the $2c$ site and/or occupies the $6k$ interstitial site of the hexagonal Fe_2P-type structure.

SAMENVATTING

De laatste Jaren hebben $(Mn,Fe)_2(P,Si)$ materialen in het centrum van de belangstelling gestaan voor hun toepassingen bij kamertemperatuur koeling en warmtepompen vanwege het grote magnetocalorische effect dat deze materialen vertonen in een laag magneetveld, de lage kostprijs van de uitgangsmaterialen en de regelbare Curie-temperatuur en thermische hysterese. Dit proefschrift heeft tot doel om de invloed van de deeltjesgrootte, de warmtebehandelingscondities en de samenstelling op de structurele eigenschappen en op het grote magnetocalorische effect te onderzoeken in (Mn,Fe)2(P,Si) gerelateerde materialen, die optimalisatie in toepassingen voor magnetisch koelen en warmtepompen mogelijk maakt.

Om uit te vinden of magnetocalorische nanodeeltjes kunnen worden geproduceerd zijn in **Hoofdstuk 4** $Mn_{1.25}Fe_{0.70}P_{0.60}Si_{0.40}$ nanodeeltjes gemaakt middels oppervlakte-actieve stoffen bij hoge-energie kogelmalen. De invloed van de kogelmalingstijd en de concentratie van de oppervlakte-actieve stoffen op de structurele en magnetische eigenschappen van de gemaakte $Mn_{1.25}Fe_{0.70}P_{0.60}Si_{0.40}$ nanodeeltjes was onderzocht met Röntgendiffractie (XRD) en magnetische metingen. De functie van de oppervlakte-actieve stoffen is om het samengaan van de gemalen deeltjes te voorkomen en de verspreiding van de nanodeeltjes in het oplosmiddel te verbeteren gedurende het kogelmalingsproces. Er is gevonden dat de kogelmalingstijd een significant effect heeft op de deeltjesgrootte en de magnetische eigenschappen, terwijl de concentratie van oppervlakte actieve stoffen geen rol speelt. De spontane magnetisatie en de thermische hysterese worden kleiner wanneer de deeltjesgrootte afneemt voor een toename in de kogelmalingstijd.

Om de optimale warmtebehandelingscondities te bepalen voor de $(Mn,Fe)_2(P,Si,B)$ materialen is in **Hoofdstuk 5** de invloed van zowel de temperatuur als de tijd van de warmtebehandeling op de structurele eigenschappen en de magnetische faseovergang van $Mn_{1.000}Fe_{0.950}P_{0.595}Si_{0.330}B_{0.075}$ verbindingen onderzocht. Er is gevonden dat de Curie temperatuur kan worden gevarieerd van 265 tot 298 K door de samples bij verschillende temperaturen tussen 1273 en 1373 K te sinteren, terwijl de duur van de warmtebehandeling nauwelijks invloed heeft op de Curie temperatuur. Verder hebben zowel de tijd als de temperatuur van de warmtebehandeling een significante invloed op de isotherme magnetische entropieverandering. De magnetische entropieverandering neemt

toe met zowel de tijd en de temperatuur van de warmtebehandeling vanwege de verhoogde homogeniteit in samenstelling van de materialen voor een warmtebehandeling voor een langere tijd en bij een hogere temperatuur. Variatie van de warmtebehandelingscondities biedt dus een extra controleparameter om de eigenschappen van $(Mn,Fe)_2(P,Si,B)$ materialen te optimaliseren.

In **Hoofdstuk 6** is de invloed van het toevoegen van stikstof op de structurele en magnetische eigenschappen bestudeerd voor de $Mn_{1.25}Fe_{0.70}P_{0.50}Si_{0.50}N_z$, $Mn_{1.25}Fe_{0.70}P_{0.50-z}Si_{0.50}N_z$ en $Mn_{1.25}Fe_{0.70}P_{0.50}Si_{0.50-z}N_z$ verbindingen. De evolutie van het volume van de eenheid-cel als functie van de stikstofconcentratie die volgt uit de Röntgendiffractie data duidt er op dat de stikstofatomen zowel substitutionele als interstitiële posities in de hexagonale Fe_2P structuur bezetten. De toevoeging van stikstof leidt verder tot een bescheiden afname van de Curie temperatuur een kleine toename in de thermische hysterese, terwijl de magnetocalorische eigenschappen behouden blijven en de mechanische stabiliteit verbetert. De toevoeging van stikstof biedt dus een nieuwe controleparameter om de Curie temperatuur te variëren en daarbij de mechanische eigenschappen van (Mn,Fe)2(P,Si) materialen te verbeteren, terwijl de magnetocalorische eigenschappen acceptabel blijven.

In **Hoofdstuk 7** is de invloed van Co-B en Ni-B co-doping op de magnetische en magnetocalorische eigenschappen bestudeerd in de volgende drie reeksen van samples $Mn_{1.25}Fe_{0.70}P_{0.50}Si_{0.50}N_z$, $Mn_{1.25}Fe_{0.70}P_{0.50-z}Si_{0.50}N_z$ en $Mn_{1.25}Fe_{0.70}P_{0.50}Si_{0.50-z}N_z$ met behulp van Röntgendiffractie, calorimetrie (DSC), magnetische en directe temperatuursveranderings-metingen. Röntgendiffractie data laten zien dat de co-substitutie van Fe door Co(Ni) en P door B geen invloed heeft op de vorming van de Fe_2P fase. Er is gevonden dat een toename in de B concentratie leidt tot een dramatische toename van de Curie temperatuur en een snelle afname van de thermische hysterese. Een toename van de Co of Ni concentratie leidt echter tot een langzame afname van de Curie temperatuur, terwijl de thermische hysterese nauwelijks verandert. Door de B concentratie constant te houden bij een veranderende Co(Ni) concentratie kan de Curie temperatuur eenvoudig worden gevarieerd tussen 272 en 316 K voor Co substitutie (tussen 265 en 308 K voor Ni substitutie), terwijl de geringe thermische hysterese en het magnetocalorische effect in het $(Mn,Fe)_2(P,Si)$ systeem behouden blijft. Zowel $(Mn,Fe,Co)_2(P,Si,B)$ als $(Mn,Fe,Ni)_2(P,Si,B)$ gerelateerde materialen kunnen worden beschouwd als een van de meest veelbelovende kandidaten voor het magnetisch koelen rond kamertemperatuur.

In **Hoofdstuk 8** is een systematische studie uitgevoerd naar het effect van koolstof toevoegingen aan de structurele, magnetische en magnetocalorische eigenschappen van $(Mn,Fe)_2(P,Si)$ gerelateerde materialen Er is gevonden dat de Curie temperatuur naar keuze kan worden gevarieerd door specifieke hoeveel-

heid koolstof toe te voegen, terwijl de thermische hysterese afneemt en de sterkte van het magnetocalorisch effect acceptabel blijft. De positie van het toegevoegde C binnen het kristalrooster is bepaald door neutronendiffractie bij kamertemperatuur. De opgeloste structuur duidt er op dat C waarschijnlijk de Si/P atomen vervangt op de 2*c* positie van de Fe_2P structuur.

ACKNOWLEDGEMENTS

Four years of my PhD journey at the section Fundamental Aspects of Materials and Energy (FAME), in the Department of Radiation Science and Technology (RST) of the Delft University of Technology (TU Delft) has come to the end. I would not be where I am today without the guidance and support of many people to whom I would like to express my gratitude.

Most importantly, I would like to express special appreciation and thanks to my promotor, Prof. dr. Ekkes Brück, for accepting me as a PhD candidate and giving me great opportunities to carry out the research at FAME. To Ekkes, thank you very much for your warm encouragements, patient guidance and genuine support during my PhD project. It has been a great honour for me to be one of your PhD students. I really appreciate that your door is always open for discussions and questions whenever I approach you. I also would like to thank you for your comments and corrections during the last three months on this thesis. Without your guidance and constant feedback, I would not be able to finish the work in time.

I am also grateful to my co-promotor, Dr. ir. Niels van Dijk for his valuable advice and feedback on my research and for always being strongly supportive of my work. To Niels, thank you very much for your patience and consistency in correcting my manuscripts quickly but extremely carefully, even a comma or extra space between words. In fact, your proof-reading, insightful comments and wise corrections make my manuscripts stronger. I also would like to thank you for translating the thesis summary into Dutch.

I also owe my deepest gratitude to the rest of my thesis committee members: Prof. dr. A. Schmidt-Ott, Prof. dr. C. Pappas, Prof. dr. G.C.A.M. Janssen, Prof. dr. N. Dempsey and Assoc. Prof. dr. N.P. Duong for their time and fruitful comments on this thesis.

I gratefully acknowledge the financial support from the Foundation for Fundamental Research on Matter (FOM) and BASF New Business via the Industrial Partnership Program IPP I28. My special thanks go to Bennie Reesink, Lian Zhang, David van Asten and Reinier Siertsema for their kind support in doing measurements at De Meern.

I especially appreciate kind supports from some wonderful staff personnel. I thank Anton J. E. Lefering for teaching me how to perform the experiments in the lab during my first year and for his daily help in the laboratory during the past

four years of my PhD. I thank Bert Zwart for making numerous quartz ampoules and inviting me to his place for his and his wife's birthday. I am deeply grateful to Dr. Jouke Heringa for his support in numerous computer-related issues, and also for his kind help in teaching me how to use Latex. Many thanks also go to Dr. Iulian Dugulan, Dr. Lambert van Eijck, Michel Steenvoorden and Kees Goubitz for their assistance in doing Mössbauer, X-ray and neutron diffraction measurements. I am thankful to Nicole Banga, Ilse van der Kraaij, and Trudy Beentjes (FAME and NPM2, TU Delft), and Annette Bor (FOM, now NWO) for their kind help in administrative matters.

Many thanks go to Ruben Geutijens, Jicheng Feng and Prof. dr. A. Schmidt-Ott for their great collaboration in the synthesis of $(La,Fe)_{13}Si$ nanoparticles by spark discharge. The promising results from that work are not included in this dissertation but are in preparation for publication in an international peer-reviewed journal.

It has been a great honour for me to know and work with such a dedicated group of people. The MCE group has been a source of friendships, excellent advice and fruitful collaborations. First and foremost, I would like to address my special thanks to Dr. N.H. Dung for having recommended me to the MCE group. I also would like to thank Maurits who accompanied me for four years and was always willing to help and give his best suggestions. I am also very grateful to Xuefei Miao and Yibole who both helped me in numerous ways during various stages of my PhD. I thank Dr. Dimitris Bessas for his useful advice on my career development and Dr. Michael Maschek for his valuable comments on the introduction of this thesis. I also would like to acknowledge other dear colleagues, former and present, at the MCE group: Dr. Luana Caron, Dr. Zhiqiang Ou, Dr. Jose Vieira Leitao, Dr. Giacomo, Dr. Francois, Francesco, Theo, Bouwei Huang, Xinmin You and Jiawei Lai for their company, friendship and kind support.

My thanks also go to all the colleagues at FAME and NPM2: Deepak Pratap Singh, Ben Herrison, Kun, Xiaoyu Zhang, Anca, Romain Blondé, Shasha, Zhou Zhou, Wenqin Shi, Yaolin, Chuang Yu, Haixing Fang, Zhaolong Li, Bo Peng, Bei Tian, Lars Bannenberg, Remco van der Jagt, Tomas Verhallen, Michel Thijs, Fred Naastepad, Shasha Lyu, Alexandros Vasileiadis, Niek de Klerk, Carla Robledo, Maxim Ariens, Martijn van Hulzen, Casper Versteylen, Swapna Ganapathy, Chao Wang, Evgenii Velichko, Violetta Arszelewska, Peter-Paul Harks and Fengjiao Qian for the interesting discussions during coffee breaks, lunches, etc. Special thanks go to my officemates: Prasad Gonugunta and Jurrian Bakker. To Prasad, thank you for supporting me a lot during the past four years and helping me buy many Chemistry books whenever you were on vacation in India. I wish you all the best with your PhD. To Jurrian, thank you for your kind help and support whenever I needed, even most of the time you were doing your experiments in Eindhoven.

My time in Delft was enjoyable in large part due to the many friends and groups that became a part of my life. First and foremost, my deep appreciation goes to my friends (in the Vietnamese Community in Delft - VCiD) whom I shared great moments of my life in Delft with, e.g. singing karaoke, playing games, having BBQ, sharing the delicious food, etc. I am so blessed to have met and spent these past four years with you all (too many to list all here but you know who you are). Special thanks go to Ricky Bui for the help of designing the cover page. Second, many thanks go to all members of the bowl up reactor group. I am grateful for the time spent with you all for playing sports, drinking beer and sharing the tasty food, which made my PhD life more colourful. I also would like to give my special gratitude to the RID table tennis team. Special thanks go to Xuefei Miao, Peter-Paul and Jawei Lai for their frequent presence to play ping pong every Friday, which has become my favourite activity for more than 2 years. Particularly, attending the Panda table tennis tournament with Peter-Paul and Xinmin You was a crazy but unforgettable experience for me.

My colleagues at Quy Nhon University (QNU) and friends in Europe were sources of laughter, joy, and support. Special thanks go to: anh Hao-chi Loan, anh Thuan-chi Tam, anh Bay-Ban Mai, Vinh, anh Hieu, anh Hien, Thuong, anh An-Y Thanh, anh Hai, chi Tra, chi Trang, anh Khai-chi Thuy, Ho, anh Dung, anh So, Thoai, anh Thoai, Tri, Dai, Hung-Hang, anh Hai-Mien Trung, anh Trung - chi Ngan, chi Ha, anh Chung and anh Hieu-Linh for their hospitality, help and friendship. It was always nice time when we were together. I truly express my sincere thanks to my teachers and colleagues at the Department of Chemistry, Quy Nhon University for the kindest help and support throughout my PhD time.

I am sincerely grateful to my uncle and his family for always welcoming and hosting me whenever I am in Ho Chi Minh city.

Above all; I would like to thank my beloved family: my parents, my elder brother, my younger sister, my sister-in-law, my brother-in-law and my nieces, for always believing in me and encouraging me to follow my dreams. Words cannot sufficiently express all my heartfelt appreciations to your love and care for me.

Delft, 5^{th} April 2017

LIST OF PUBLICATIONS

PUBLICATIONS RELATED TO THE THESIS

5. **N. V. Thang**, X. F. Miao, H. Yibole, K. Goubitz, L. van Eijck, N. H. van Dijk and E. Brück, *Effect of carbon doping on the structure and magnetic phase transition in $(Mn,Fe)_2(P,Si)$*, submitted.

4. **N. V. Thang**, N. H. van Dijk and E. Brück, *Tuneable giant magnetocaloric effect in $(Mn,Fe)_2(P,Si)$ materials by Co-B and Ni-B co-doping*, Materials, **10**, 14 (2017).

3. **N. V. Thang**, H. Yibole, N. H. van Dijk and E. Brück, *Effect of heat treatment conditions on MnFe(P,Si,B) compounds for room temperature magnetic refrigeration*, Journal of Alloys and Compounds, **699**, 633 (2017).

2. **N. V. Thang**, X. F. Miao, N. H. van Dijk and E. Brück, *Structural and magnetocaloric properties of $(Mn,Fe)_2(P,Si)$ materials with added nitrogen*, Journal of Alloys and Compounds, **670**, 123 (2016).

1. **N. V. Thang**, N. H. van Dijk and E. Brück, *Effects of milling conditions on nanoscale MnFe(P,Si) particles by surfactant-assisted high-energy ball milling*, Physics Procedia, **75**, 1104 (2015).

OTHER PUBLICATIONS

5. M. F. J. Boeije; M. Maschek, X. F. Miao, **N. V. Thang**, N. H. van Dijk and E. Brück, *Mixed magnetism in magnetocaloric materials with first-order and second-order magnetoelastic transitions*, Journal of Physics D: Applied Physics (2017).

4. N. T. K. Lien, **N. V. Thang**, N. D. Hung, N. D. Cuong, N. D. T. Kien, C. X. Thang, P. H. Vuong, D. X. Viet, N. T. Khoi, and P. T. Huy, *Influence of annealing temperature and Gd and Eu concentrations on structure and luminescence properties of $(Y,Gd)BO_3:Eu^{3+}$ phosphors prepared by sol-gel method*, Journal of Electronics Materials, (2017).

3. E. Brück, H. Yibole, **Nguyen Van Thang**, Xuefei Miao, Maurits Boeije and Niel van Dijk, *Transition metal based magnetocaloric materials for energy efficient heat pumps*, Solid state phenomena, **257**, 129 (2016).

2. X. F. Miao, **N. V. Thang**, L. Caron, H. Yibole, R. Smith, N. H. van Dijk and E. Brück, *Tuning the magnetoelastic transition in $(Mn,Fe)_2(P,Si)$ by B, C and N doping*, Scripta Materialia **124**, 129 (2016).

1. X. F. Miao, Y. Mitsui, I. Dugulan, P. Roy, L. Caron, **N. V. Thang**, K. Koyama, K. Takahashi, R. A. de Groot, N. H. van Dijk and E. Brück, *Kinetic-arrest induced phase coexistence and metastability in (Mn,Fe)$_2$(P,Si)*, Physical Review B, **94**, 094426 (2016).

PATENTS

4. E. Brück and **N. V. Thang**, *Heat treatment of magnetocaloric materials comprising Mn, Fe, one or both of Ni and Co, P, Si, N, C and B* , European Patent, application no. 16203485.4, 2016.

3. E. Brück, **N. V. Thang** and P. Roy, *Magnetocaloric materials comprising Mn, Fe, one or both of Ni and Co, P, Si and B*, European Patent, application no. 16191432.0, 2016.

2. E. Brück, **N. V. Thang** and X. F. Miao, *Magnetocaloric materials comprising manganese, iron, silicon, phosphorus and carbon*, European Patent, application no. 16173919.8, 2016.

1. E. Brück, **N. V. Thang** and X. F. Miao, *Magnetocaloric materials comprising manganese, iron, silicon, phosphorus and nitrogen*, European Patent, application no. 15192313.3, 2015.

CONFERENCE PRESENTATIONS

5. Effect of heat treatment conditions on MnFe(P,Si,B) compounds for room-temperature magnetic refrigeration, Thermag VII, 2016, Turin, Italy (Poster presentation).

4. Effect of nitrogen addition on the structure and magnetocaloric properties of (Mn,Fe)$_2$(P,Si) materials, 13^{th} Joint MMM-Intermag, 2016, San Diego, USA (Oral presentation).

3. Effects of milling conditions on nano-scale MnFe(P,Si) particles by surfactant-assisted high-energy ball milling, 20^{th} ICM, 2015, Barcelona, Spain (Poster presentation).

2. Preparation and characterization of nano-scale Fe_2P-based particles by surfactant-assisted high-energy ball milling, Thermag VI, 2014, Victoria, BC, Canada (Poster presentation).

1. Synthesis of red-emitting phosphors (Y,Gd)B_3: Eu^{3+} by sol-gel process, 6^{th} National Conference on Solid State Physics and Materials Science, 2009, Da Nang, Vietnam (Oral presentation)

CURRICULUM VITÆ

Thang Van Nguyen was born on August 1^{st}, 1984 in Binh Dinh, Vietnam. He received his BSc. degree in Chemistry at Quy Nhon University, Vietnam in June 2006. After his graduation, he was appointed to work as a teaching assistant at the Department of Chemistry, Quy Nhon University, where he was involved in teaching several courses on General and Inorganic Chemistry. In October 2007, he went to Hanoi to study at Hanoi National University, University of Natural Science and obtained his MSc. degree in Inorganic Chemistry in November 2009.

Between March 2013 and February 2017, he was employed by the Dutch Foundation for Fundamental Research on Matter (FOM) to work as a PhD student at the section Fundamental Aspects of Materials and Energy (FAME), Department of Radiation Science Technology of Delft University of Technology (TU Delft), the Netherlands. Under the supervision of Prof. dr. E. Brück and Dr. ir. N.H. van Dijk, his PhD project aims to tailor the properties of $(Mn,Fe)_2(P,Si)$-based materials for room-temperature magnetic refrigeration. This thesis summarized the main results obtained from this study, which have been published in five international peer-reviewed journals (four published and one submitted) and have been filed in four European patents.